

ROLE OF ENGINE AGE AND LUBRICANT CHEMISTRY
ON THE CHARACTERISTICS
OF EGR SOOT

BY

OLUSANMI ADENIJI ADENIRAN

Presented to the Faculty of the Graduate School of
The University of Texas at Arlington in Partial Fulfillment
of the Requirements
for the Degree of

MASTERS OF SCIENCE DEGREE IN MATERIALS ENGINEERING

THE UNIVERSITY OF TEXAS AT ARLINGTON

December 2013

Copyright © by Olusanmi Adeniji Adeniran

All Rights Reserved



Acknowledgements

I would sincerely like to express a deep appreciation and gratitude to my Research Advisor and Committee Chair, Dr. Pranesh Aswath, for the opportunity to work and learn from him, and for instilling in me research acumen throughout my time as a graduate student in the Department of Materials Science & Engineering at the University of Texas at Arlington. His knowledge of subject matter and willingness to guide makes him a remarkable mentor. My sincere gratitude goes to my other committee members Dr. Yaowu Hao and Dr. Fuqiang Liu for their contributions to my completing the graduate program.

I would like to acknowledge my past and present colleagues in the Tribology & Bio-materials group who we worked together at some point; Megen Velten, Pradip Sairam, Sujay Bagi, Vibhu Sharma, Olumide Aruwajoye, Ami Shah, Kush Shah, Gaurav Nagalia and Kavisha Tekade for all the support I got from them. I am also grateful for the Camaraderie and knowledge shared with office mates from other groups, Dong Liu, Amir Salehi, Manoucher Teimouri, Zi Wei, Syed Sajjad, and Alex Hsu; their support also made my time in the program worthwhile.

My sincere words of appreciation also go to Jennifer Standlee, Libia Cuauhtli, and Beth Robinson for helping me with administrative matters

during my program. My acknowledgement also goes to Dr. Jiechao Jiang and David Yen for their various help at the CCMB characterization facility.

My sincere words of appreciation go to my family members and friends for their prayers, support and encouragement which saw me through completing the program. I am most grateful to My Parents Mr. Adeniji Adeniran and Mrs. Oyebola Adeniran for their continual affection, love and support which saw me through achieving this fit. I would like to thank my siblings; Ayodele, Adedolapo, Kayode and Adeola for the guidance and how their contributions have made me what I am today.

I would also like to acknowledge all my mentors and older colleague in the field who has been sources of encouragement to me throughout the Masters program; Dr. Kola Akinade and Dr. Dwayne Shirley. I appreciate my boss at LuK USA LLC Dr. Rashid Farahati for giving me an opportunity to work in his team on an internship position and for offering me a full-time position as a Development Engineer. I appreciate all the many friends that I made at the University, the list is endless and they all made my time in UT Arlington and the city of Arlington fun. I wish them all a good time and all the very best of life.

December 3, 2013

Abstract

ROLE OF ENGINE AGE AND LUBRICANT CHEMISTRY
ON THE CHARACTERISTICS
OF EGR SOOT

Olusanmi Adeniji Adeniran, M.S.

The University of Texas at Arlington, 2013

Supervising Professor: Pranesh Aswath

Exhaust products of Diesel Engines serves as an environmental hazard, and to curtail this problem a Tier 3 emission standard was introduced which involves change in engine designs and introduction of EGR systems in Diesel engines. EGR systems, however has the challenge of generating soot which are abrasive and are major causes of wear in Diesel engines.

This work has studied the characteristics of EGR soot formed in different range of engine age and in different lubricant chemistries of Mineral and Synthetic based diesel Oils. It is found that lubricant degradation is encouraged by less efficient combustion as engine age

increases, and these are precursors to formation of crystalline and amorphous particles that are causes of wear in Diesel Engines. It is found that soot from new engine is dominated by calcium based crystals which are from calcium sulfonate detergent, which reduces formation of second phase particles that can be abrasive. Diverse crystalline peaks with increased intensity are noticed in soot samples generated from EGR engine of increasing ages. This understanding of second phase particles formed in engines across age ranges can help in improving on durability design of engine, improvement of Diesel oil for EGR engines, and in development of chemistries for after-treatment solutions that can inhibit formation of abrasive particles in Oils.

Table of Contents

Acknowledgement.....	iii
Abstract	v
List of Illustrations.....	xiii
List of Tables	xvi
Chapter 1 General Overview	1
1.1 Current Understanding of Research.....	4
1.2 Objective and Drive for the research.....	7
1.3 Outline of the Research work.....	9
Chapter 2 Background.....	11
2.1 Controlled Emission in Heavy Duty Diesel Engine Design.....	12
2.2 Paradigm Shift in Diesel Engine Oil Technology	17
2.2.1 2010 Engine Technology	18
2.2.2 Proposed 2018 Engine Technology.....	19
2.3 Role of Lubricant Chemistry in Soot Formation.....	23
2.3.1 Basestock	24
2.3.1.1 Group I Base Oil.....	25
2.3.1.2 Group II Base Oil.....	26
2.3.1.3 Group III Base Oils	26

2.3.1.4	Group IV Base Oils.....	26
2.3.1.5	Group V Base Oils.....	27
2.3.2	Lubricant Additives	27
2.3.2.1	Detergent and Dispersants.....	29
2.3.2.2	Oxidation Inhibitors.....	31
2.3.2.3	Antiwear Additives	32
2.4	Role of Engine Age in Soot Formation	33
2.5	Soot Formation in EGR Diesel Engine	35
2.5.1	Soot processes.....	37
2.5.1.1	Oxidation	38
2.5.1.2	Fuel pyrolysis.....	39
2.5.1.3	Nucleation	40
2.5.1.4	Surface growth	42
2.5.1.5	Coalescence and Agglomeration.....	43
2.5.2	Kinetic mechanisms and models of soot formation.....	45
2.6	Wear Induced Mechanism of soot.....	45
2.7	Field based condition monitoring of soot	50
Chapter 3 EGR Soot from Mineral based Diesel Oil.....		54
3.1	Introduction	55
3.2	Soot Extraction.....	55
3.2.1	Oil Dissolution.....	55

3.2.2	Centrifuging Process	56
3.2.3	Soxhlet Process.....	57
3.2.4	Drying and Storage.....	58
3.3	Elemental Composition Studies of Used Oil Samples	59
3.3.1	Spectrochemical Analysis for wear metals	60
3.4	Raman studies of Soot samples.....	63
3.4.1	Experimental Procedure for Raman Studies.....	63
3.4.2	Raman Spectra Analysis by Curve Fitting	65
3.4.3	Raman Spectra Analysis of Soot Samples	66
3.4.4	Discussion of Raman Spectra of EGR Soot Samples.....	68
3.5	X- Ray Diffraction studies of Diesel Soot	70
3.5.1	Experimental Procedure	70
3.5.2	X-Ray Diffraction Analysis of EGR Soot Samples	70
3.5.3	Discussion of XRD Spectra of EGR Diesel Soot Samples	76
3.6	HR-TEM Studies of EGR Soot Samples	78
3.6.1	Experimental Procedure for HR- TEM Soot Studies.....	78
3.6.2	HR-TEM Analysis of EGR Soot Samples	79
3.6.2.1	Lattice Fringe Image Analysis.....	79
3.6.2.2	SAED Analysis of Soot Samples	89

3.6.3	Discussion of HR-TEM Analysis of EGR Soot	
	Samples	92
3.7	XANES Studies of EGR Soot Samples	95
3.7.1	Experimental Procedure for XANES Studies	96
3.7.2	XANES Analysis of Soot Samples	96
3.7.2.1	Phosphorus L edge XANES Spectral Analysis	97
3.7.2.2	Sulphur L Edge XANE Spectra Analysis	99
3.7.2.3	Phosphorus K edge XANE Spectra Analysis	100
3.7.2	Discussion of XANES Spectra	102
Chapter 4	EGR Soot from Synthetic based Diesel Oil	103
4.1	Introduction	104
4.2	Soot Extraction	104
4.2.1	Oil Dissolution	104
4.2.2	Centrifuging Process	105
4.2.3	Soxhlet Process of Soot Sample	107
4.2.4	Drying and Storage	108
4.3	Elemental Composition Analysis of Used Diesel Oil	108
4.3.1	Spectrochemical Analysis for wear metals	109
4.4	Raman Studies of EGR Soot Samples	112
4.4.1	Experimental Procedure for Raman Studies	113
4.4.2	Raman Spectra Analysis by Curve Fitting	114

4.4.3	Raman Spectra Analysis of Soot Samples	115
4.4.4	Discussion of Raman Spectra of EGR Diesel Soot	117
4.5	X- Ray Diffraction studies of Diesel Soot	119
4.5.1	Experimental Procedure	119
4.5.2	XRD Analysis of Soot Samples	120
4.5.3	Discussion of XRD Spectra of EGR Diesel Soot Samples	124
4.6	HR-TEM Studies of EGR Soot Samples	125
4.6.1	Experimental Procedure for HR-TEM Soot Studies	126
4.6.2	HR-TEM Analysis of Soot Samples	126
4.6.2.1	Lattice Fringe Image Analysis.....	127
4.6.2.1	SAED Analysis of Soot Samples	134
4.6.3	Discussion of HR-TEM Analysis of EGR Soot Samples	135
4.7	XANES Studies of EGR Soot Samples	136
4.7.1	Experimental Procedure for XANES Studies	137
4.7.2	XANES Analysis of Soot Samples	137
4.7.2.1	Phosphorus L edge XANES Spectral Analysis	138
4.7.2.1	Sulphur L edge XANE Spectra Analysis	140
4.7.1.3	Phosphorus K edge XANE Spectra Analysis.....	142
4.7.2	Discussion of XANES Spectra	143

Chapter 5 Conclusions	144
Chapter 6 Suggested Future Work	147
Appendix A API Diesel Oil Grades [81]	148
References	150
Biographical Information	162

List of Illustrations

Fig 2-1 Diesel Engine Design Strategies from 1985 to date [32]	13
Fig 2-2 (a) Diesel engine particulate filter (b) Single stage DPF [26]	15
Fig 2-3 Schematic of Typical EGR Engine	17
Fig 2-4 2010 Diesel Engine Technology [26]	19
Fig 2-5 Schematic path leading to soot formation [47]	40
Fig 2-6 Schematic of primary soot particles	44
Fig 2-7 ASTM standard measurement of Diesel soot in used lubricant using Trend Analysis in FTIR spectroscopy [69]	52
Fig 3-1 Weighted used oil sample	56
Fig 3-2 (a) Sorvall SS34 centrifuge (b) Centrifuge bottle holder	57
Fig 3-3 Soxhlet setup in an experimental fume hood (b) 8 um cellulose thimble	58
Fig 3-4 Deconvoluted Raman spectra fitted with Lorentzian curve fit for G, D ₁ , D ₃ and D ₄ peaks for (a) Carbon Black (b) Sample SP A, (c) Sample SP B and (d) Sample SP C	67
Fig 3-5 XRD spectra of Carbon black and soot samples SP A, SP B and SP C	72
Fig 3-6 Turbostratic region of soot sample SP A showing (a) Crystal fringe lattice image (b) EDS spectra	81

Fig 3-7 Turbostratic Region of Soot Sample SP B Showing (a) Crystal Fringe Lattice Image (b) EDS Spectra	84
Fig 3-8 Turbostratic Region of Soot Samples SP C Showing (a) Crystal Fringe Lattice Image (b) EDS Spectra	87
Fig 3-9 SAED Image of soot samples (a) SP A (b) SP B and (c) SP C ...	90
Fig 3-10 Normalized TEY and FLY Phosphorus L Edge spectra of soot samples SP A, SP B, SP C and model compounds	98
Fig 3-11 Normalized TEY and FLY Sulfur L Edge of soot samples SP A, SP B and SP C and model compounds	99
Fig 3-12 Normalized FLY and TEY Phosphorus K Edge spectra of soot samples SP A, SP B, SP C and model compounds	101
Fig 4-1 Weighted used synthetic oil sample	105
Fig 4-2 (a) Sorvall SS 34 Centrifuge (b) Centrifuge Bottle Holder	107
Fig 4-3 (a) Soxhlet Setup in an experimental Fume Hood (b) 8 μ m cellulose thimble	108
Fig 4-4 Deconvoluted Raman Spectra fitted with Lorentzian fit for G, D ₁ , D ₃ and D ₄ peaks for (a) Carbon black (b) Sample AM A (c) Sample AM B (d) Sample AM C	116
Fig 4-5 Fig 4.5 XRD spectra of Carbon black, soot samples AM A, AM B, and AM C	121

Fig 4-6 Turbostratic region of soot sample AM A showing (a) Crystal fringe lattice image (b) EDS spectra	128
Fig 4-7 Turbostratic region of soot sample AM B showing (a) Crystal fringe lattice image (b) EDS spectra	130
Fig 4-8 Turbostratic region of soot sample AM C showing (a) Crystal fringe lattice image (b) EDS spectra	132
Fig 4-9 SAED Lattice image of soot samples (a) AM A (b) AM B and (C) AM C	134
Fig 4-10 Normalized TEY and FLY Phosphorus L Edge spectra of soot samples AM A, AM B, AM C and model compounds.....	139
Fig 4-11 Normalized TEY and FLY Sulfur L Edge spectra of soot samples AM A, AM B, AM C and model compounds.....	141
Fig 4-12 Normalized FLY Phosphorus K Edge spectra of soot samples AM A, AM B, AM C and model compounds	142

List of Tables

Table 2-1 API Base Stock Categories [37]	24
Table 2-2 Lubricant Additives, Tasks and Examples [39]	29
Table 2-3 Major Classes of Oxidation Inhibitors and Their Applications..	32
Table 2-4 Exhaust Gas Comparison in Different Engine Ages [42]	35
Table 3-1 Spectrochemical Analysis of mineral based SAE 15-40 used oil samples	60
Table 3-2 Spectrochemical Analysis of Wear Metals.....	61
Table 3-3 Spectrochemical Analyses of Lubricant Additives	62
Table 3-4 Spectrochemical Analysis of Contaminants.....	62
Table 3-5 Raman Peak Analysis of Carbon Black and Soot Samples SP A, SP B and SP C	68
Table 3-6 XRD Analysis of nano crystalline peaks of soot sample SP A.	73
Table 3-7 XRD Analysis of nano crystalline peaks in soot sample SP B.	74
Table 3-8 XRD Analysis of nano crystalline peaks of soot sample SP C.	75
Table 3-9 Crystalline nano particles in the turbostratic structure of sample SP A	82
Table 3-10 Crystalline nano particles in the turbostratic structure of sample SP B	85
Table 3-11 (a) crystalline nano particles in the turbostratic structure of sample SP C in region 1	88

Table 3-11 (b) crystalline nano particles in the turbostratic structure of sample SP C in region 2.....	88
Table 3-12 d-spacing measurement of diffraction patterns in sample SP A, SP B and SP C.....	91
Table 3-13 d Lattice size matching of abrasive component of sample SP A, SP B and SP C.....	91
Table 4-1 Spectrochemical Analysis of Synthetic based SAE 15-40 used Oil Samples.....	109
Table 4-2 Spectrochemical Analysis of Wear Metals.....	110
Table 4-3 Spectroscopic Analysis of Lubricant Additives	111
Table 4-4 Spectroscopic Analysis of External Contaminants	111
Table 4-5 Deconvoluted Raman Peak Data for Carbon Black, Samples AM A, AM B and AM C.....	117
Table 4-6 Analysis of nano crystalline peaks of soot sample AM A.....	122
Table 4-7 Analysis of nano crystalline peaks of soot sample AM B.....	123
Table 4-8 Analysis of nano crystalline peaks of soot sample AM C.....	123
Table 4-9 HR-TEM Analysis of lattice fringes for possible nano crystalline particles in sample AM A.....	129
Table 4-10 HR-TEM Analysis of Lattice fringes image for possible nano crystalline particles in sample AM B	131

Table 4-11 HR-TEM Analysis of Lattice Fringes for Possible Nano crystalline particles	133
Table 4-12 d- spacing measurement for electron diffraction patterns for Samples AM A, AM B and AM C	135

Chapter 1

General Overview

The popularity of Diesel Engines has in recent years increased as preferred choice of transportation engines because of their higher efficiency and low maintenance cost. The Compression-Ignition-Direct Injection (CIDI) or Diesel Engines give a higher efficiency as compared to Spark-Ignited Gasoline Engines, hence improved fuel economy and consequently reduction in greenhouse gas emission. Fuel consumption reduction [1] from CIDI or diesel engines compared to gasoline fueled engines is estimated to result in as much as 30–35% reduction in greenhouse gases. However, a major obstacle to the extensive application of Diesel Engines, especially for automotive applications, is their high level of Nitrogen Oxides (NO_x) and Particulate Matter (PM), both of which have possible negative effects on the environment and health. Major efforts are being directed at development of technologies that can reduce Diesel Engine NO_x and particulate matters (PM).

A greater concern to protect the environment has informed a requirement for engine manufacturers set by API. The American Petroleum Institute (API) requires engine manufacturers to reduce the level of nitrogen oxides (NO_x) in Diesel Engine exhaust to meet Tier 3 emission standards. API CJ 4 is the current required standard required for

four stroke diesel engines by the Environment Protection Agency (EPA) where maximum limit has been put on the emission of NO_x to 0.2 gram/BHP hr and PMs to 0.01 gram/BHP hr by 2010 [2]. This requirement is accomplished by *changes in engine designs* that include retarded timing, raised piston rings, selective catalytic reduction and *the use of Exhaust Gas Recirculation (EGR)*. [3]. The effect of the standard is that the 2007 engines will generate more soot and experience higher peak cylinder temperatures due to the higher levels of EGR. A newer standard PC-11 is in progress to serve as latest engine and environmental standard superseding the API CJ 4.

The Exhaust Gas Recirculation (EGR) is an effective means to reduce the NO_x emission from Diesel Engines [4,5]. Oxides of nitrogen (NO_x) are formed when the combustion temperatures are too high. Any measure that reduces the combustion temperature will thus lead to decreased NO_x formation and emissions. EGR involves recirculation of exhaust gas back into the intake stream, the recirculated gas is burned a second time and therefore reduces emission associated with health risk. Returning exhaust product to the Diesel Engine combustion chamber will however accelerate the degradation of the lubricant engine oil, primarily by increasing the total acid number (TAN) as well as the soot content and, consequently, the viscosity. Engine durability may be compromised by

EGR due to acceleration of oil contamination and degradation by engine Exhaust Gas Recirculation (EGR) soot and other products [6,7].

The use of EGR has increased soot and other solid particulate loading of the lubricant oil, which degrades the lubricating oil properties physically and chemically, and thereby result in wear of engine parts [6-9]. Modern Cummins engine M-11 engines, have been reported to contain up to 9% soot in used oils [10,11]. This condition goes against the current desire for an extended oil drain interval in Diesel Engines. The enormous amount of soot degrades oil increasing its viscosity [12,13] and hence, its pumpability between surfaces in relative motion. In engine tests, wear of engine components such as the valve train, piston rings, and cylinder linings have been found to be promoted by increasing level of EGR [10-12].

Another restriction on the amount of some chemicals that should be used in lubricant formulation also compounds the problem of wear in Diesel Engines. The EPA regulation known as SAPS has imposed a (1wt %) sulfated ash, (0.1wt %) Phosphorus and (0.1 wt %) Sulfur limit in engine oil formulation. Phosphorus and Sulfur on the other hand are major contributors in formation of antiwear film in engine oil, and their restriction in Diesel Engine Oils will aggravate wear of diesel engine components equipped with EGR protocol.

The increase in soot and solid particulate content in the engine oil results in accelerated abrasive wear of critical engine components. Similarly, the increase in the oil acid content (sulfuric acid) increases corrosive wear of lubricated surfaces. The synergistic impact of these two detrimental effects in the form of abrasive–corrosive wear is also possible in some EGR-equipped Diesel Engine components. EGR soot is believed to contain abrasive nano crystalline particles embedded within turbostratic structure of soot, which are the major causes of wear in EGR Diesel Engines.

Four-ball wear tests with M-50 balls have shown that, although the used oils slightly decrease the friction coefficients, they increased the ball wear by two orders of magnitude when compared to tests with clean oil. Wear in EGR engines from increased viscosity is primarily by an abrasive mechanism, but in oil with the highest soot loading of 12%, scuffing and soot particle embedment had been observed. Laboratory wear tests by S. Aldajah et al. [6] had shown a linear correlation with the TAN, while the crosshead wear during the engine test was proportional to the soot content.

1.1 Current understanding of Research

Significant work has been done to understand formation and structure of soot in Diesel Engines using simulation and various

characterization methods. Various characterization tools and techniques have been used to understand structure and composition of “Exhaust Gas Recirculation” soot. Some of techniques used have been X-ray diffraction, Raman Spectroscopy, Electron Energy Loss Spectroscopy (EELS), High Resolution Transmission Electron Microscope (HRTEM), X-ray Adsorption Near Edge Spectroscopy, etc [14-17].

Significant effort has been made to understand the nature of soot formed in EGR Diesel Engines, its structure and composition. EGR soot is believed to have compositions of graphitic soot and other crystalline abrasive components. The abrasive components are believed to come from interaction of degraded oil chemistries (from both base oil and engine oil additives) with wear particles of Diesel Engine. Antusch et al [18] characterized soot using various microscopy and spectroscopy techniques, and his result suggested that wear from EGR soot does not depend on the mechanical properties of the different soot particles, but is closely related to their reactivity and the amount of defect sites. The reactivity is believed to be informed by the chemistries of the different lubricants, but the mechanism of how these chemistries affect the characteristics of EGR soot has not been understood.

Significant efforts have been made to understand the role of crankcase soot, available inside the oil sump, to promote higher wear of

Diesel engine equipped with EGR. Many conflicting, incomplete ideas and explanations about the properties and effects of soot particulates on wear mechanisms have been published. Rounds [19] showed that soot is not abrasive but adsorb anti-wear additive in lubricants, thus diminishing the anti-wear properties. Ryason et al [20] concluded that soot particles are abrasive because they are found to generate groves and breakouts in metal surfaces.

The idea of Nagai et al [21] was that soot particles are very hard and acts abrasively on metal surface. The authors also found that intensified EGR raises the soot concentration in oil, thus enhancing wear. Gautam et al [5] found more wear with soot contamination of the oil than without. It has been an established fact that higher soot concentration in oil generates more wear whereas a higher concentration of phosphorus in the oil leads to less wear. Soejima et al [22]. Yamaguchi et al [11] and, Aldajah et al [6] found that the presence of soot particles reduces the thickness and extension of anti-wear films and are abrasive. Truhan et al [23,24] concluded that chemical activity of soot particles and their reaction with ZDDP prevents the formation of liquid boundary layers on the metal surface.

Properties of soot particulate emission has been found to very much depend on thermodynamics of combustion in the engine and

consequently on the final structure of the carbonaceous matter such as the average primary particle and aggregate size and size distributions, and the degree of graphitization. Thermodynamics of combustion in engine will be informed by lubricant chemistries and their reactivity with engine material, and the reactivity of the engine material can be traced to depend on engine age. It has been established that older Diesel Engines will generate higher levels of PM, NO_x and CO emissions; but this has not been related to nature of soot that can be generated as Diesel Engine ages. Hence, there's a need to relate the nature of soot generated with engine age and lubricant chemistries. It is believed that there will be diminished combustion efficiency in combustion systems of engine which can be related to the nature of EGR soot that is generated in engines of different ages.

1.2 Objective and Drive for the Research

Engine Age can be a determinant factor on nature of EGR soot formed. As Diesel Engine ages, it is believed that there will be less efficiency of combustion systems, and thermodynamics of combustion will change which will result in different characteristics of EGR soot formed across different engine age range. The reactivity of ageing Diesel Engines with oil chemistries will differ, which will also influence nature of EGR soot formed. New engine generally have a break- in period of surface

asperities from early cycle of operation and this may affect interaction with lubricant chemistries.

The works of many authors carried out in this area in the past have not studied the effect of engine age and lubricant chemistries on characteristics of soot generated in EGR engines. This work by characterizing soot samples generated in new to older Diesel engines will predict the effect of engine age and lubricant chemistry on the characteristics of EGR soot generated across different Diesel Engine age ranges from Mineral based and Synthetic based Diesel Oil. Understanding the characteristics of EGR soot formed in various engine ranges will also give an insight and better understanding in the development of after-treatment oil additive which can mitigate and inhibit the formation of likely abrasive product of soot which are causes of wear in Diesel engines.

The structural complexity of soot varies depending on the type of engine, age of engine, lubricant chemistry and its operating conditions. Uncertainty is avoided by focusing on EGR soot samples from same engine make, the Detroit DD15 engines under similar operating conditions for varying Diesel Engine age ranges which allows for comparability. Lubricant chemistries employing Mineral and Synthetic base stocks were studied to learn the effect of basestock chemistry on nature of EGR soot. The conclusion from work of the several authors in this area has not been

able to relate nature of EGR soot formed from different engine ages and lubrication chemistries, therefore more fundamental knowledge is needed in this area. This informed the need to carry out this study to get the idea of the nature of EGR soot produced in diesel engine as they go older. The study examined how engine ages and lubricant chemistries affect the characteristics of EGR soot in diesel engines.

1.3 Outline of the Research work

This thesis is presented in a total of five chapters. Following is a list of the chapters with a brief outline of contents presented.

Chapter 1: This chapter gives the reader a general overview of state of research by previous authors, research work carried out, and it highlights the objectives and drive for the research.

Chapter 2: This chapter gives a background to study and explains in depth all fundamentals related to soot Tribology of diesel soot.

Chapter 3: This chapter gives a detailed experimental description and studies of nature of EGR diesel soot generated mineral based formulated diesel oil for new to older engines of 54,000 miles, 247,000 miles and 306,000 miles respectively.

Chapter 4: This chapter gives a detailed experimental description and studies of nature of EGR diesel soot generated mineral based formulated

diesel oil for new to older engines of 127,000 miles, 187,000 miles and 248,000 miles respectively

Chapter 5: This chapter concludes on the findings of the Studies

Chapter 6: This Chapter suggests future work that can be carried out.

Chapter 2

Background

Diesel Engines have always been the preferred mode of transportation because of their superior fuel efficiency as a result of their higher compression ratio, lean mixture operation, and the absence of throttling losses. They have found applications in both Heavy Duty and Off-highway vehicles and equipment. Today, Diesel Engines are developed to be more environmentally friendly due to lower emission of carbon dioxide CO₂ [25], which is the main cause of greenhouse effect. Economic-wise, Diesel Engine is also better since there are more taxes on gasoline. Current advancements in diesel emission control are constantly upgraded to keep pace with increasing targets in emission control. Nitrogen oxides (NO_x) emissions, which includes nitric oxide (NO), and nitrogen dioxide (NO₂), as well as particulate matters (PMs) from Diesel Engines is being minimized to necessary levels in order to lower the concentration of these pollutants in the atmosphere. Various legislations have been put in place to guard diesel engine manufactures and lubricant oil formulation requirements for reduced NO_x emissions into the atmosphere.

In the US, the API CJ-4 is the latest specified standard for Diesel Engine oils to meet tier 3 emission standard of the Environmental Protection Agency (EPA) where maximum limit has been put on the emission of NO_x to 0.2 gram/BHP hr and PMs to 0.01 gram/BHP hr from 2010 [26], and a “proposed category” PC-11 in the process to take effect from 2018. The European Union has an updated specification, where Emission standard laws for diesel engines meet up till 2016 requirements. Euro 5 emission standard, applied since Jan 2011 for diesel engine vehicles targeted reduction of NO_x and PM from 0.25 g/km to 0.18 g/km, and from 0.025 g/km to 0.005 g/km respectively from the previous Euro 4. The Euro 6 is expected to be enforced from Jan 2015 for the registration of new engine vehicles [27]. The main driver for the change in diesel emissions regulations of tailpipe NO_x and PM lies in the fact that both pollutants pose significant health and environmental risks [28].

2.1 Controlled Emission in Heavy Duty Diesel Engine Design

Modifications to engine design features and operating strategies have been employed to reduce NO_x emissions and control soot in response to environmental legislations. Most of the direct approaches explored have been regulating pre- and in-cylinder process such as controlling flame temperature and local equivalence ratio since formation of NO_x and soot are function of temperature and equivalence ratio [29]. Modification of

engines to achieve efficiency in response to environmental legislation is usually achieved by optimizing combustion chamber geometry [30,31], by employing the exhaust gas recirculation (EGR) system [32] and by injection strategies [33,34]. Engine design strategies employed in the last three decades is shown in Fig 2.1 below.

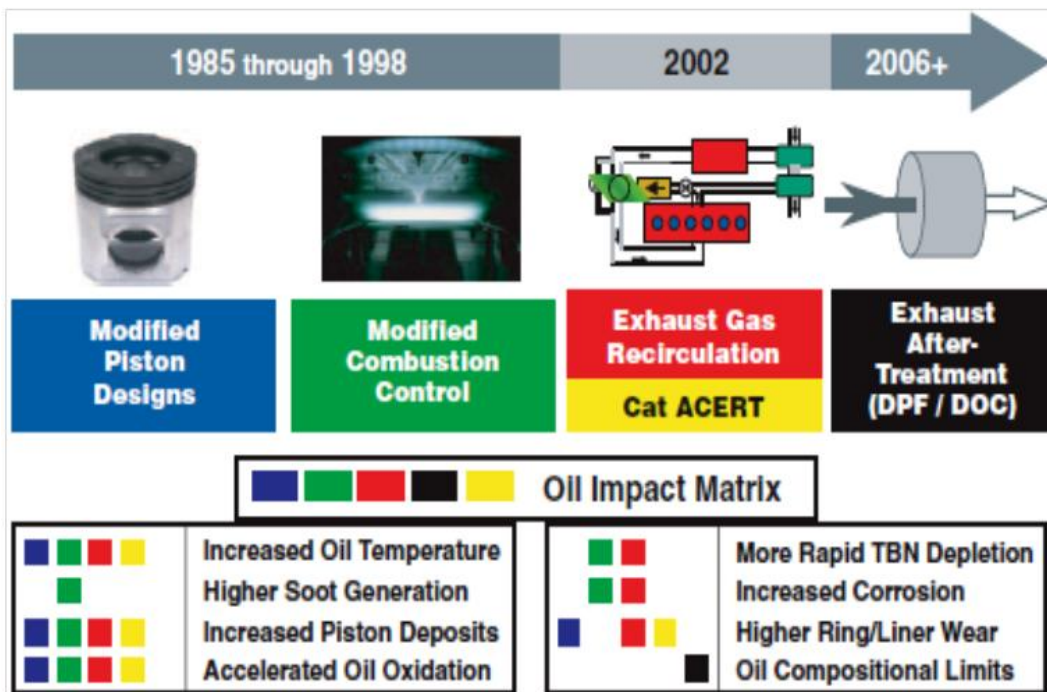


Fig 2-1 Diesel Engine Design Strategies from 1985 to date [32]

In modification to diesel engines employing injection strategies, the multiple fuel injection schemes is commonly used as it offers significant advantages over single injection, particularly with regards to limiting NO_x and soot formation. Injection parameters are optimized such that the amount of fuel required can be delivered in many discrete steps according

to local oxygen availability for optimum combustion process. This scheme (multiple injections) is aimed at achieving a drastic reduction in local gas temperature, to lean out the combustion zones as well as to eliminate soot formation originating from spray wall impingement. However, as changes in operating strategies were implemented, there comes into place an unexpected increase in soot concentration. Lockwood et al [35] while studying the effect of injection loading on diesel engine oil found an increase in soot concentration for typical used engine oil at drain from a line haul operation, from 0.5 – 1.0 wt% to 2.0 – 4.0 wt% in comparable operations. This shows that engine operating conditions and choice of calibration controls play a major part in dictating the transport processes of in-cylinder soot into the crankcase, which ultimately determine the level of soot in engine oil.

Increased generation of soot in oil usually leads to significant wear and damage, which ultimately reduces the lifecycle of engines. For multiple injection schemes, there exists the possibilities of available in-cylinder soot that can be transferred into the oil sump is significantly raised due to the resulting changes in the distribution of combustion events. Research is ongoing by various authors and there is still the need to expand on the limited knowledge of the nature and factors contributing to soot transport into engine oil when injection patterns are varied. Detailed

understanding of the effects of injection parameters on diesel spray combustion process, soot formation processes, and also the in-cylinder soot transport still needs to be grasped.

Exhaust Gas Recirculation (EGR) and after-treatment devices such as Catalytic Diesel Particulate Filters and oxidation catalysts were developed as means to achieve these emission limits. They result in new generation of engine oils that provide emission control system durability, prevent catalyst poisoning and particulate filter blocking, while still offering optimum protection for control of piston ring deposits, oxidative thickening, oil consumption, high- temperature stability, soot handling properties, foaming and viscosity loss due to shearing. Typical diesel engine particulate filter is shown in fig 2.2 below.



Fig 2-2 (a) Diesel engine particulate filter (b) Single stage DPF [26]

Cummins, Detroit Diesel, International- Navistar, Mack and Volvo North America have employed the use of heavy EGR (30 to 35 percent)

closed crankcase ventilation and diesel particulate traps to remove soot and other particulates. Caterpillar uses its Advanced Combustion Emission Reduction Technology (ACERT), an advanced combustion process called Clean Gas Induction (CGI), closed crankcase ventilation and diesel particulate filters. CGI employs the use of remote EGR, a closed crankcase ventilation system and diesel particulate filter system with active regeneration.

CGI draws clean inert soot-free exhaust gas from downstream of the particulate filter and then puts the clean gas into the intake system. This clean gas does not induce wear and the low intake manifold gas temperature of the CGI contributes to lower NO_x emissions, with particulate filter employing a walled-flow filter technology. Regeneration is necessary to activate the process of oxidation that eliminates the soot that collects along the inlet walls of the filter. To aid regeneration, the exhaust gas is heated by auxiliary means. The regeneration process takes place only when needed. Caterpillar engines that are 500 horsepower or less will require one diesel particulate filter and engines of more than 550 horsepower will require dual particulate filters [25].

All diesel engines OEM choose closed crankcase ventilation in order to remove harmful vapor generated in the crankcase; with the vapors discharged into the engine's intake system (usually via the intake

manifold), where they are burned as part of the combustion process rather than being discharged into the atmosphere. Fig 2.3 below shows general schematic of an EGR Diesel Engine.

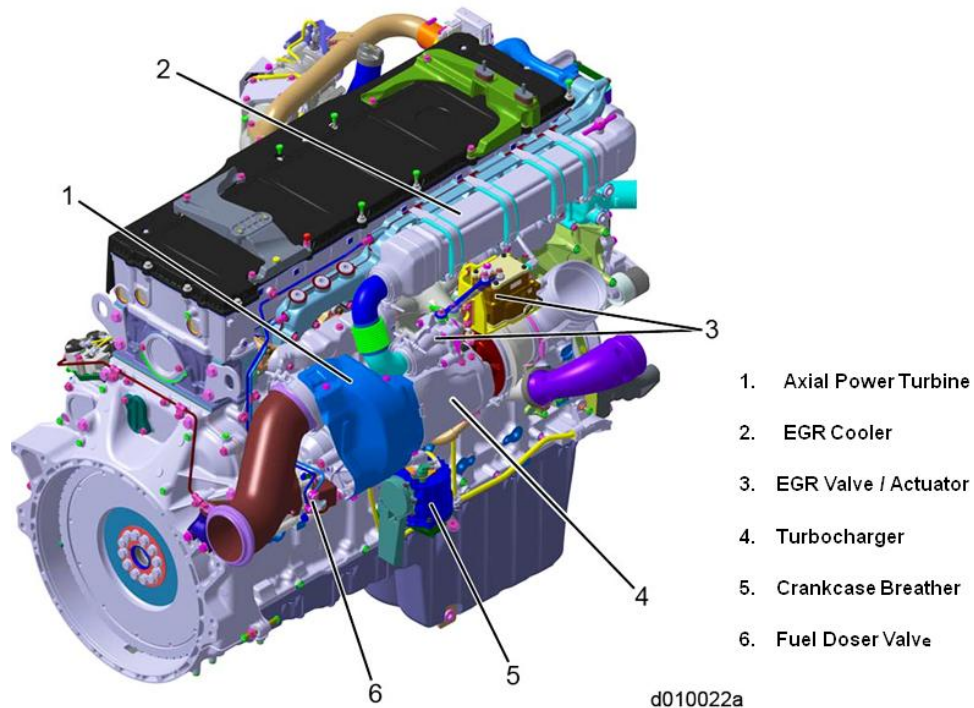


Fig 2-3 Schematic of Typical EGR Engine

2.2 Paradigm Shift in Diesel Engine Oil Technology

Regulations and standards over the years have evolved which have been main driving factors for the development of API commercial “C” Diesel Engine Oil classification. The first standard being API CA for engines built by 1959 and the latest being API CJ- 4 which took effect in 2010. PC-11 is currently proposed and being developed and will take full effect in 2018.

2.2.1 2010 Engine Technology

On-highway diesel emissions was expected to be further reduced to 0.2 g/ bhp-hr for NO_x, and particulate emissions remain at 0.01 g/bhp-hr. On-highway diesel emission levels, in conjunction with mandated use of ultra low sulfur diesel fuel for off-highway diesel engines begun in June 2010, which resulted in further engine design changes and the use of additional after-treatment technologies as well as the use of the current diesel particulate filter technology. Fig 2.4 on page 19 illustrates the 2010 engine technology requirements. The additional after-treatment devices that are used in the engine are:

- lean NO_x catalysts (LNC)
- lean NO_x traps (LNT)
- NO_x storage reduction catalysts (NSRC)
- DeNO_x catalysts
- NO_x absorbers
- selective catalytic reduction (SCR)
- diesel oxidation catalysts (DOC)

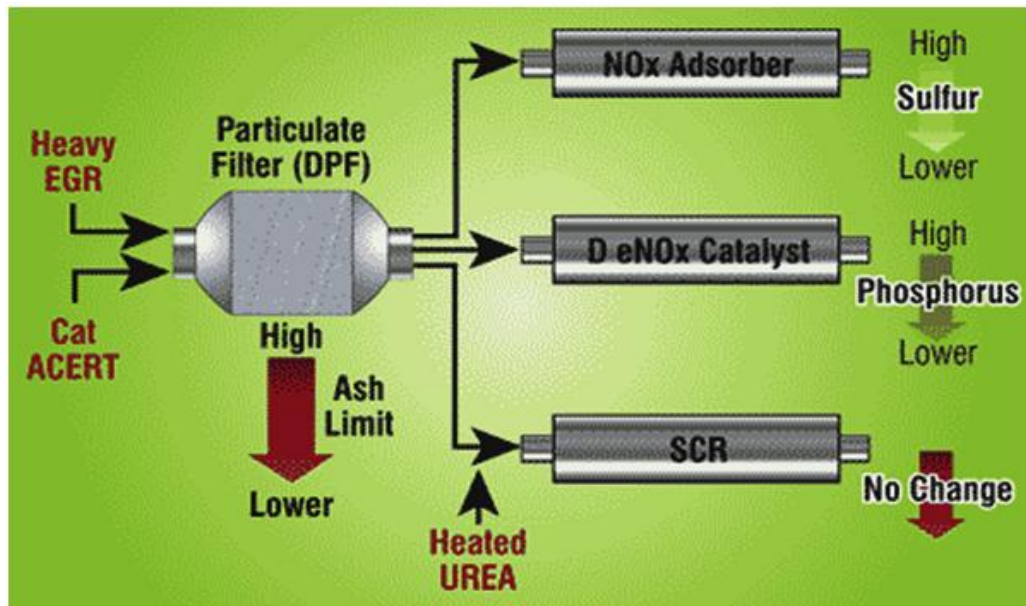


Fig 2-4 2010 Diesel Engine Technology [26]

The use of these after-treatment devices result in further chemical limits being placed on future heavy-duty diesel engine oils to ensure catalyst compatibility. This will result in the development of a new engine oil service classification for heavy-duty diesel engine oils that will require a careful balancing act in providing engine durability to existing engines while still providing after-treatment compatibility and life.

2.2.2 Proposed 2018 Engine Technology

The latest applicable standard for diesel engine oil is the API CJ-4; with “proposed category” PC-11 in the process to take effect from 2018. Development of a new American Petroleum Institute (API) service category for heavy diesel engine oil always starts with a discussion by

engine makers, additive suppliers and lube formulators of a “Proposed Category (PC) [36].”

The PC-11 may well lead to the release of not one but two new API service categories, according to industry experts. PC-11 is said to be launched both to address the coming reduction in carbon dioxide [CO₂] emissions from truck engines and to help engines be more fuel-efficient [36]. The PC-11 is also intended to deliver lubricants that protect engine life and durability. The proposed two subcategories is due to desire to improve fuel efficiency while ensuring corresponding performance levels, and both subcategories would help engines meet the lower NO_x standards that will start coming into effect for engines in model year 2014 trucks. Engine Manufacturers Association (EMA) has specifically recommended is that there be two API service categories created. Both would help engines meet the lower NO_x standards that will start coming into effect for engines in model year 2014 trucks.

The first of the new API categories would be formulated to “preserve the historical heavy-duty oil criteria as represented by the current CJ-4 category and be backward-compatible with existing on- and off-highway engines. While the second new category would also “maintain engine durability but by using a lower-viscosity formula it would provide additional fuel-efficiency gains vs. current SAE 15W - 40 oils and it would

offer only limited backward-compatibility,” which would be dependent on OEM and engine maker requirements and vehicle applications. List of expected improvement for what PC-11 will accomplish in heavy-duty motor oil includes better oxidation stability, aeration, shear stability; less adhesive wear or “scuffing,” and compatibility with engines running biodiesel blends. Decision on whether or not to split PC-11 into two proposed categories would likely be made by 2014 and the goal of the industry is to have new oil formulations- whether one or two- on the market by 2016.

The API CJ-4 currently in use has a goal of backward compatibility with the oil formulations of the older API CI - 4 and CI - 4 Plus classifications. Restrictions in SAPS for the oil brought a paradigm shift to engine oil technology. The reduction in ash levels from the norm of 1.3 percent to 1.5 percent to the mandatory maximum of 1.0 percent and the additional reduction in sulfur levels of the base oil and additives to 0.4 percent maximum required replacing conventional metal-containing additive chemistries with alternative additive chemistries that are low in metallic content, sulfur and in some cases ashless. The use of these alternative additive chemistries has reduced the engine oil's BN to a level ranging from 8 to 10. This lowering BN can reduce oil drain intervals in off-highway diesel engines that will still be allowed to use low sulfur diesel

fuel (500 ppm maximum) till 2010. For on-highway diesel engines, this reduction in BN is not anticipated to affect current oil drain intervals because the use of ultra low sulfur diesel fuel (15 ppm maximum) will be the balancing factor in the oil drain interval equation. These factors could result in a differentiating of two different engine oils: one for off-highway diesel engines and the other for on-highway diesel engines for the next few years. Further, it is anticipated that some OEMs will require BN minimums depending upon the application their engines are used in.

To meet the API CJ-4 limit of 0.12 percent phosphorus, the amount of ZDTP used in the formulation of heavy-duty diesel engine oils has been reduced. This reduction in ZDTP requires the use of alternative ashless antiwear agents to protect the valve train from wear. The reduction in sulfur levels to 0.4 percent maximum along with the NOACK volatility limits of 13 percent maximum and the need for increased oxidation stability due to the increased thermal stress placed on the engine oil from the use of heavy EGR rates and after-treatment have resulted in an increased use of Group II, Group III and Group IV basestock.

Consumer demand for longer lasting oils and the concern over increased engine and oil sump temperatures due to current and future engine design to meet these emission standards have further driven the

development of new engine oil service categories. Summary of Diesel Oil API grades over the past fifty years is Appendix A

2.3 Role of Lubricant Chemistry in Soot Formation

Gautam et al [5] investigated the effects of base stock, dispersant level, and ZDDP level on nature of soot formed and resulting three-body wear. Their statistical analysis of Lubricant formulation suggested that base stock and dispersant levels were significant on oil's wear performance, while the effect of ZDDP was negligible within the range of concentrations tested. They investigated the effects of soot contaminated engine oil on three-body wear. The effect of Phosphorus, dispersant and sulfonate levels as oil additives were tested and they concluded that there is an interaction between oil additives and soot in reducing the oil's anti-wear properties.

Modern oil formulations for diesel engines contain the base oil and several lubricant additives, which are used to control deposits, wear corrosion, friction, oxidation, rust, etc. The principal compounds which are present in diesel engine oils for today's engines include ashless dispersants, metallic detergents, oxidation inhibitors, rust inhibitors, anti-wear additives, and oil-soluble polymers. Formulation of lubrication chemistry will go a long way to affect the nature of soot generated in engines. The basestock group used, additive properties and nature of their

degradation will determine nature of soot formed in diesel engines. Different formulation of soot will produce different nature of soot from the different additive and basestock composition. Different types of base stock used in modern engine oil formulation are described in Table 2.1 below.

Table 2 2-1 API Base Stock Categories [37]

API BASE OIL CATEGORIES				
	Base Oil Category	Sulfur (%)	Saturates (%)	Viscosity Index
Mineral	Group I (solvent refined)	>0.03	and/or <90	80 to 120
	Group II (hydrotreated)	<0.03	and >90	80 to 120
	Group III (hydrocracked)	<0.03	and >90	>120
Synthetic	Group IV	PAO Synthetic Lubricants		
	Group V	All other base oils not included in Groups I, II, III or IV		

2.3.1 Basestock

Base Oils for lubricant formulations are usually mineral (Petroleum) or Synthetic, with vegetable Oils also becoming common in some specialized applications. Synthetics are made from petroleum or vegetable feedstocks and are made to be long lasting. The API has a classification for based Oils which are categorized into five categories (API 1509). The first three groups are refined from crude oil and are generally mineral oils, Group IV are full synthetics (Polyalphaolefin) oils, and Group V is all other

base oils not belonging to group I to IV. Basestock generally serves as the platform on which additives ride.

In recent years, these categories have been informally subdivided into Group I+, Group II+, Group III+. Based on sources, base oil are classified as:

- Paraffinic (Neutral Oils)- Derived from Paraffinic crude stocks
- Naphthenic (Pale Oils)- Derived from Naphthenic Crude Stocks
- Synthetics- Derived from Chemical Reactions or Highly Refined Paraffinic Stocks
 - Traditional Synthetics are Poly Alpha Olefins (PAO's), Esters, etc
 - Hydro processed Synthetics are Group III Base Oils derived from Crude
 - GTL Synthetics are derived from Natural Gas

2.3.1.1 Group I Base Oil

Oils are classified as group I based on its less than 90 percent saturates quantity, greater than 0.03 percent sulfur and a viscosity-index range of 80 to 120. Oil temperature compatibility is usually within the range of 32 to 150 °F. The base oil type of this group is produced by the simple solvent-refining method which makes them cheap and readily available.

2.3.1.2 Group II Base Oil

Oils in group II have more than 90 percent saturates, less than 0.03 percent sulfur and a viscosity index of 80 to 120. They are produced by hydrocracking process and more complex than Group I base Oil production. Group II base oil has better antioxidant characteristics from its saturated hydrocarbon molecules chains. They are clear Oils than Group I base Oils but cost more.

2.3.1.3 Group III Base Oils

Oils in Group III have greater than 90 percent saturates, less than 0.03% sulfur and viscosity index above 120. The Oils are refined from series of hydrocracking process under higher heat and pressure with the longer process ensuring purer base oil. The Oils are made from crude Oil but are sometimes referred to as crude hydrocarbon. These Oils are more expensive from the series of production process but are becoming more prevalent.

2.3.1.4 Group IV Base Oils

Group IV base oils are synthetics made from synthesizing process. They are polyalphaolefins (PAOs) and have much broader temperature range that is able to withstand extremely cold and high heat conditions. Synthetics are built from simpler substances to give desired oil properties required. Polyalphaolefins are all hydrocarbon structures, and contains no

sulfur, phosphorus or metals. They are wax-free with low pour points usually below -40°F (-40°C) with Viscosity grades ranging from 2 to 100 cSt and Viscosity index for almost all grades exceeding 140.

2.3.1.5 Group V Base Oils

All other Oils not classified in group I – IV are classified as Group V. They include silicone, phosphate ester, polyalkylene glycol (PAG), polyester, biolubes, etc. Basestock in this group are sometimes mixed with basestock from other groups for enhanced properties. Esters are common examples of base V oils used to enhance properties of other existing base oils. Esters will withstand higher operating temperatures and will provide superior detergency compared to synthetic base oil which will make it last extended hours of use.

2.3.2 *Lubricant Additives*

Lubricants play an important role in reducing wear and friction in Automobile engines, and potentially increase efficiency. The base Oil acts as transport upon which the additives ride. Additives are used to supplement the limitations of lubricants and to enhance the performance of base oils. The base oils as main lubricants must be viscous enough to maintain a lubricant film under operating conditions; they should be as fluid as possible to remove heat and to avoid power loss due to viscous drag. It should also be stable under thermal and oxidative stresses, have

low volatility and possess some ability to control friction and wear by itself. Base Oils used should have ability to dissolve the additives but to be inert toward metal surfaces, rubber seals and gaskets [38]. Lubricant additives are added to oils in small amounts to improve the lubricating capacity and durability of the oil. Each lubricant additive has its own primary purpose. Table 2.2 on page 29 shows each additive's role for the overall mechanism of lubrication in oils with common examples.

Table 2-2 Lubricant Additives, Tasks and Examples [39]

Lubricant Additive	Main Task	Examples
Antioxidants	Preventing peroxides and stabilizing radicals (enhancing oxidation stability of oil)	Alkylated Diphenol Amine, Hindered Phenol
Antiwear Additives	Preventing wear in mild condition	Zinc Dialkyl Dithiophosphate (ZDDP), Tricresylphosphate (TCP)
Extreme Pressure Additives	Preventing wear in severe condition	Dibenzylidissulphide, Sulfurized Derivatives, Molybdenum Disulphide
Adsorption or Boundary Additives	Preventing slip-stick phenomena	Sulphurized Fatty Acid Derivatives, Phosphonic Acids
Detergents	Protecting oils against sludge formation	Calcium Sulfonate
Dispersants	Dispersing particles	Polyisobutylene (PIB) Succinimide
Corrosion and Rust Inhibitors	Preventing corrosion or rust of engine surface and bearings	Barium Sulfonates, Calcium Phenates
Viscosity Index Improvers	Reducing difference in viscosities at different temperatures	Olefin Co-polymers, Polymethacrylates
Friction Modifiers	Performing lower friction behavior on surfaces	Organomolybdenum, Molybdenum Dithiocarbonates
Foam Inhibitors	Retarding the formation of foam in oil	Hydrogen and silicon compounds
Pour Point Depressants	Preventing the generation of wax crystals at low temperatures	Polymethacrylates

2.3.2.1 Detergent and Dispersants

Detergent and dispersants control deposits and wear in oil. They keep sludge, carbon and other deposit precursors derived from partial oxidation of the fuel or lubricating oil suspended in the oil. There are

various detergents and dispersants which have been used for the control of deposits. The earliest of these are phenate and sulfonate metallic detergents, and more recently ashless dispersants such as the succinimides and the polymeric dispersant viscosity index improver (oil-soluble polymers)

Ashless dispersants are used in modern oil formulations for control of deposits. A common feature of the ashless dispersant structure is an oil solubilizing tail, usually based on polybutene of 700 - 3000 molecular weight, and a polar group usually derived from a polyamine or polyol. The linking of the polar head to the oil solubilizing tail is accomplished by diverse chemical reactions. The three main ashless dispersant types which are in use today are succinimides, Succinate esters and Alkylphenol amines. The succinimide dispersants represents the largest volume of ashless dispersant manufactured.

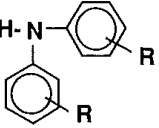
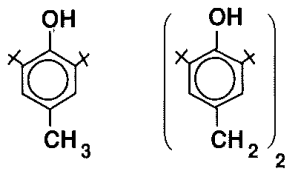
Calcium sulfonate detergent is the most widely used metallic detergent additives. They are produced from oil soluble Mahogany sulfonic acids obtained in the refining of lubricating oils and by sulfonation of synthetic alkylbenzenes. The alkyl solubilizing group is approximately C_{18} to C_{20} or higher. The molecular weight of the sulfonic acid is normally 450 or higher to provide adequate oil solubility. In addition to the metallic detergent such as the neutral sulfonate, modern oil formulations contain

basic metal which provide some detergency. Their main function is to neutralize acid and prevent corrosion from acids attack. Sulfuric acids results from oxidation of sulfur in diesel fuels. Overbased sulfonate, while providing base for neutralizing of acid, also acts as a pro-oxidant and can degrade anti-oxidant performance. Addition of overbased phenate does not degrade the antioxidant performance of other inhibitors and, in fact in some formulations will increase oxidation inhibition

2.3.2.2 Oxidation Inhibitors

The most important classes of oxidation inhibitors are Zinc Dialkyl Dithiophosphates (ZDDP), Aromatic Amines, Hindered Phenols, Sulfurized Products. The most commercially important class is the ZnDTPs which are used in most diesel and industrial oils. In certain special applications, including natural gas engines and turbine oil, ashless oxidation inhibitors such as hindered phenolics, aromatic amines, and organic sulfur compounds are used instead of the ZnDTPs. Types of Oxidation inhibitors and their uses is described in Table 2.3 on page 32 below.

Table 2-3 Major Classes of Oxidation Inhibitors and Their Applications

NAME	TYPICAL	APPLICATION
Zinc Dithiophosphates	$\left(\begin{array}{c} \text{S} \\ \parallel \\ \text{RO} \text{---} \text{P} \text{---} \text{S} \\ \diagup \quad \diagdown \\ \text{RO} \end{array} \right)_2 \text{Zn}$	Industrial, Diesel, and Gasoline Engine Oils
Amines		Industrial Oils Gasoline Engine Oils
Sulfides	$\text{R-S}_x\text{-R-S-R}$	Industrial and Railroad Oils
Phenols		Industrial and Railroad Oils

2.3.2.3 Antiwear Additives

Extreme pressure (EP) and Antiwear additives are used to form a protective film on metal surfaces. Practically all modern engine oil formulations rely on the use of ZnDTP for the control, not only of oxidation, but also of corrosion and EP wear. In certain special applications, other phosphorus, sulfur and chlorine containing compounds are used. ZnDTP is the oxidation and wear inhibitor of choice, wherever the application allows on a cost performance basis. This class of additive is normally prepared by the reaction of an alcohol or an alkyl phenol with phosphorus pentasulfide to produce an acid which is neutralized with zinc oxide to

yield a zinc salt, ZnDTP. Since the alkyl and aryl ZnDTPs provide a different balance of functions, a single ZnDTP or a mixture of ZnDTPs is used in modern oil formulations, depending upon service requirement.

2.4 Role of Engine Age in Soot Formation

Two separate factors are basically identified to affect nature of soot formed in oil as engine age increases. It is assumed that as diesel engine ages and accumulates high mileage, the diesel engine produce higher emissions which are recirculated into the engine through the Exhaust Gas Recirculation System (EGR). These emissions come in the form of CO, NO_x and Particulate Matters and their thermo oxidative reaction with degraded composition of lubricant chemistries are determinant of nature of soot generated in diesel engine. A 10 year old diesel engine will for example produce more emissions than a new engine and will be believed to generate soot with more abrasive composition.

The combustion process can also influence soot characteristics, with combustion efficiency changing in different engine ages. Vander Wal and Tomasek [40] using a high flow reactor found that the nanostructure of soot depends upon its formation conditions, such as temperature and residence time. Zhu et al. [41] found that the crystallite degree of soot increases with engine load and exhaust temperature. In addition, it is also found that soot particle size tends to decrease when the exhaust

temperature increases due to the particle oxidation at high temperature. The combustion process can also change with different engine technology that change will change in diesel engine across different engine age range. With improvement in engine technology; NO_x, CO and PM produced in diesel engines has been seen to reduce [42]. From the EPA emission standard used for certifying engines, a 1998 model year heavy-duty engine (used in a bus) would produce less NO_x by a factor of 2.5 and less PM by a factor of 12 relative to a 1988 model year engine. Effect of technology level on vehicle emission in engines was also determined by comparing test data from two Detroit Diesel 6V-92TA engines. The newer engine made five years after the older engine produced emissions for NO_x and CO that were lower than those of the older engine. A reduction of 71% CO and 45% PM was observed with only increase in the HC composition produced by a factor of 11%. Comparison of the two engines showed that majority of the exhaust gas constituents have reduced over five years period. Exhaust Gas composition changes for two engines due to change in engine technology is shown in Table 2.4 on page 35 below.

Table 2-4 Exhaust Gas Comparison in Different Engine Ages [42]

Vehicle	1	2	
Type	Transit bus	Transit bus	
Model Year	1988	1993	
Transmission	3-speed auto.	4-speed auto.	
Test Weight	15,297 kg	15,048 kg	
Test Cycle	CBD	CBD	
Test Date	June 4, 1994	March 16, 1994	
Odometer	287,747 km	171,794 km	
			Difference
NO_x (g/km)	23.7	15.5	-35 %
CO (g/km)	13.8	4.00	-71 %
HC (g/km)	1.99	2.20	+11 %
PM (g/km)	1.92	1.06	-45 %
Fuel Consumption (L/100 km)	75.6	84.0	+11 %

Technology advances that have improved exhaust gas products over years include improved engine combustion chamber design and introduction of variable geometry turbochargers.

2.5 Soot Formation in EGR Diesel Engine

Soot is in the form of necklace-like agglomerates of around 100 nm size. They are composed of collections of smaller, basic particle units that are spherical or nearly spherical in shape. Soot clusters may contain as many as 4000 spherules. The size of the spherules varies in diameter from 10–80 nm, but mostly lies between 15–50 nm. The surface of the

spherules has adhering hydrocarbon material and inorganic material (mostly sulfates). The inorganic materials are main sources of abrasives that impacts wear.

Exhaust gas recirculation (EGR) has proved to be an improved method of reducing NO_x emission and is mostly practically implemented in most diesel engines worldwide. The EGR however leads to increase in soot recirculation because of soot- NO_x trade- off. The EGR generated soot leads to several problems in engines like oil thickening, oil degradation, and enhanced engine wear, etc. Singh et al [9] investigated the effect of EGR on characteristics of lubricating oil with time of its usage; he found higher soot loading with deposits of graphitic carbon and ionic metal compounds on vital parts of the engine operating with EGR. Experimental investigations by Wade [43] and Needham et al [44] has also shown that particulate matter (PM) emission increases consistently as the rate of EGR increases.

$$EG\% = \frac{V_{EGR}}{[V_{AIR} + V_{EGR}]} \times 100$$

Where, V_{EGR} = volume of recirculating exhaust gas, V_{AIR} = volume of fresh air entered into intake manifold

Majority of particulate matters (PM) originates with soot particles which are formed in fuel rich regions of burning diesel jets. The fundamentals of soot formation and oxidation in compression ignition

diesel engine had been described by Smith [45], Haynes and Wagner [46], and Glassman [47]. Work by these authors gives a background to the physical processes involved in the formation and oxidation of soot. Soot is a solid substance consisting of roughly eight parts carbon and one part hydrogen. Newly formed particles has the highest hydrogen content with C/H ratio as low as one, but as soot matures, the hydrogen content decreases. C Zhou, Zhi- Qiang et al [48] has reported soot to have a density of $1.84 \pm 0.1 \text{ g/cm}^3$ and result by other authors fall in range. Soot is formed from unburnt fuel which nucleates from the vapor phase to a solid- phase in fuel rich regions at elevated temperatures. Hydrocarbon or other available molecules may condense on, or be absorbed by soot depending on the surrounding conditions.

Particulate matter (PM) is formed which is a combination of soot and other liquid- or solid- phase materials that are collected when product exhaust gases pass through a filter. The fraction of particulate which is soot is often estimated by finding the insoluble portion of the particulate. The portion of soot in PM is estimated by finding insoluble portion of the PM, this may vary but typically higher than 50% of the total PM. The other constituent in the PM will include unburned/ partially burned fuel/ lubricant oil, bound water, wear metals and fuel derived sulfate [47]

2.5.1 Soot processes

The transformation of liquid- or vapor- phase hydrocarbon to solid soot particles, and possibly back to gas- phase products involves six commonly identified processes: Pyrolysis, Nucleation, Surface growth, Coalescence and Agglomeration, and Oxidation. The sixth process, which is oxidation, converts hydrocarbons to CO, CO₂ and H₂O at any point in the process. 'Net soot formation' describes the overall combination of soot formation and oxidation.

2.5.1.1 Oxidation

This involves the conversion of carbon or hydrocarbon to combustion products. Oxidation process can be anytime during the soot formation process from pyrolysis to agglomeration. The most active oxidation specie depends on the process and state of oxidation at the time. Glassman [47] states that soot particle oxidation occur when the temperature is higher than 1300 K. Oxidation of small particles is considered a two stage process. First, chemical attachment of oxygen to the surface (absorption), and second, desorption of oxygen with attached fuel component from the surface as a product [47]. Bartok and Sarofim [49] believe that OH is most likely to dominate soot oxidation under fuel-rich and stoichiometric conditions; soot is oxidized by both OH and O₂. Haynes and Wagner [46] state that about 10- 20% of all OH collisions with soot are effective at gasifying a carbon atom

2.5.1.2 Fuel pyrolysis

This is the process of alteration of molecular structure of organic compounds (Fuel) at very high temperatures without significant oxidation even at the presence of oxygen species. These reactions are endothermic and temperature dependent [45] and are also a function of concentration. The process results in production of species which are precursors or building block for soot. The soot precursor formation is competitive between rate of pure fuel pyrolysis and precursor oxidation by hydroxyl radical, OH. Both pyrolysis and oxidation rate increases with temperature, but the oxidation rate increases faster. Radical diffusion is necessary for diffusion flames, especially H which accelerates pyrolysis when diffused into the fuel- rich zone. Smith [45] commented that small amounts of O, O₂, OH is expected to accelerate pyrolysis since many of the reaction takes place by means of free radicals mechanism.

All fuels undergo pyrolysis and produce essentially the same specie: Unsaturated hydrocarbons, polyacetylenes, polycyclic aromatic hydrocarbons (PAH) and most especially acetylene. Smith [45] adds that in the presence of sufficient O and OH, some acetylene is oxidized to relatively inert products. Haynes and Wagner [46] listed C₂H₂, C₂H₄, CH₄, C₃H₆ and benzene as typical pyrolysis products in laminar diffusion flames. Radicals are formed during pyrolysis and Glassman [47] in his

work has shown that larger molecules increase the radical pool size. Fig 2.5 below shows a schematic of sequence of the first five processes of soot formation.

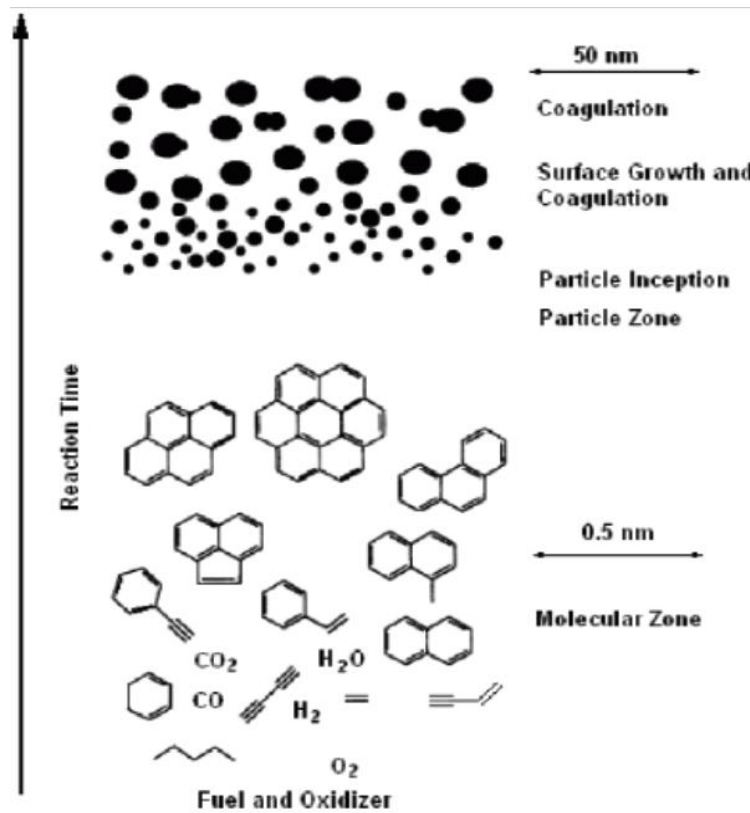


Fig 2-5 Schematic path leading to soot formation [47]

2.5.1.3 Nucleation

This is a soot particle inception process which involves formation of particles from gas-phase reactants. Bartok and Sarofim [49] found the smallest identifiable solid particles in luminous flames to have diameters in the 1.5 - 2.0 nm range; these particles are referred to as nuclei. They

further suggested the particle inception process to probably consist of radical additions of small, probably aliphatic hydrocarbons to larger aromatic molecules. Reports on particle nucleation temperatures may vary from 1300 to 1600 K. The particle nuclei do not contribute significantly to the total mass, but do have a significant influence on the mass added later, because they provide sites for surface growth. Nucleation is spatially restricted to regions near the primary reaction zone where the temperatures, radicals, and ion concentrations are the highest in both premixed and diffusion flames [49]

In the investigation of nucleation of soot by Glassman [47], he found that a fuel-independent soot formation mechanism may exist, which has alternate routes to immediate species. The routes are affected by temperature and initial fuel type. Propensity for soot is determined by the initial rate of formation of the first and second ring structures. The process of growth to larger aromatic ring structures leading to soot nucleation and growth are similar for all fuels and faster for subsequent rings than the first. The relatively slow formation of the initial aromatic aromatic rings controls the incipient soot formation rate, which determines amount of soot formed. Two propynyl radicals, C_3H_3 are likely to form the first ring. The aromatic ring is believed to add alkyl groups turning into a PAH structure which grows in the presence of acetylene and other vapor phase soot

precursors. At some point, PAH becomes large enough to develop into particle nuclei, which at this point contains large amount of hydrogen. Haynes and Wagner [46] notes that ring-rupture slows down the rate of soot formation and reduces final yield

Bryce et al [50] observed three soot nucleation routes viz:

- (1) Cyclization of chain molecules into ring structures. This is found when acetylene molecules combine to form a benzene ring
- (2) A direct path where aromatic rings dehydrogenate at low temperature and form polycyclics
- (3) Breakup and recrystallization of rings at higher temperatures

2.5.1.4 Surface Growth

This is the addition of mass to the surface of a nucleated soot particle. There are no clear distinction between the end of a nucleation and the beginning of surface growth, in reality both process are concurrent. During the process, hot reactive surface of soot particles readily accepts gas- phase hydrocarbons which are mostly acetylenes. This leads to an increase in soot mass, while the number of particles remains constant. Surface growth continues as the particles move away from the primary reaction zone into cooler and less reactive regions, even where hydrocarbon concentrations are below the soot inception limits [43]. The majority of the soot mass is added during surface growth and thus,

the residence time of the surface growth process has a large influence on the total soot mass or soot volume fraction. Surface growth rate are higher for small particles than for larger particles because small particles have more reactive radical sites [46].

2.5.1.5 Coalescence and Agglomeration

These two processes are both combination processes for primary soot particles. Coalescence (also called coagulation) occur when particles collide and coalesce, decreasing number of primary soot particles and holding a constant combined mass for the combined particles. During the coalescence, two or more roughly spherically shaped particles combine to form a single spherically shaped particle. Agglomeration occurs when individual or primary particles stick together to form large groups of primary particles, and then the primary particles maintain their shape. Typically, the combined soot particles form chain- like structures, but clumping of particles has also been observed in some cases. Schematic of primary soot particle is shown in Fig 2.6 on page 44 below.

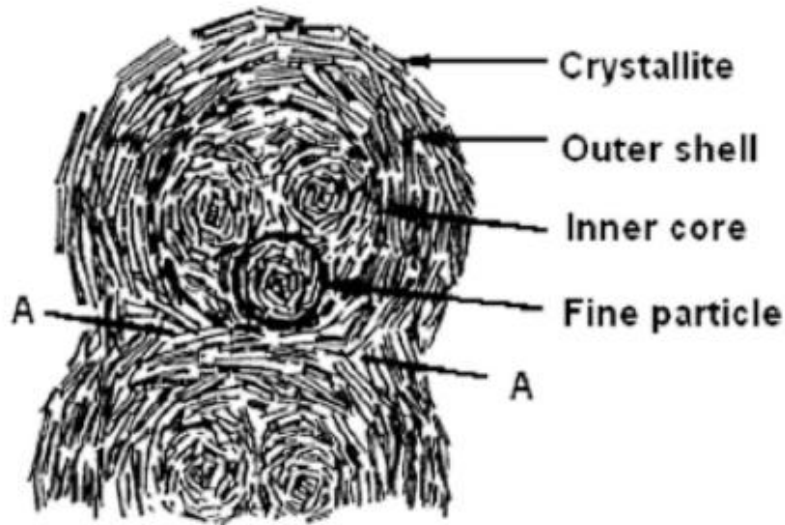


Fig 2-6 Schematic of primary soot particles

EGR soot from diesel engines consists of primary particles of spherical shape which agglomerate to form long chain-like structures. The primary soot size particle size will vary depending on operating conditions, injector type and injector conditions, but most of the size observed has been in 20 - 70 nm range. In the work of Mitchell et al [51], they measured soot particle size by using a sampling probe and observed primary particle size of 20 - 50 nm with an average of 30 nm. Peck et al [52] used the optical scattering technique and reported a range of 30 - 70 nm for the primary particle diameter. In-cylinder scattering measurement by Tree and Foster [53], and Pinson and Litzinger [54] have shown result for estimates of 30 - 50 nm and 40 - 65 nm respectively. After combustion ends, soot

particles agglomerate further to form chain- like structures of 100 nm to 2 μm size.

2.5.2 Kinetic Mechanisms and Models of Soot Formation

The work of various authors has modeled formation of soot in diesel engines, but three representative models are more common, which ranges from the simple to complex. Most commonly used model uses one global rate expression for soot formation and one rate expression for soot oxidation. Most commonly used models for formation soot are those of Nakanishi and Kadota [55] and Nagle and Strickland-Constable [56] respectively. Formation and oxidation are both high temperature dependent represented by Arrhenius type expressions. Rate of formation is proportional to fuel vapor concentration and oxidation increases with increasing oxygen partial pressure and increasing soot mass.

2.6 Wear Induced Mechanism of Soot

Work by various researchers has been carried out to understand soot induced wear mechanism and they have come up with various possible models. All the models do not necessarily agree but they give a better understanding of the subject matter. Rounds [19,57-59] in his four-ball wear test of soot contaminated oil came up with an idea that soot itself is not abrasive but soot preferentially adsorb the antiwear additive, and the adsorption of antiwear additive was the reason for wear in the engine. This

was the plausible reason he provided for the wear taking place in a diesel engine. He also performed hardness tests to compare soot and alumina which is a known abrasive, and disagreed with the concept that soot removed the surface coating by abrasive action, since the hardness of soot is lower than the hardness of alumina. He believes that engine load and EGR have a large effect on the pro-wear characteristics of soot. Several authors have disputed the adsorption theory proposed by Rounds.

Nagai et al. [21] performed tests on valve train to study soot induced wear. They concluded that the wear of cam noses and rocker arm tips was found to increase significantly with the increase in EGR rate. The drain oil analysis at the end of each EGR test run indicated evidence of elements such as zinc and phosphorous, which contradicted the adsorption theory proposed by Rounds. They also carried out tests using the four-ball wear tester and it was concluded that, soot strips off the anti-wear film formed on lubricated metal surface and that subsequent metallic contact accelerated the wear process. They also concluded that soot might incorporate very hard particle from thermo oxidation of the wear metal and oil additives under the high-pressure conditions and might be abrasive to the metal.

Berbeizer et al. [60] evaluated special test blends of different types of commercial carbon black and concluded that bore polishing is

influenced more by the size, nature, and concentration of carbon black rather than by the products of oil degradation. They suggested that decreasing the amount of carbon black reaching the piston or suspension in the lubricant could reduce bore polishing and that bore polishing can be reduced by reducing the elementary carbon black particles, or by completely changing the microstructure of graphitized carbon. They also suggested that abrasive wear is not the sole factor contributing to increased wear, but two other phenomena also play important roles; decreased surface coverage rate by ZDDP molecules due to physical adsorption of carbon black on the surface and subsequent modification of physical and mechanical properties of the reaction film by the introduction of carbon in their composition.

Kim et al. [61] investigated the effects of oil formulations on diesel engine valve train wear and concluded that laboratory wear tests could properly differentiate the anti-wear performance provided by different engine oils. The anti-wear properties of the diesel engine oil could be improved by increasing the ZDDP concentration. They suggested that improved engine oil specifications, as the existing diesel engine oil at the time was not adequate to protect every engine. Chinas-Castillo and Spikes [62] studied the behavior of diluted soot containing oils in lubricated contacts using carbon black colloid, lampblack colloid, and used

engine oil. Ultra-thin film interferometry and image analysis techniques showed that soot colloid particles are entrained in the lubricated contact inlets which can influence the friction and wear characteristics of the base stock. Their study showed that the entrainment of soot particles occur at slow speeds, affecting the film characteristics of clean engine oils and the process is more pronounced at high temperatures.

Needelman and Madhavan [63] concluded that contamination of the lube oil causes wear of engine components and also suggested that, a special relationship is present between the size of the contaminant particles and the thickness of dynamic oil films. The contaminant particles larger than the oil film cause wear of engine components by making simultaneous contact with both the surfaces. Cadman and Johnson [64] analyzed used oil samples for wear debris using analytical ferrography technique. Result of a 15% EGR in their test showed significant increase in the concentration of the wear particles ten times higher than normal baseline levels, which made them to conclude that soot acts as an abrasive to remove the anti-wear surface coating provided by the additives in the lubricant. Corso and Adamo [65,66] suggested that soot contaminants interact with the adsorption/ chemisorption mechanism of ZDDP on metal surfaces causing a transition from anti-wear Fe_3O_4 to pro-

wear FeO aided by the soot in the lubricant which prevents access of oxygen to the metal surfaces.

Akiyama et al. [67] believes that cylinder wear of diesel engine equipped with EGR increases at low temperatures and suggested that the abnormal wear may be due to corrosion of cast iron caused by formation of sulfuric acid from reaction of condensed water with combustion SO_x. This model may however not be a primary reason for engine wear as the sulfur content in diesel engines has been reduced to 0.05 wt.%. Gautam et al. [5,68] investigated the effects of soot contaminated engine oil on three-body wear. The effect of Phosphorus, dispersant and sulfonate levels as oil additives were tested and they concluded that there is an interaction between oil additives and soot in reducing the oil's anti-wear properties. They also concluded that wear increases with higher soot concentration and decreases with higher phosphorous concentration. They performed tests on the ball-on-flat-disk setup with soot and alumina comparing their wear ratios, and they concluded that abrasion could be the major mechanism involved in the diesel engine wear. They [5] also investigated the effects of base stock, dispersant level, and ZDDP level on three-body wear. Their result indicated that the oil's anti-wear properties were reduced as a result of soot. The statistical analysis led to the conclusion that base stock and dispersant levels were significant on oil's

wear performance, while the effect of ZDDP was negligible within the range of concentrations tested. Ball-on-flat-disk tests showed that the wear scar diameter as a result of soot was similar to that due to alumina indicating that the wear due to soot is abrasive in nature. EDAX (energy dispersive X-ray analysis) tests performed on soot samples showed that there was no adsorption of anti-wear agents by soot

2.7 Field based Condition Monitoring of Soot

The ASTM D7686 - 11 is the currently used standard for field based condition monitoring of soot in- service petroleum and hydrocarbon based lubricants. The standard is applicable to oils having soot levels under 12%, a level under which EGR soot usually falls. The standard is intended for field test only and its objective is to help diagnose the operational condition of the engine based on measuring the level of soot in the oil, this standard measures only soot content in lubricant oil and there are other methods for more complex analysis for all degradation products in the oils. The test method used filter based infrared technology to acquire spectral data for measuring soot for in- service used lubricant samples employing a fixed - filter IR instrument. Calibration is done against prepared soot standard which is usually a new unused lubricant oil sample.

The ASTM E2412 - 10 is also used for more complex condition monitoring. It monitors additive depletion, contaminant build- up, and base

stock degradation in normal machinery operation. Contaminants monitored include soot, water, ethylene glycol, fuels and incorrect oil. Oxidation, nitration and sulfonation of base stock can also be monitored as evidence of degradation. The practice is based on trending and distribution response analysis from mid-Infrared absorption measurements. Interpretation parameter for this standard allows a universal comparison of measurement and data from FTIR spectrometry by different operators. The data generated from this practice is used in conjunction with other testing methods to get a full view of the elemental analysis of the wear metal levels. Illustration of the ASTM standard for measurement of Diesel soot in used lubricant using Trend Analysis in FTIR Spectroscopy is shown in Fig 2.7 on page 52 below.

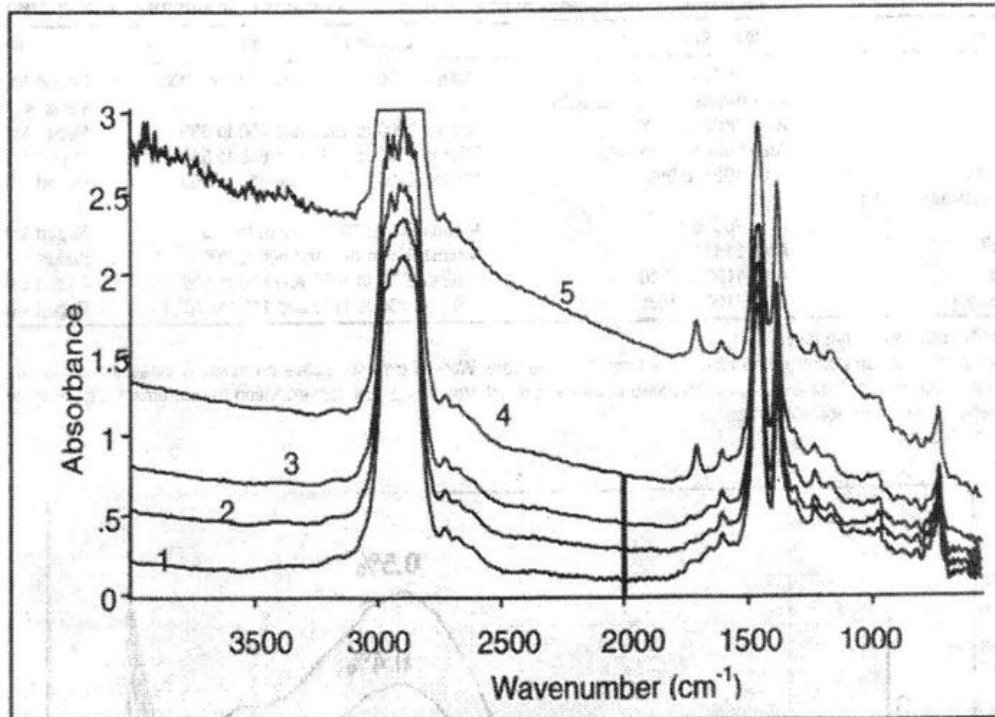


Fig 2-7 ASTM standard measurement of Diesel soot in used lubricant using Trend Analysis in FTIR spectroscopy [69]

Fig. 2 7 shows the mid- infrared measurement of soot at baseline offset at 2000 cm^{-1} . The spectra shows low, intermediate, high, and very high soot loading levels (increasing levels from 1 through 5). High water levels can interfere with the measurement of soot in internal combustion engine crankcase. However, this only become significant when water level is in the order of $> 5\%$ (50 000 ppm), which will immediately condemn the lubricant and require immediate maintenance action irrespective of any other indicators.

Soot does not have a specific frequency of absorption in the infrared spectrum, but a change in concentration will cause a shift in the in the baseline of the spectrum due to absorption and scattering of light. Since there are no other spectral features in the region at 1950 cm^{-1} , spectra shift at this area is used to assess the level of soot in the sample as can be seen above. The baseline absorbance is measured prior to reference oil subtraction. The baseline shift caused by soot is affected by the amount of soot present and the effective particle size. The amount of soot and effective particle size is determined by nature of combustion system, and dispersant in the oil. This makes it inherent to establish engine types and lubricants of interest for which test is applied.

Chapter 3

EGR Soot from Mineral based Diesel Oil

This chapter discusses the role of lubricant chemistry from mineral base stock and role of engine age on the nature of EGR soot generated in diesel engine of different ages. Mineral based lubricants are classified in the API Base Oil categories of Group I to III and usually contain about 0.03 or greater percentage of Sulphur. The presence of sulfur in base stock can easily lead to other corrosive reactions which are catalysts for corrosive and other forms of wear in Diesel engines; this will be a determinant to formation of other crystalline nano particles in diesel soot which will induce wear. Degradation of other lubricant additives used in formulation of lubricant chemistry can also be a determinant of contribution of lubricant chemistry to nature of EGR soot formed under engine operating conditions. Efficiency in combustion capacity of diesel engine with age will change and this is studied to understand its contributions to nature of EGR soot generated in engines of different engine ages. Factors such as change in engine technologies overtime will also affect combustion with different diesel engines and hence nature of soot generated. The discussion is as seen for an Exhaust Gas Recirculation (EGR) diesel engine.

3.1 Introduction

EGR soot samples analyzed was extracted from SAE 15W-40 type Mineral based used Diesel Oil of approximately 50,000 miles of oil change from Detroit DD15 engines. The used Oil was acquired from Speedco Oil change facility, Indianapolis, IN. The Oil type is from a known diesel Oil manufacturer with known Oil properties. Three samples of different engine ages are analyzed labeled SP A, SP B and SP C of 54,000 miles, 247,000 miles, and 306,000 miles respectively to study the role of engine age and lubricant chemistry on nature of EGR soot formed.

3.2 Soot Extraction

The EGR soot is formed from recirculated particulate matter (PM), NO_x and CO combustion product in Diesel Oil. EGR soot sample is not readily obtained, but is extracted from used Oil from a series of extraction processes to get sample for further analysis. The extraction and handling processes is as described.

3.2.1 *Oil Dissolution*

Used diesel oil is mixed with hexane as solvent in approximately 50 wt % dilution. A proper mix of used oil and hexane is ensured by heating together in an ultrasonic heater for about 10 minutes. A 1000ml glass tube is recommended to achieve extraction of more quantity of soot at a time; the weight of the glass tube is noted, and weight of used oil sample and

hexane at each mix should also be noted. Weighted dissolved used oil in hexane is shown in Fig 3.1 below. Noting the quantity/ weight of used oil sample and comparing with quantity/ weight of soot obtained can give an idea of % soot concentration of used oil sample (though % soot concentration obtained from extraction will not give an exact concentration of soot in used oil because some of the soot will have been lost during the extraction).



Fig 3-1 Weighted used oil sample

3.2.2 *Centrifuging Process*

After ensuring a proper mix of the used oil sample with about 50% quantity of hexane, the mixture was centrifuged in a SORVALL SS 34 centrifuge which accommodated up to eight (8) numbers of 32mm x 100mm centrifuge bottles at a time. All the centrifuge bottles were filled to

the same volume which ensured a proper balancing of the centrifuge disc. To fill the centrifuge bottle, a standard volume of oil sample mixture was measured for all the bottles using a measuring cylinder. Fig 3.2 below shows a typical centrifuge and centrifuge bottle holder (disc).

After balancing of centrifuge bottles in the disc, centrifuge parameters were set for operations to give optimal soot sediment. Operating conditions for optimal extraction was set at 12000 rpm for 2 hours duration. The supernatant from each bottle were carefully removed into a glass tube to remove the soot particles settled at the bottom of the tube. Solid soot particle settled at the bottom of the bottle which can be scooped out with a spatula. The process is repeated for all centrifuge bottles to extract soot particles.



(a) Sorvall SS34 centrifuge (b) Centrifuge bottle holder

3.2.3 Soxhlet Process

Soot obtained from the centrifuging is not clean enough and still contains some oil in it, and soot samples were further cleaned in a soxhletting process. The soxhletting process removed oil still attached to soot particles to give oil-free soot. The process was carried out for 48 hours period. Cleaning was achieved by heating up hexane to boiling point and leaving it to condense into the soot sample to wash out oil through the pores of the thimbles in which soot is placed; thimbles size of 8 μ m pore size was used in the process. The whole soxhletting process was carried out in an experimental fume hood to ensure safety precautions, as seen in Fig 3.3 below.

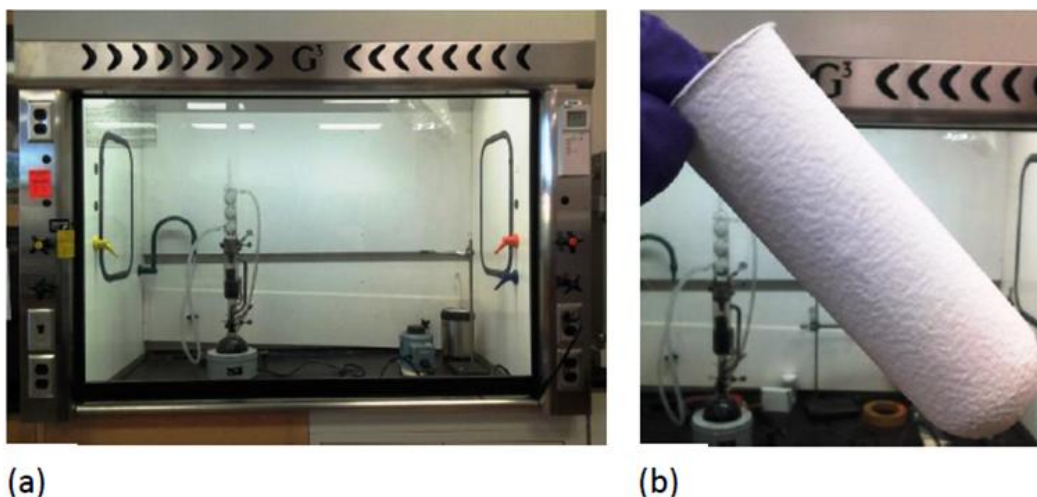


Fig 3-3 Soxhlet setup in an experimental fume hood (b) 8 um cellulose thimble

3.2.4 Drying and Storage

On completion of soxhletting, the thimble is removed from the Soxhlet and left in the fume hood for soot to dry up. Dried soot should be carefully removed from the thimble to maximize extraction and minimize waste. The dried soot is ground to fine powder using an experimental mortar and pestle. The final weight of soot is obtained using the weigh balance and recorded before storage in a glass tube properly closed in a dry environment. The soot samples are then stored for further analysis.

3.3 Elemental Composition Studies of Used Oil Samples

Elemental Analysis of used Diesel Oil sample shows the level of contamination from wear metals, lubricant degradation and external contaminants. Contaminations and degraded lubricant chemistries in diesel oil under the high operating conditions of diesel engines are believed to result in formation of crystalline nano particles within soot, which are abrasive and are causes of wear in EGR Diesel Engine. Table 3.1 on page 60 below shows detail of chemical analysis for the used oil samples from which studied EGR soot was extracted.

Table 3-1 Spectrochemical Analysis of mineral based SAE 15-40 used oil samples

SAMPLE	ENGINE AGE	ELEMENTAL COMPOSITION															
		METAL (ppm)							CONTAMINANTS (ppm)		ADDITIVES (ppm)						
		Fe	Cr	Pb	Cu	Sn	Al	Ni	K	Na	Mg	B	Ca	P	Zn	Mo	Si
		Contributions from equipment wear							From engine coolant	From detergents			From ZDDP antiwear	Friction Modifier	Anti-foam additive		
SP A	54,000	61	5	4	432	8	68	2	221	13	791	83	2393	1041	2104	112	17
SP B	246,513	38	3	2	16	4	18	1	32	18	1149	13	2644	1034	2017	55	15
SP C	306,000	42	2	2	12	4	17	1	507	676	1355	15	2395	1042	2059	133	15

The spectrochemical analysis measures different metals in parts per million (ppm) that represent equipment wear, lubricant additives and system contaminants. The ICP - AES (Inductively coupled plasma atomic emission spectroscopy) is used to carry out the test observing wear metals and other contaminants in used lubricants.

3.3.1 Spectrochemical Analysis for Wear Metals

Abnormal wear is indicated by combination of metals and/or reaction of wear metals with degraded lubrication chemistries. There could also be other possible secondary sources. The interpretation of sources of elements in the stoichiometric analysis of the used engine oil lubricant sample is given in tables 3 – 2 to 3. - 4 in pages 61 – 62 below.

Table 3-2 Spectrochemical Analysis of Wear Metals

ELEMENT	SOURCE
Iron (Fe)	Major component Material in Equipment manufacturing, housing/ blocks, bushing, bearing, shafts, valves, Rings, Rusts, etc
Chromium (Cr)	Cylinder Liners and Guides, Bushings, Bearing, Shafts, Valves, Rods, Rings, Hydraulic Cylinders
Lead (Pb)	Bearing/ Bushings, Thrust Plates, Washers
Copper (Cu)	Bearings/Bushings, Thrust Plates, Washers, Oil cooler, Pumps, Disc/ Disc Lining
Tin (Sn)	Bearings/Bushings, Pumps, Motors, Compressor, Piston, Piston skirt overlay
Aluminum (Al)	Piston, Bearings/Bushings, Thrust washers, Rings, Housing/blocks, Oil cooler, Cylinders and Cylinders Guides, Engine aftercooler
Nickel (Ni)	Gears, shafts, Rings, Valve Trains, Bearings/Bushings, Pumps

Table 3-3 Spectrochemical Analyses of Lubricant Additives

ELEMENT	SOURCES
Boron (B)	Extreme pressure additive, Detergency
Calcium (Ca)	Detergency, Alkalinity Reserve (Contributes to base number)
Molybdenum (Mo)	Extreme Pressure Additive, Lubricity Additive
Phosphorus (P)	Antiwear when present with Zinc, Extreme Pressure Additive, Friction modifier
Zinc (Zn)	Antiwear when present with Phosphorus, Antioxidant, Anticorrosive
Silicon (Si)	Anti-foam Additive

Table3-4 Spectrochemical Analysis of Contaminants

ELEMENT	SOURCE
Potassium (K)	Engine coolant, aftercooler brazing flux
Sodium (Na)	Engine coolant
Aluminum (Al)	Aftercooler brazing flux, Dirt if in combination with Silicon

The various elements which make up the chemistry of the used oil samples are from oil composition and possible reaction products formed under engine operating conditions. Some of the reaction products form third body nano- sized particles which are incorporated and become part of the turbostratic structure of soot. These nano - sized particles in the form of crystalline or amorphous can be source of abrasion and causes of wear in EGR engines. From the stochiochemical analysis, contributions from equipment wear, engine oil additives and contaminants are seen in

the oil. Reaction of the breakdown of additive chemistry of the oil with equipment wear product and contaminants are believed as possible result of the nano- sized crystalline and amorphous phases.

Stoichiometric result show the presence of high amount of Zinc and Phosphorus from ZDDP antiwear additive, high amount of Calcium from detergent, and high level of Iron from equipment wear. Possible reaction of these chemistries to form second phase crystalline and amorphous nano-sized abrasive particles which influence nature of soot formed in EGR engines were further studied using the Raman, HR-TEM, XRD, and XANES Spectroscopy. This will validate suggestions about formation of nano crystalline abrasive particles in EGR soot.

3.4 Raman studies of Soot samples

Raman spectroscopy has been used to investigate short-range highly disordered graphitic structures. Studies have shown that different soot types can be distinguished based on the degree of graphitization. The integrated intensity ratio of D and G (D/G) peaks is inversely proportional to microcrystalline planer size L_a that corresponds to the in - plane dimension of the single microcrystalline domain in graphite [70-72]. Information is obtained from analyzing spectral features such as intensity, peak position, line shape, and bandwidth between 800 and 2000 cm^{-1} .

3.4.1 *Experimental Procedure for Raman Studies*

The equipment used for the Raman test was the Thermo scientific DXR spectrometer which employs a diode pumped solid-state type laser as a source of illumination. The collection system is configured to use backscattered configuration. Soot samples were analyzed by visualizing using a 10x microscope objective lens. A solid-state laser of 532 nm frequency and maximum power output of 10 mW was used. A low laser power was used to avoid excessive heating of soot sample; a laser power of 1 mW was used in analyzing the Raman Spectra. Laser spot diameter was 2 μm with 25 μm slit size for the fully focused laser beam. Spectral resolution was 5 cm^{-1} at 532 nm with wavelength range from 800 cm^{-1} to 2000 cm^{-1} .

Soot thickness of about 1 mm thick was densely pressed on a glass slide to create a macroscopically smooth surface of sample as they were analyzed. The glass slide is held by a sample holder and positioned under the microscope to focus white light. On getting a focus of sample, the white beam is replaced with laser beam which acquire the Raman spectra of sample. Curve fitting for the determination of spectral parameters was performed using the OriginLab software. Curve fit was plotted from combination of various line shapes. Best fit of the curve was accomplished without fixing or limiting the range of any spectral parameters during iteration.

3.4.2 Raman Spectra Analysis by Curve Fitting

Studies have found that different types of soot could be distinguished according to their degree of graphitization [73]. In this study, the Lorentzian line shape was evaluated for the analysis and determination of spectral parameters by curve fitting. Raman spectra of carbonaceous materials exhibit a broad band at about 1500 cm^{-1} which is associated with amorphous sp^2 bonded carbon. It is noted that sp^3 bonded carbon have vibrational frequency below 1500 cm^{-1} and this observation suggests a higher probability of sp^2 bonded amorphous carbons. The best fit for the samples was achieved combination of line shape for G, D_1 and D_3 peaks. The Lorentz line shape can be used for all four G, D_1 , D_3 and D_4 peaks or the Lorentzian line shape for G, D_1 , and D_4 peak and Gaussian line shape for D_3 peak. The Lorentzian line shape was used to fit G, D_1 and D_4 , while Gaussian was used to fit D_3 at approximately 1350, 1595, 1200 and 1520 respectively in agreement with studies by Sadezky et al [73].

Studies from previous work showed that the intensity maximum at $\sim 1590\text{ cm}^{-1}$ (known as G band) is analogous to ideal graphitic vibration mode. Increased degree of disorder in the graphite structure gives rise to the peak maxima at $\sim 1350\text{ cm}^{-1}$ which corresponds to disordered graphite, this peak maximum is known as D_1 peak (Defect bands). Strong signal

intensity designated as D_3 (A) can also be noticed at $\sim 1500\text{ cm}^{-1}$ which originates from the amorphous carbon fraction of soot (organic molecules, fragments or functional groups) and/ or amorphous sp^2 bonded forms of carbon. A fourth peak D_4 in the fitting took into account disordered graphitic lattice due to polyenes and/or ionic impurities.

3.4.3 Raman Spectra Analysis of Soot Samples

Analysis of the spectra was obtained by analyzing full width half maximum (FWHM) of the peaks, peak intensity and peak position; curve fitted data and ratio of D/G peak intensity. Deconvoluted Raman peaks for samples SP A, SP B, SP C and Carbon black are shown in Fig 3.4 on page 67 and Table 3.5 on page 68 below. The ratio of I_D/I_G is related to the structural defects in the basal plane of individual graphene layers. With a high amorphous content of soot, the D_3 band broadens and differences in intensities may become significant [74]. D_1 implies disordered graphitic lattice and is indicative of polycrystalline materials consisting of large number of small poly-oriented graphite - like structures. A high D_1 will imply high intensity of disordered graphitic structures, which are caused from contributions from other crystalline phases. These other crystalline phases may be from small poly-oriented structures likely formed from thermo oxidative reaction of degraded lubricants chemistries.

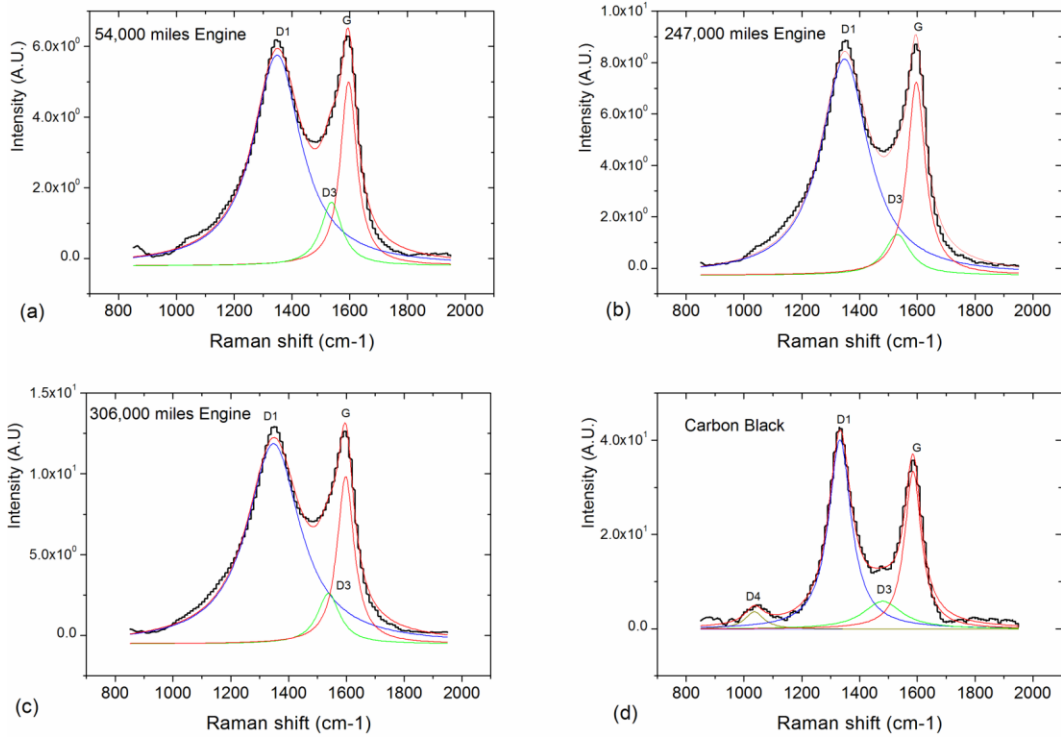


Fig 3-4 Deconvoluted Raman spectra fitted with Lorentzian curve fit for G, D₁, D₃ and D₄ peaks for samples (a) SP A, (b) SP B (c) SP C and (d) Carbon black

Table 3-5 Raman Peak Analysis of Carbon Black and Soot Samples

SP A, SP B and SP C

SAMPLE	PEAK	PEAK POSITION	INTENSITY	D ₁ /G	D ₃ /G	D ₄ /G	(D ₁ + D ₃ + D ₄) / G
SP A (54,000 miles Engine)	G	1596.38	741.22	-	-	-	2.52
	D1	1348.59	1703.87	2.30	-	-	
	D3	1536.91	168.40	-	0.227	-	
	D4	-	-	-	-	-	
SP B (247,000 miles Engine)	G	1596.44	838.16	-	-	-	3.10
	D1	1348.08	2344.19	2.80	-	-	
	D3	1530.90	253.78	-	0.303	-	
	D4	-	-	-	-	-	
SP C (306,000 miles Engine)	G	1597.86	1109.76	-	-	-	3.83
	D1	1348.24	3784.20	3.41	-	-	
	D3	1538.57	435.65	-	0.393	-	
	D4	-	-	-	-	-	
Carbon Black	G	1585.16	67.35	-	-	-	5.16
	D1	1332.19	93.96	1.40	-	-	
	D3	1480.20	182.69	-	2.71	-	
	D4	1035.90	70.24	-	-	1.04	

G = Ideal Graphitic Lattice

D1 = Disordered graphitic lattice (graphene layer edges)

D3 (A) = Amorphous carbon

D4 (I) = Disordered graphitic lattice, polyenes, ionic impurities

3.4.4 Discussion of Raman Spectra of EGR Soot Samples

Degree of graphitization of EGR soot formed will generally decrease from loss of efficiency in combustion process in diesel engines as engine age increases. The G peak gives the intensity of the ideal graphitic lattice, with D_1 representing disordered graphitic lattice. An increase in the intensity ratio of D_1 to G (D_1/G) meaning more level of disorder as compared to ordered graphitic lattice is a means of classifying degree of graphitization in Diesel soot. This is a basis used to compare level of graphitization for the three soot samples from different engine ages. The ratio of I_D/I_G is related to the structural defects in the basal plane of individual graphene layers.

The three EGR soot samples are compared with Mogul L type Carbon Black which is known to have lower degree of graphitization. From Fig 3.4 and Table 3.5, it is seen for samples SP A, SP B and SP C that intensity ratio D_1/G for the soot samples increased as the age of source engine increased. Quantity of soot generated in older engines is also seen to increase from increased intensity of both G and D_1 , and overall increase in $(D_1 + D_2 + D_3)/G$ ratio with decreased degree of graphitization.

Lattice disorder of soot particles will enhance interaction of other particles with disordered graphene edges. The graphene layer edges encourage reaction and formation of other crystalline phases. Studies in functionalizing of graphene have shown that functionalized edges of the

graphene layer reacts more easily with other phases resulting in larger D₁/G ratios [75]. The graphene edges serves as preferential location for absorption of reactive decomposition species. It is seen in this study that soot samples generated in older engines has higher D₁/G which suggests that older engines will produce soot which have larger proportion of their of their graphene layer edges more easily able to react with other crystalline phases, which will result in a higher level of crystal disorder. More specific complimentary tests to validate tests were carried out using the XRD and HR-TEM.

3.5 X- Ray Diffraction Studies of Diesel Soot

3.5.1 *Experimental Procedure*

The X- Ray diffraction spectra were collected using a Bruker AXS D8 High Resolution X-ray Diffractometer at the Center for Characterization of Materials and Biology (CCMB) at the University of Texas- Arlington using a CuK α ($\lambda = 1.54059 \text{ \AA}$) radiation. Samples were prepared by pressing soot into a Lucite holder. The Lucite holder was fixed in an orientation that ensured that the three pins of the sample holder in D8 held firmly. A Scintag counter detector was used to collect scattered x-ray from the sample. The 2θ angle ranged from 10° to 60° with step size of 0.02° and an acquisition of 1s for every step.

3.5.2 *X-Ray Diffraction Analysis of EGR Soot Samples*

XRD spectra for Carbon black, soot sample SP A, SP B and SP C are seen in Fig 3.5 on page 72 below. Soot spectra were analyzed to identify possible nano crystalline phases in the individual soot samples. Spectra peaks for the samples were matched with peaks of crystalline compounds in the Jade5 database on the Bruker ASX D8 XRD machine using metallic element composition of Ca, Zn, Fe and non - metallic composition H, C, O, S, P. The search match procedure was performed using elements of known chemical composition of lubricant chemistry and equipment wear. Interpretation and matching of XRD result of samples are further explained in Tables 3.6 - 3.8 on pages 73 - 75 below.

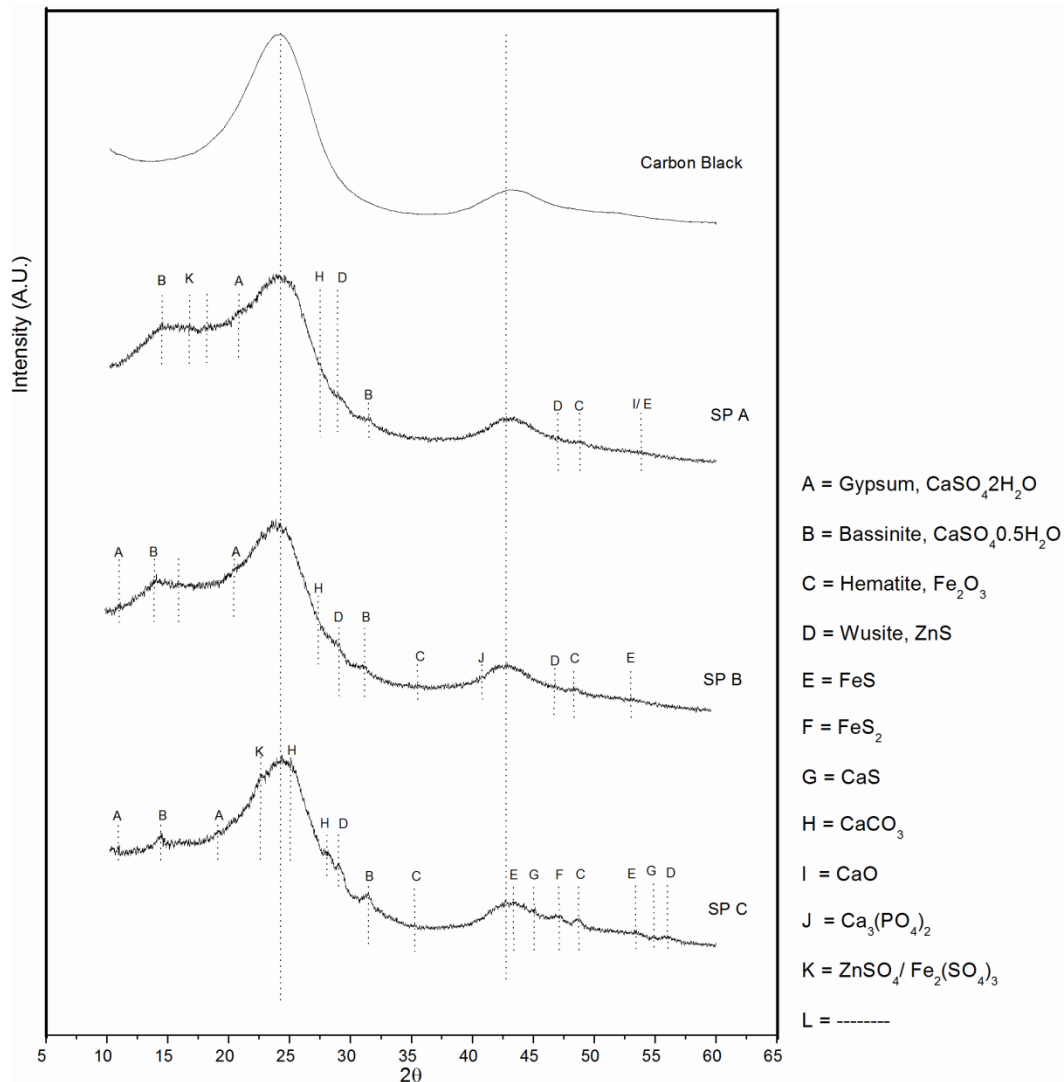


Fig 3-5 XRD spectra of Carbon black and soot samples SP A, SP B and
SP C

The three soot samples exhibited two broad peaks are at approximately 24.5° (002) and 43.5° (101) which are from the graphitic nature matched with graphite 2H peak in the Jade5 database. There are common crystalline peaks at 14.66° , 25.49° , 29.69° and 31.50° which matched with

Bassinite and Gypsum in all three samples. Other Hematite peaks are also noticed in various intensities in all three samples. Peaks in soot sample from the older engines show more intensities establishing the presence of nano crystal represented. The peculiar peaks observed in individual samples gave their individual characteristics, and are indicated in Tables 3.6 – 3.8 in pages 73 - 75 below.

Table 3-6 XRD Analysis of nano crystalline peaks of soot sample SP A

Sample		Suspected Compounds	Crystalline Peak	Crystalline compounds	(h k l)
SP A	A	Gypsum (PDF #33-031)	20.8	CaSO ₄ .2H ₂ O (20.69)	(0 2 1)
	B	Bassinite (PDF #41-0224)	14.7	CaSO ₄ .0.5H ₂ O(14.66)	(2 0 0)
			31.9	CaSO ₄ .0.5H ₂ O(31.90)	(2 0 4)
	C	Hematite (PDF #33-0664)	48.8	Fe ₂ O ₃ (49.48)	(0 2 4)
	D	Wurtzite, 2H (PDF #65-0309)	28.9	ZnS (28.6)	(1 1 1)
			47.2	ZnS (47.5)	(2 2 0)
	H	Calcium Carbonate (PDF #41-1475)	27.5	CaCO ₃ (27.20)	(0 2 1)
I/E	Calcium Oxide (PDF #37-2497)/ Iron Sulfide (PDF #57-0477)	53.5	CaO (53.85)/ FeS (53.12)	(2 2 0)/ (3 0 0)	

Table 3-7 continued

Sample		Suspected Compounds	Crystalline Peak	Crystalline compounds	(h k l)
SP A	J	Ca ₃ (PO ₄) ₂ (PDF #09-0169)	16.9	Ca ₃ (PO ₄) ₂ (17.00)	(1 1 0)
	-		-		

Table 3-8 XRD Analysis of nano crystalline peaks in soot sample SP B

Sample		Suspected Compounds	Crystalline Peak	Crystalline compounds	(h k l)
SP B	A	Gypsum (PDF #33-031)	11.5	CaSO ₄ .2H ₂ O (11.59)	(0 2 0)
			29.0	CaSO ₄ .2H ₂ O (29.11)	(4 0 0)
	B	Bassinite (PDF #41-0224)	14.7	CaSO ₄ .0.5H ₂ O(14.66)	(2 0 0)
			31.5	CaSO ₄ .0.5H ₂ O (31.90)	(2 0 4)
	C	Hematite (PDF #33-0664)	35.2	Fe ₂ O ₃ (35.61)	(1 1 0)
			48.8	Fe ₂ O ₃ (49.48)	(0 2 4)
	D	Wurtzite, 2H (PDF #65-0309)	47.2	ZnS (47.56)	(1 1 0)
	E	Iron Sulfide (PDF #57-0477)	53.2	FeS (53.12)	(3 0 0)
	H	Calcium Carbonate (PDF #41-1475)	27.5	CaCO ₃ (27.20)	(0 2 1)
	L	-	41.8	-	-

Table 3-9 XRD Analysis of nano crystalline peaks of soot sample SP C

Sample	Suspected Compounds	Crystalline Peak	Crystalline compounds	(h k l)
SP C	A	11.5	CaSO ₄ .2H ₂ O (11.59)	(0 2 0)
		20.5	CaSO ₄ .2H ₂ O (20.69)	(0 2 1)
	B	14.8	CaSO ₄ .0.5H ₂ O(14.66)	(2 0 0)
		25.1	CaSO ₄ .0.5H ₂ O(25.67)	(0 2 0)
		31.8	CaSO ₄ .0.5H ₂ O(31.90)	(2 0 4)
	C	35.4	Fe ₂ O ₃ (35.61)	(1 1 0)
		48.8	Fe ₂ O ₃ (49.48)	(0 2 4)
	D	28.7	ZnS (28.6)	(1 1 1)
		56.2	ZnS (56.47)	(3 1 1)
	E	42.7	FeS (43.15)	(1 1 4)
		53.3	FeS (53.12)	(3 0 0)
	F	46.8	FeS ₂ (47.43)	(0-2 2)
	G	45.1	CaS (45.00)	(2 2 0)
		55.3	CaS (55.8)	(2 2 2)
H	27.5	CaCO ₃ (27.20)	(0 2 1)	
K	22.6	ZnSO ₄ (21.39)/ Fe ₂ (SO ₄) ₃ (21.59)	(1 1 1)/ (1 1 0)	

Sample A from a new engine of 54,000 miles is dominated by presence of Bassinite, Gypsum, and other calcium based crystal particles; with low peaks of Hematite and sulfides. Soot sample SP B from an older engine of 247,000 mile show stronger Hematite and various of sulfide peaks of Iron and Zinc, with additional sulfates of Iron and Zinc, Calcium Sulfides observed in soot sample C from the oldest engine of 306,000 miles.

3.5.3 Discussion of XRD Spectra of EGR Soot Samples

Various variation of Calcium based crystal particles are observed in the soot samples in varying level of domination depending on the engine age in which sample was generated The origin of the observed phases are from overbased calcium sulphonates, which forms the core of detergents used in Lubricants. It is believed that the general effectiveness of the lubricant will depend on engine age; this will also be seen in the effectiveness of calcium sulphonate detergent which is the source of the calcium based particles

Soot sample SP A from a new engine of first oil change is dominated by Bassinite, gypsum and other Calcium based crystal particles which have low abrasion. They are in the form of micelles preventing formation of sludge and reducing oil degradation. These particles generally have hardness value of 2 on the Mohr hardness scale, and will

not be contributor to wear, but rather improve lubrication. The new engine from more efficient combustion and lubrication system will generally offer less degradation of lubricant chemistries that can be precursor to formation of third body abrasive products. Hematite (Fe_2O_3) is noticed in all three samples, with very weak peaks in new sample SP A and more profound peaks in soot sample generated in older engines. The strength of the peak may be used as an indication of how strong they are present in such sample

It is observed that soot samples from older engines show more diverse crystalline peaks representing other crystal particles in the soot samples; this can be related to the less graphitized soot generated from such engines. The less graphitized soot will have more disordered graphene edges that will more easily react to degrade lubricant chemistries; and form other phases. Soot sample SP B from an older engine of 247,000 mile show stronger Hematite and various sulfide peaks of Iron and Zinc, with additional sulfates of Iron and Zinc, Calcium Sulfides observed in soot sample C from the oldest engine of 306,000 miles. The oxides, sulfates and sulfides dominating in the older engines are abrasives and will influence the characteristics of soot. The abrasive nature of these particles will be causes abrasive wear in diesel engines, with their

influence increasing as the age of engine increases. The nature of other crystalline particles found in soot can give characteristics of such soot.

The distinctiveness of the individual crystalline peaks can be used as a measure of their presence in the soot samples. Crystalline peaks are observed to be more intense for soot samples formed from older engines, giving credence to presence of such nano particle they represent. There are fewer crystalline peaks in soot samples generated in newer engines, which is indication of lower presence of those phases. The results are further verified by complimentary studies using HR-TEM.

3.6 HR-TEM Studies of EGR Soot Samples

HR-TEM was used to determine possible nano crystalline particles embedded in diesel soot; studying structure, morphology and composition of soot formed from reaction of decomposed lubricant chemistry and wear metals. Selected Area Diffraction (SAED) was used to probe structural information. Energy Dispersive X-ray Spectrometer (EDS) coupled to HR-TEM was used to acquire compositional information of nano crystalline particles embedded within the amorphous structure of the soot. Bright field image of the soot samples clearly shows turbostratic structure in the range of 5 - 35 nm in diameter.

3.6.1 Experimental Procedure for HR- TEM Soot Studies

The HR-TEM Studies of the soot samples were conducted using a Hitachi H -9500 microscope with an accelerating voltage of 300 kV and lattice resolution of 0.18 nm. High resolution lattice image of the nanoparticle crystals from reaction of degraded lubricant chemistries with wear particles were acquired and measured. Energy Dispersive Spectra (EDS) and Selected Area Diffraction (SAED) were also obtained for various crystalline regions in the different soot samples. These were used to determine the chemical make-up of the nano-particles for each crystalline region.

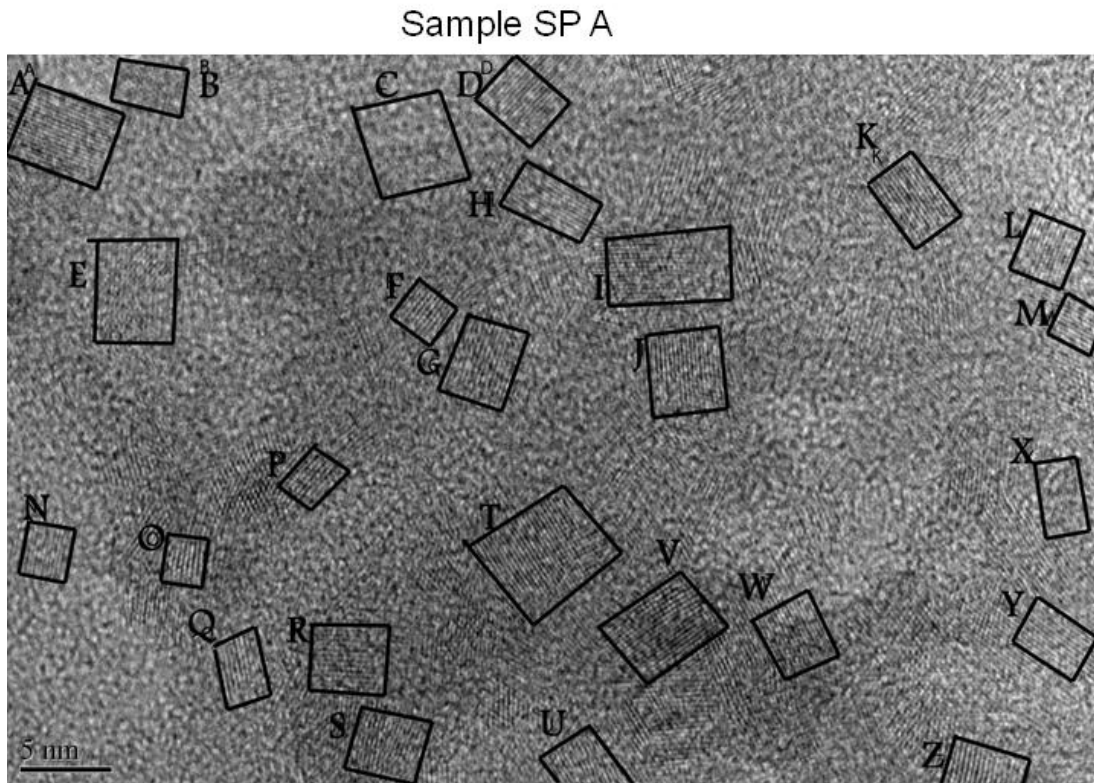
3.6.2 HR-TEM Analysis of EGR Soot Samples

Lattice fringe image, EDS spectra and SAED of the crystalline domains were taken from turbostratic region of soot. The crystalline domain was packed into hexagonal closed packed structure similar to graphite in a turbostratic fashion and an interpretation of the lattice fringes and EDS chemical make-up gave an idea of possible nano - crystalline particles embedded within the individual soot samples.

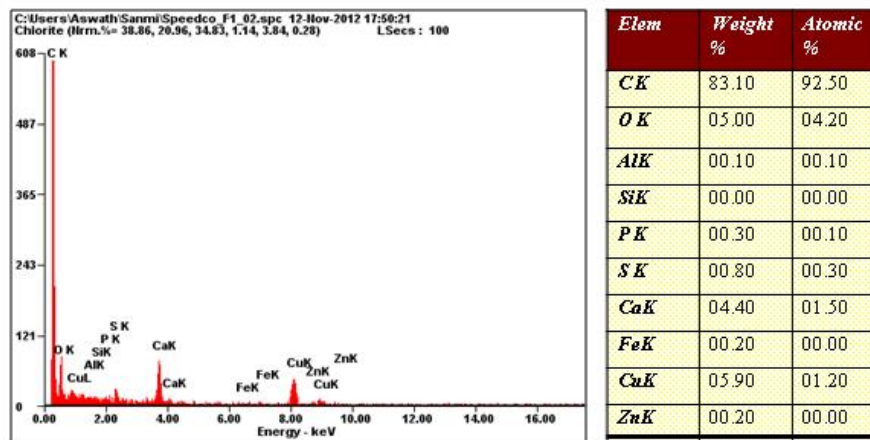
3.6.2.1 Lattice Fringe Image Analysis

The lattice fringes observed within the turbostratic layers of soot samples were analyzed by manual measurement of the lattice fringe using the image J software and comparing with similar d-spacing of possible

compounds from EDS result. Image of lattice fringes and EDS results for the three samples are seen in Fig 3.9 - 3.11 in pages 81, 84 and 87.



(a)



(b)

Fig 3-6 Turbostratic region of soot sample SP A showing (a) Crystal fringe lattice image (b) EDS spectra

Table 3-10 Crystalline Nano particles in the Turbostratic Structure of
Sample SP A

Crystal Lattice Fringe	Suspected Compound	d-spacing (Å ^o)		Nano Crystal Particle
		Standard Value	Measured Value	
C	Hematite	1.69	1.65	Fe ₂ O ₃
F		2.70	2.71	Fe ₂ O ₃
G		2.70	2.76	Fe ₂ O ₃
O		2.70	2.72	Fe ₂ O ₃
Q		2.70	2.72	Fe ₂ O ₃
S		2.51	2.52	Fe ₂ O ₃
Z		2.70	2.72	Fe ₂ O ₃
A	Calcium Oxide	2.41	2.37	CaO
B		2.41	2.38	CaO
H		2.41	2.37	CaO
I		2.41	2.42	CaO
J		2.41	2.44	CaO
K		2.41	2.40	CaO
L		2.41	2.46	CaO
M		2.41	2.43	CaO
N		2.41	2.37	CaO
T		2.41	2.36	CaO
Y		2.41	2.39	CaO
P	Calcium Sulfate	2.82	2.77	CaSO ₄
R	Sulfate	2.82	2.82	CaSO ₄

Table 3-11 continued

Crystal Lattice Fringe	Suspected Compound	d-spacing (Å ^o)		Nano Crystal Particle
		Standard Value	Measured Value	
X	Calcium Sulfate	1.75	1.74	CaSO ₄
V	Gypsum	2.87	2.83	CaSO ₄ .0.5H ₂ O
D	Zinc Oxide	2.47/ 2.43	2.45	ZnO/ZnO ₂
E		2.47/ 2.43	2.45	ZnO/ ZnO ₂
W		2.43	2.45	ZnO ₂
U		2.43	2.44	ZnO ₂

Sample SP B

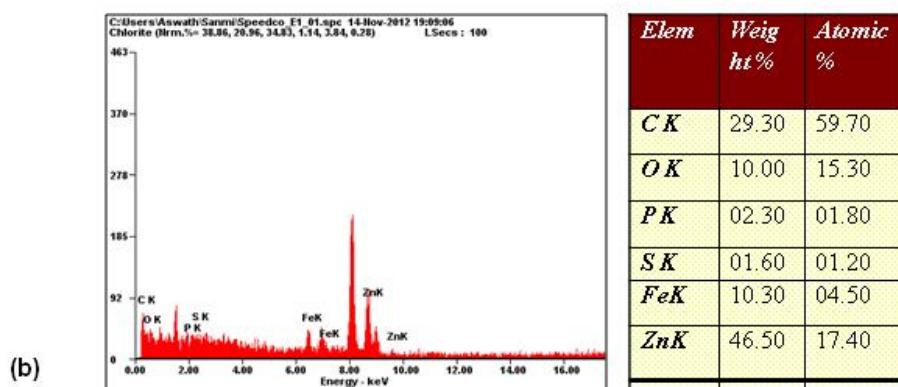
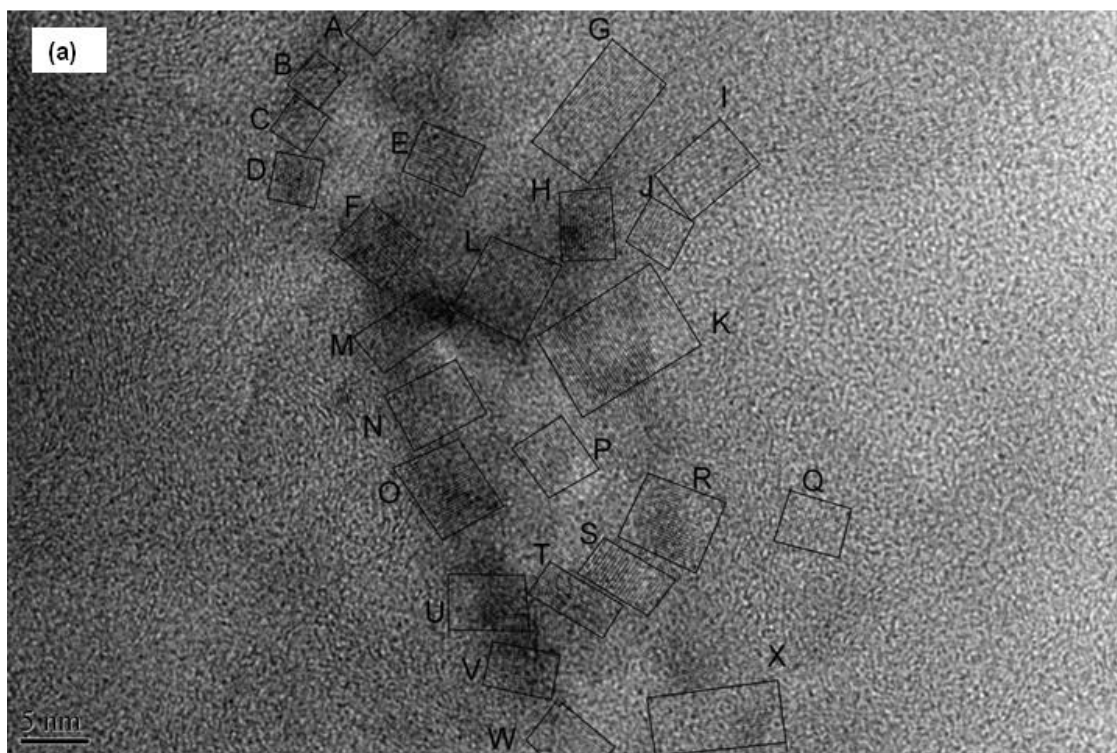


Fig 3-7 Turbostratic Region of Soot Sample SP B Showing (a) Crystal Fringe Lattice Image (b) EDS Spectra

Table 3-12 Crystalline nano particles in the turbostratic structure of sample

SP B

Crystal Lattice Fringe	Suspected Compound	d-spacing (Å ^o)		Nano Crystalline Particle
		Standard Value	Measured Value	
Region A				
A	Zinc Phosphate	3.00	3.05	Zn ₃ (PO ₄) ₂
B		3.00	3.05	Zn ₃ (PO ₄) ₂
C		3.00	3.04	Zn ₃ (PO ₄) ₂
F		3.00	3.10	Zn ₃ (PO ₄) ₂
I		3.00	2.97	Zn ₃ (PO ₄) ₂
D	Hematite	1.69	1.71	Fe ₂ O ₃
G	Magnetite	2.53	2.56	Fe ₃ O ₄
K	Wustite	2.22	2.24	FeO
L		2.22	2.26	FeO
W		2.24	2.26	FeO
J	Iron Sulfate	2.62	2.97	FeSO ₄
U	Iron Sulfide	2.31	2.32	FeS
E	Wutzite 2H	1.91	1.87	ZnS
N		2.93	2.89	ZnS
T		2.93	2.86	ZnS
V		3.12	3.20	ZnS
H	Zinc Oxide	2.43	2.34	ZnO ₂
M		2.43	2.43	ZnO ₂
O		2.47	2.48	ZnO
P		2.43	2.40	ZnO ₂

Table 3-13 continued

Crystal Lattice Fringe	Suspected Compound	d-spacing (Å ^o)		Nano Crystalline Particle
		Standard Value	Measured Value	
Region A				
Q	Zinc Oxide	2.43	2.42	ZnO ₂
R		2.43	2.38	ZnO ₂
S		2.43	2.39	ZnO

Sample SP C

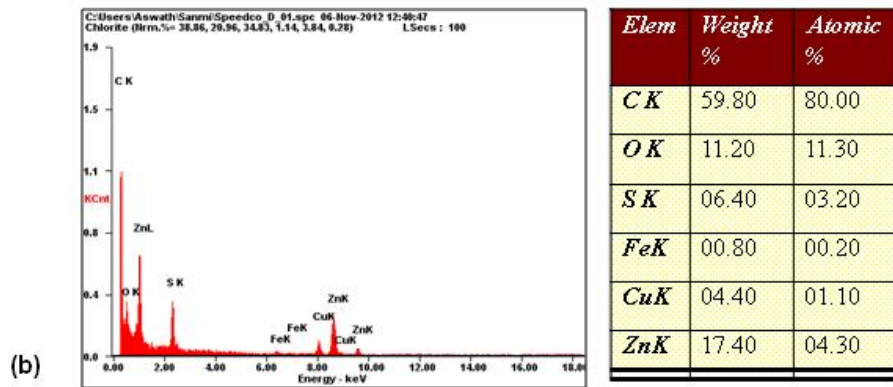
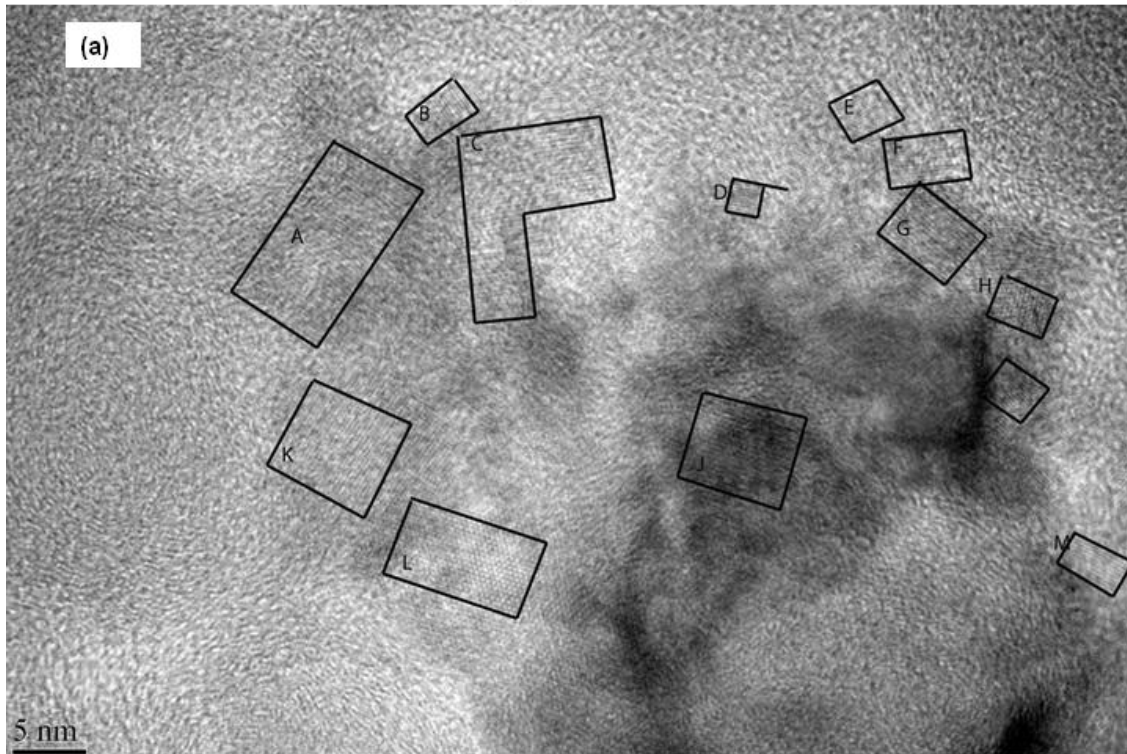


Fig 3-8 Turbostratic Region of Soot Samples SP C Showing (a) Crystal

Fringe Lattice Image (b) EDS Spectra

Table 3-14 (a) crystalline nano particles in the turbostratic structure of
sample SP C in region 1

Crystal lattice fringe	Suspected particles	Inter-planer crystal spacing d (Å°)		Nano crystalline particle
		Standard Value	Measured Value	
Region A		Standard Value	Measured Value	
A	Wurtzite 2H	3.31	3.24	ZnS
C		3.31	3.32	ZnS
G		3.31	3.31	ZnS
J		3.31	3.30	ZnS
K		2.93	2.87	ZnS
L		3.31	3.27	ZnS
N		1.91	1.91	ZnS
B	Wustite	2.59	2.57	FeO
E	Hematite	2.87	2.83	Fe ₂ O ₃
F	Magnetite	2.94	2.99	Fe ₃ O ₄
I	Iron Sulfate	2.62	2.64	FeSO ₄
M		2.62	2.61	FeSO ₄
H	Iron Sulfide	2.97	3.05	FeS
D	Zinc Oxide	2.43	2.36	ZnO ₂

Table 3-11 (b) crystalline nano particles in the turbostratic structure of sample SP C in region 2

Crystal lattice fringe	Suspected particles	Inter-planer crystal spacing d (Å°)		Nano crystalline particle
		Standard Value	Measured Value	
Region B	Suspected Particles	Standard Value	Measured Value	Crystalline Particle
A	Iron Sulfate	2.75	2.79	Fe ₂ (SO ₄) ₃
K		3.60	3.57	Fe ₂ (SO ₄) ₃
D	Iron Sulfide	2.97	3.00	FeS
E	Hematite	2.70	2.69	Fe ₂ O ₃
F		2.70	2.66	Fe ₂ O ₃
C	Zinc Sulfate	4.15	4.13	ZnSO ₄
G	Wurtzite 2H	3.12	3.20	ZnS
B		3.12	3.07	ZnS
I		3.31	3.30	ZnS
J		3.31	3.31	ZnS
H	Zinc Oxide	2.47/ 2.43	2.46	ZnO/ ZnO ₂

3.6.2.2 SAED Analysis of Soot Samples

SAED analyses are used for structural characterization of sample. Interpretation and Analysis for the samples SP A, SP B and SP C are compared in Fig 3.9 on page 90 and Tables 3.12 - 3.13 on page 91 below.

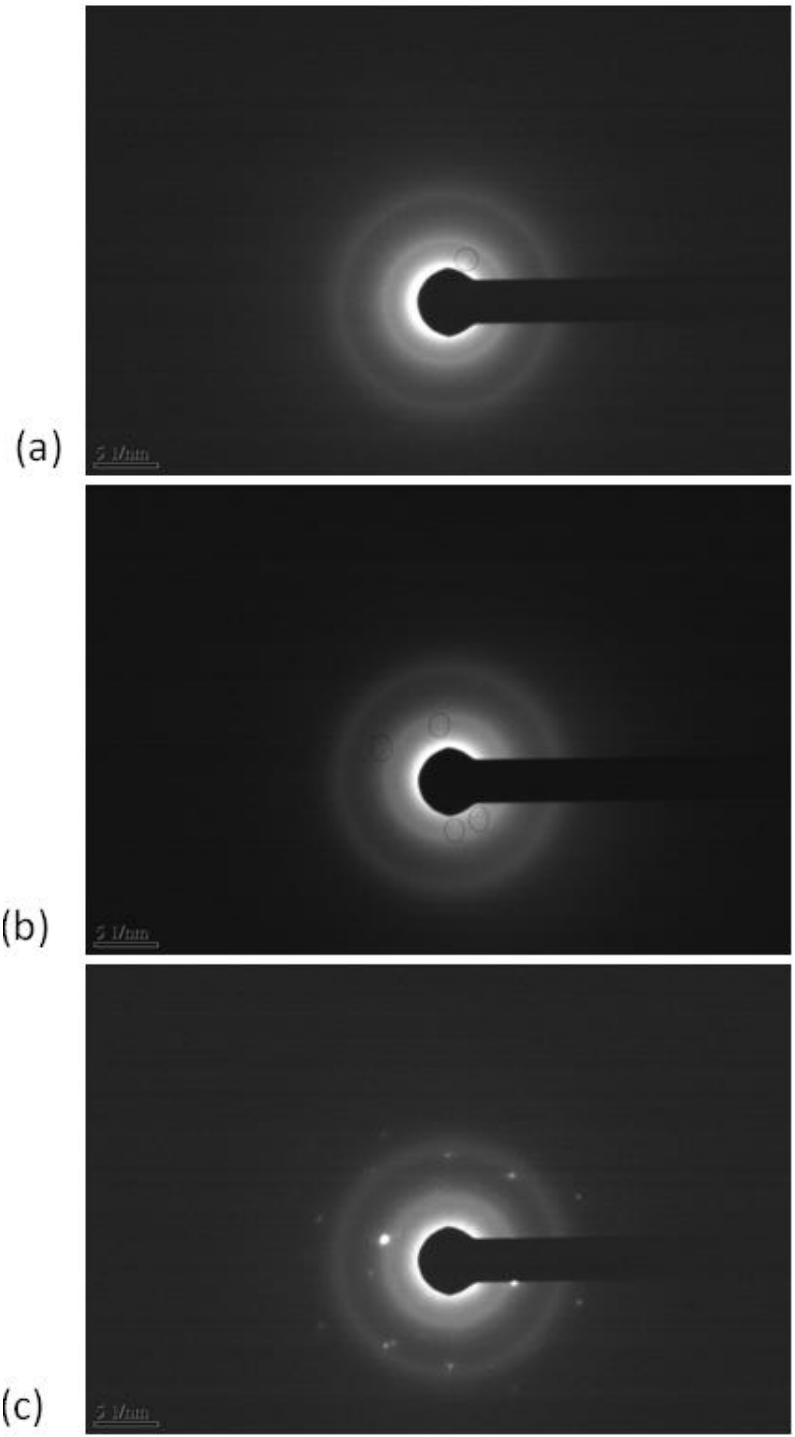


Fig 3-9 SAED Image of soot samples (a) SP A (b) SP B and (c) SP C

Table 3-15 d-spacing measurement of diffraction patterns in sample SP A,
SP B and SP C

	1 st ring d-spacing (R ₁)	2 nd ring d-spacing (R ₂)	3 rd ring d-spacing (R ₃)	R ₂ /R ₃	R ₁ /R ₃
SP A	0.321 (002)	0.197 (10)	0.117 (11)	1.68	2.74
SP B	0.318 (002)	0.196 (10)	0.115 (11)	1.70	2.76
SP C	0.323 (002)	0.194 (10)	0.118 (11)	1.64	2.73

The SAED diffraction patterns seen in Fig 3.9 majorly has the intense rings arising from (200) basal planes, (10) prismatic plane and (11) from the pyramidal planes. The diffraction patterns primarily arise from the crystalline portion of the turbostratic structure. The d- spacing that give rise to the rings are calculated from the electron patterns.

Table 3-16 d Lattice size matching of abrasive component of sample SP
A, SP B and SP C

	SP A			SP B			SP C		
	Measured d(A°)	Standard d(A°)	Nano Particle	Measured d(A°)	Standard d(A°)	Nano Particle	Measured d(A°)	Standard d(A°)	Nano Particle
R ₁	2.622	2.700	Fe ₂ O ₃	2.512	2.519	Fe ₂ O ₃	2.944	2.967	Fe ₃ O ₄
R ₂	1.670	1.690	Fe ₂ O ₃	1.661	1.608	Fe ₂ O ₃	1.833	1.841	Fe ₂ O ₃
R ₃	-	-	-	-	-	-	1.557	1.525	FeO
R ₄	-	-	-	-	-	-	1.191	1.237	
R ₅	-	-	-	-	-	-	1.182	-	
R ₆	-	-	-	-	-	-	0.925	0.957	
R ₇	-	-	-	-	-	-	0.879	-	-

Table 3-17 continued

	SP A			SP B			SP C		
	Measured d(A°)	Standard d(A°)	Nano Particle	Measured d(A°)	Standard d(A°)	Nano Particle	Measured d(A°)	Standard d(A°)	Nano Particle
R ₈	-	-	-	-	-	-	0.869	-	-

Reciprocal lattices of additional crystalline species are evident within the diffraction rings of graphitic soot. A closer look at the SAED image of sample SP A and SP B reveal a couple, while other multiple reciprocal lattices can be in soot sample from the oldest engine, sample SP C. Reciprocal lattice $d(A^\circ)$ is calculated by the formula, $d(A^\circ) = 10/ R$. Where R is radius of point- to- point lattice within crystal rings, and analysis as seen on Table 3.13 on pages 91 – 92 above.

3.6.3 Discussion of HR-TEM Analysis of EGR Soot Samples

The EDS for sample SP A reveals presence of Calcium and Oxygen in notable amounts, with insignificant amount of Zn, P, and S. Matching of lattice fringes in the Jade5 database using compositions of Ca, Fe, Zn, P, S and O, showed strong possibility of Gypsum ($\text{CaSO}_4 \cdot 2\text{H}_2\text{O}$), Calcium Oxide (CaO), Hematite (Fe_2O_3) and Zinc Oxide (ZnO_2). Most of the nano crystalline particles generated in the new engine are Calcium based particles from Calcium sulfonate detergent. More graphitized soot and better efficiency in the engine will offer less

degradation of lubricant additives which will otherwise produce a feed for formation of other crystalline and amorphous phases within soot particles. SAED result for sample SP A confirmed the presence Hematite (Fe_2O_3) which is a general constituent of EGR soot.

EDS of region imaged in SP B showed presence of Zn, P, S, O and Fe, and the matching of lattice fringes from manual measurement with the Jade5 database suggests the presence of Magnetite (Fe_3O_4), Hematite (Fe_2O_3), Wustite (FeO), Iron Sulphate (FeSO_4), FeS (Iron Sulfide), Wurtzite 2H (ZnS), Zinc Oxide (ZnO), and $\text{Zn}_3(\text{PO}_4)_2$. The SAED result confirmed the presence of Fe_2O_3 . The additional Oxides, Iron sulfate and Iron Sulfide found in older engine SP B are abrasive and are characteristics of EGR soot in older engines, suggesting that older soot will generate soot that will cause more wear in engine.

Soot from oldest sample SP C of 306,000 miles show higher numbers of crystalline nano particles than in the new and older engines. Overall, the turbostratic soot regions imaged showed the presence of Zn, S, O, and Fe. The old engine condition, generating less graphitized soot that is more reactive with lubricant chemistry will generally change the chemical make-up of the soot.

The soot sample is matched to contain Magnetite (Fe_3O_4), Hematite (Fe_2O_3), Wustite (FeO), Iron Sulphate (FeSO_4), FeS (Iron Sulfide),

Wurtzite 2H (ZnS) and Zinc Oxide (ZnO_2). SAED result confirmed the presence of Wustite (FeO), Hematite (Fe_2O_3) and Magnetite (Fe_3O_4) in this sample from the very old engine suggesting that the three oxidative state of Iron oxide are composition of soot generated in very old engine. These are highly abrasive materials which can result in accelerated wear in diesel engines.

Overall, range of crystalline nano particles is seen to increase in soot formed as age of engine increases. As seen in soot samples SP B and SP C, older engines under operating conditions showing less combustion and lubrication efficiency which will produce less graphitized soot which will degrade lubricant chemistry and aid reaction with contaminants and equipment wear. Nano particles observed in the result above are products of reactions of degraded lubricant chemistries and engine contaminants under operating conditions. Most of these particles are abrasive and influence the abrasive nature of EGR soot. The three phases of Iron Oxide especially are seen to be dispersed within otherwise amorphous soot graphitic structure in the older engines.

The origin of the nanoparticles could be from oxidation of asperity particles of iron that are subsequently incorporated into soot particles and from intrinsic oxidation of the constituents of tribofilm resulting in the nano crystals of oxides. The likely mechanism for the formation of the

nanoparticles is the intrinsic reaction of the Lubricant additive metals and other chemistries with wear debris together with available oxygen dissolved in the lubricant and during contact of debris with air. Formation of these particles from within an amorphous matrix involves a complex interplay between the kinetics of oxidation, thermodynamic stability of the phases, and interfacial energy between the nano particles and the amorphous matrix.

3.7 XANES Studies of EGR Soot Samples

The X-ray Absorption Near Edge Spectroscopy (XANES) is used as a non destructive tool to characterize chemical substances at nano scale [76]. It employs high energy/ soft X-ray photon from synchrotron radiation source with high flux where photon beam of known energy is directed incident on a sample surface with sufficient energy which excites a core level electron of an atom in the sample. On excitation, a photoelectron is created which moves into unoccupied states of the atom and photon is absorbed. Holes created in either of the K or L levels from movement of photoelectron are filled up by electrons from other shells. These electron movement to fill the 'holes' generate an emission of a Fluorescent Yield (FLY) Spectra. Another approach used is to ground the sample and measure neutralization current which yields Total Electron Yield (TEY) spectra. Total Electron Yield is surface sensitive while the Fluorescent

Yield spectra give information to higher depth of sample [77]. The Absorption Edge of photon energy in samples can be used as finger-print to identify their chemical make-up.

3.7.1 Experimental Procedure for XANES Studies

The XANES experiment was carried out at the Canadian Light source, Saskatoon, Canada using the 2.9 GeV storage ring. Two beam lines were used to obtain the K and L absorption edge spectra. Phosphorus and Sulphur L Edge were obtained using the Variable Line Grating – Plane Grating Monochromator (VGM – PGM) beam line covering region of 5 – 250eV with photon resolution of 0.2eV and spot size of 500 μ m x 500 μ m. Phosphorus K Edge was recorded using the Soft X-ray Micro-characterization Beamline (SXRMB) covering region of 1700 – 10000 eV with photon resolution of 0.2eV and spot size of 300 μ m x 300 μ m. XANE spectra for the L edge were all acquired in both the Total Electron Yield (TEY) and Fluorescent Yield (FLY) modes while XANES spectra for the K edge was acquired in FLY mode. The spectra data for the soot samples were analyzed with the OriginPro software to get final XANES spectra.

3.7.2 XANES Analysis of Soot Samples

XANES Spectroscopy of extracted soot samples from used Diesel Oil were acquired in the Total Electron Yield (TEY) mode for chemical

information of surface or near surface regions and the fluorescence Yield (FLY) mode was acquired to determine chemical property of bulk soot sample. The sampling depths for the soot sample in the TEY mode of the Phosphorus and Sulfur L Edge are at about 5 nm at the L- Edge and about 50 nm at the K- Edge. Sampling depth for the FLY mode was taken at about 50 nm at the L Edge and about 400 nm at the K Edge [78].

3.7.2.1 Phosphorus L edge XANES Spectral Analysis

The FLY spectra and the TEY spectra of nano particles created with soot are compared with model compounds of FePO_4 , $\text{Zn}_3(\text{PO}_4)_2$, $\text{Ca}_2\text{P}_2\text{O}_7$, $\text{Ca}_3(\text{PO}_4)_2$ as shown on Fig 3.10 in page 98. Iron phosphates have a slightly higher energy states than zinc phosphates. FePO_4 is at 139 eV and $\text{Zn}_3(\text{PO}_4)_2$ is at 138.7 eV).

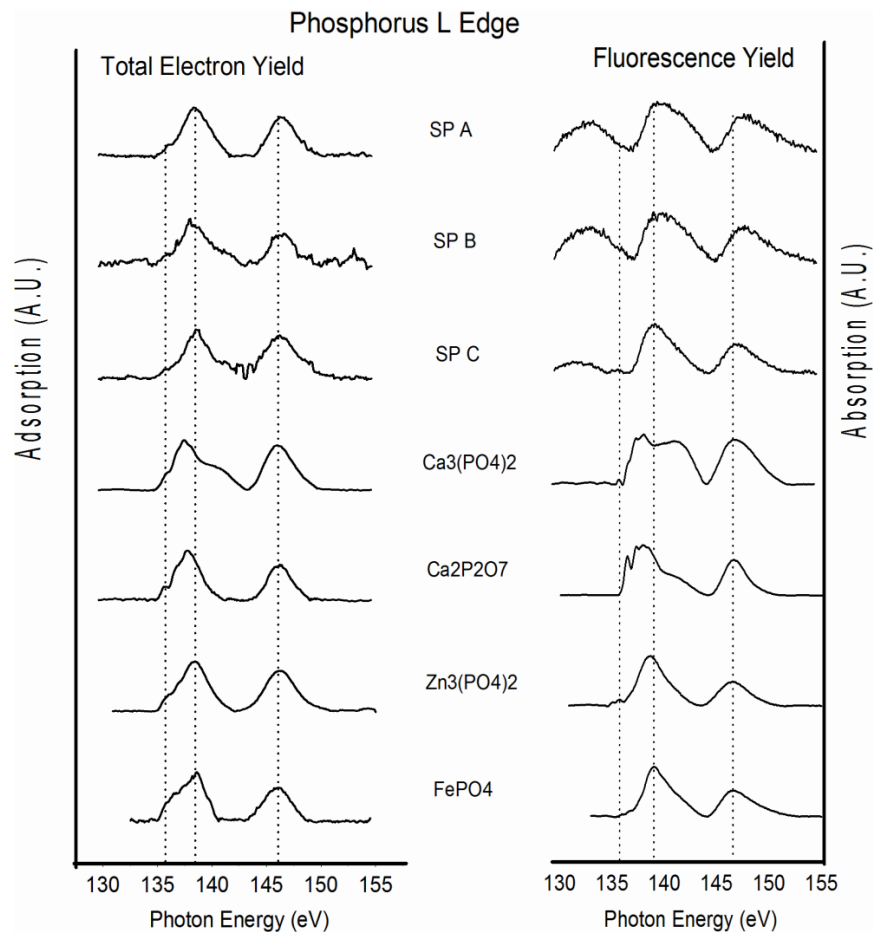


Fig 3-10 Normalized TEY and FLY Phosphorus L Edge spectra of soot samples SP A, SP B, SP C and model compounds

The plot and match of the XANES spectra of soot samples SP A, SP B and SP C with phosphate model compounds suggests the presence of Calcium, Zinc and iron Phosphate. A closer look at both TEY and FLY modes of the three samples suggests Iron Phosphate, but overall Zinc Phosphate and Iron Phosphate is believed to be present in the three samples in different degrees.

3.7.2.2 Sulphur L Edge XANE Spectra Analysis

The FLY spectra and the TEY spectra of nano particles created with soot are compared with model compounds of ZnSO_4 , CaSO_4 , FeSO_4 , $\text{Fe}_2(\text{SO}_4)_3$, FeS_2 , FeS and ZnS as shown in Fig 3.11 below.

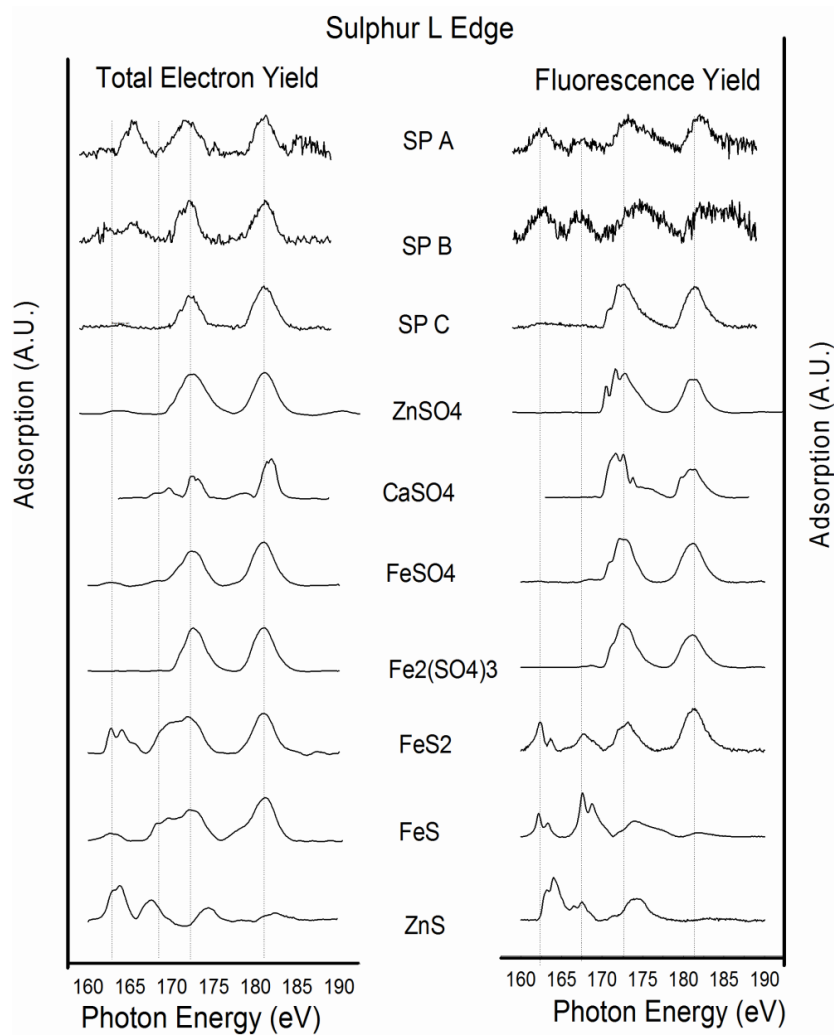


Fig 3-11 Normalized TEY and FLY Sulfur L Edge of soot samples SP A, SP B and SP C and model compounds

Sulfur L Edge provides local coordination of sulfur near the surface soot sample [79,80]. The XANES spectra indicate the presence of sulfates and sulfides of Iron. XANES spectra of sample SP A and SP B are more similar to spectra of Iron sulfide, FeS_2 and suggest the presence of FeS_2 in the soot samples. Matching of samples SP C closely matched with Iron Sulfate and can be suggested as Iron Sulphate, FeSO_4 . There could be possibilities of ZnSO_4 and $\text{Fe}_2(\text{SO}_4)_3$ in sample SP C which are also loosely matched with SP C spectra.

3.7.2.3 Phosphorus K edge XANE Spectra Analysis

Absorption peak in phosphorus K- edge spectrum arises from transition of 1s electrons to unoccupied 2p shells. Soot spectra for the three samples are compared with phosphates of zinc, calcium, and iron. Spectra plot of soot samples with phosphate model compounds is shown in Fig 3.12 on page 101 below.

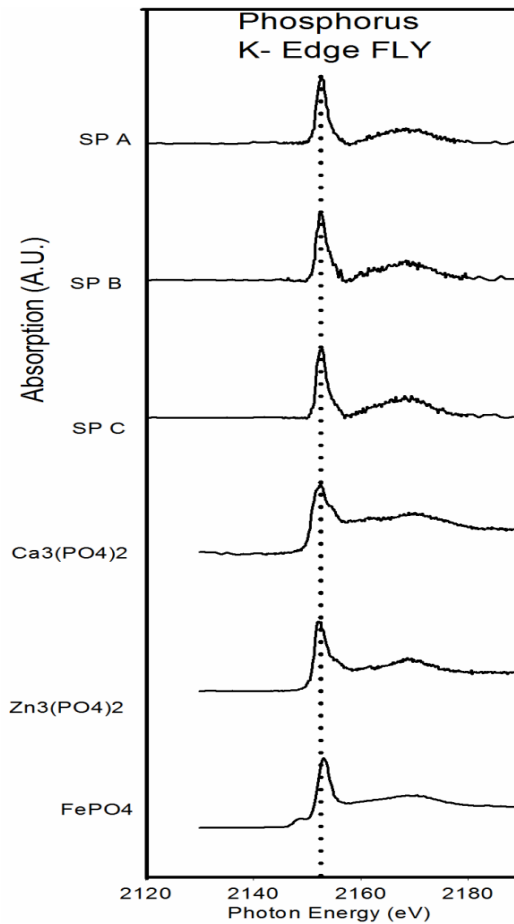


Fig 3-12 Normalized FLY and TEY Phosphorus K edge Spectra of Soot Samples SP A, SP B, SP C and Model Compounds

The peaks observed for the three samples SP A, SP B and SP C are similar. The P K Edge which is at a higher depth can be used to confirm result in the P L Edge where samples closely matched with Iron phosphate and Zinc phosphates. In this case of the P K Edge, the phosphate peak is also closer matched to Zinc phosphate, but the presence of Iron phosphate will not be ruled out. The absence of pre edge

peak at 2148eV in the soot sample which is seen in Iron can also be used to corroborate the match.

3.7.2 Discussion of XANES Spectra

XANES Analysis result was able to show the presence of a number of crystalline particles formed with EGR Soot. The presence of Iron Sulfide, Iron Sulfate and the possibility of other sulfates is confirmed in results from the Sulphur L Edge. Results from both Phosphorus L and K Edge also confirm the presence of Iron Phosphate and a high likelihood of Zinc phosphates. These nano particles reveals by the XANES analysis are all abrasive and are believed to cause and encourage wear in Diesel engines. Their ease of formation and effect on wear will be more aggravated in older engines with less operating combustion efficiency.

Chapter 4

EGR Soot from Synthetic based Diesel Oil

This chapter discusses the role of lubricant chemistry from synthetic base stock and role of engine age on the nature of EGR soot generated in diesel engine. Synthetic base stocks are classified in the API Base Oil categories of Groups IV to V and contain no Sulphur. Majority of Synthetic base stocks are from Polyalphaolefin (PAO) molecule which is a largely stable and highly purified ethylene derivative that make far superior oils than mineral oils. PAO generally have the advantages of greater oxidative stability, superior volatility, excellent low-temperature viscosities, extremely high viscosity index, excellent pour points, and pure petrochemical feedstocks. PAO have great oxidative stability and will form less thermo-oxidative reaction products than in mineral base stocks. However, lubricant additives added in formulation of synthetic Diesel Oils may degrade at certain operation conditions forming abrasive crystalline phases in soot particles. The possibility and extent of formation of these third body particles is studied in this chapter, characterizing soot generated from synthetic based oils.

Engine age can also be a determinant factor in nature of soot formed from change in efficiency of engine combustion system with increasing engine age. Factors such as change in engine technologies will

also affect combustion design with different diesel engines and hence nature of soot generated. The discussion is focused on an Exhaust Gas Recirculation (EGR) Diesel Engine.

4.1 Introduction

EGR soot samples analyzed was extracted from SAE 15W-40 type Synthetic based used Diesel Oil of approximately 50,000 miles of oil change from Detroit DD15 engines. The used oil was acquired from Amsoil oil change facility, Superior, Wisconsin. The Oil type is from a known Diesel Oil manufacturer with known oil properties. Three samples of different engine ages are analyzed labeled AM A, AM B and AM C of 127,000 miles, 187,000 miles, and 248,000 miles respectively to study the role of engine age and lubricant chemistry on nature of EGR soot formed.

4.2 Soot Extraction

The EGR soot is formed from recirculated particulate matter (PM), NO_x and CO combustion product in diesel Oil. EGR soot sample is not readily obtained, but is extracted from used Oil from a series of extraction processes to get sample for further analysis. The extraction and handling processes is as described.

4.2.1 Oil Dissolution

Used engine oil is mixed with hexane as solvent in approximately 50 wt % dilution. A proper mix of used oil and hexane is ensured by

heating together in an ultrasonic heater for about 10 minutes. A 1000ml glass tube is recommended to achieve extraction of more quantity of soot at a time; the weight of the glass tube is noted, and weight of used oil sample and hexane at each mix should also be noted. Weighted dissolved used oil in hexane is shown in Fig 4.1 below. By taking note of the quantity/ weight of used oil sample and comparing with quantity/ weight of final soot extracted give an idea of percentage soot concentration of used oil sample, though percentage soot concentration obtained from extraction may not always give exact concentration of soot in used oil because of possible soot loss during extraction process.

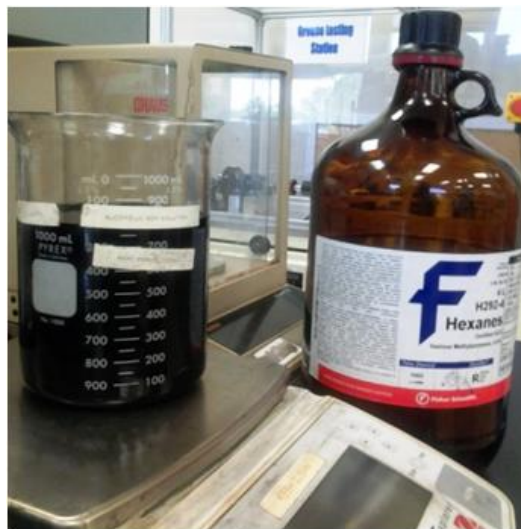


Fig 4-1 Weighted used synthetic oil sample

4.2.2 Centrifuging Process

After ensuring a proper mix of the used oil sample with about 50% quantity of hexane, the mixture was centrifuged and a SORVALL SS 34 was used for the centrifuging process which accommodated up to eight (8) numbers of 32mm x 100mm centrifuge bottles at a time. All the centrifuge bottles were filled to the same volume which ensured a proper balancing of the centrifuge disc. To fill the centrifuge bottle, a standard volume of oil sample mixture was measured for all the bottles using a measuring cylinder. A typical centrifuge and centrifuge bottle holder is shown in Fig 4.2 on page 107 below.

After balancing of centrifuge bottles in the disc, centrifuge parameters were set for operations to give optimal soot sediment. Operating conditions for optimal extraction was set at 12000 rpm for 2 hours duration. The supernatant from each bottle were carefully removed into a glass tube to remove the soot particles settled at the bottom of the tube. Solid soot particle settled at the bottom of the bottle which can be scooped out with a spatula. The process is repeated for all centrifuge bottles to extract soot particles.

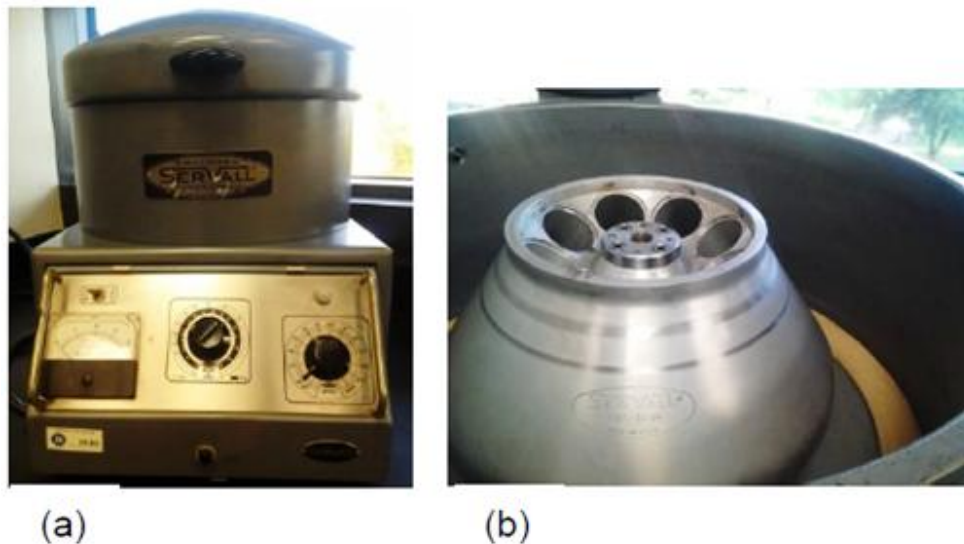


Fig 4-2 (a) Sorvall SS 34 Centrifuge (b) Centrifuge Bottle Holder

4.2.3 Soxhlet Process of Soot Sample

Soot obtained from the centrifuging is not clean enough and still contains some oil in it, therefore soot samples were further cleaned a soxhletting process. The soxhletting process removed oil still attached to soot particles to give oil-free soot. The process was carried out for 48 hour period. Cleaning was achieved by heating up hexane to boiling point and leaving it to condense into the soot sample to wash out oil through the pores of the thimbles in which soot is placed; thimbles size of $8\mu\text{m}$ pore size was used in the process. The soxhletting process was carried out in an experimental fume hood to ensure safety precautions, as shown in Fig 4.3 on page 108 below.

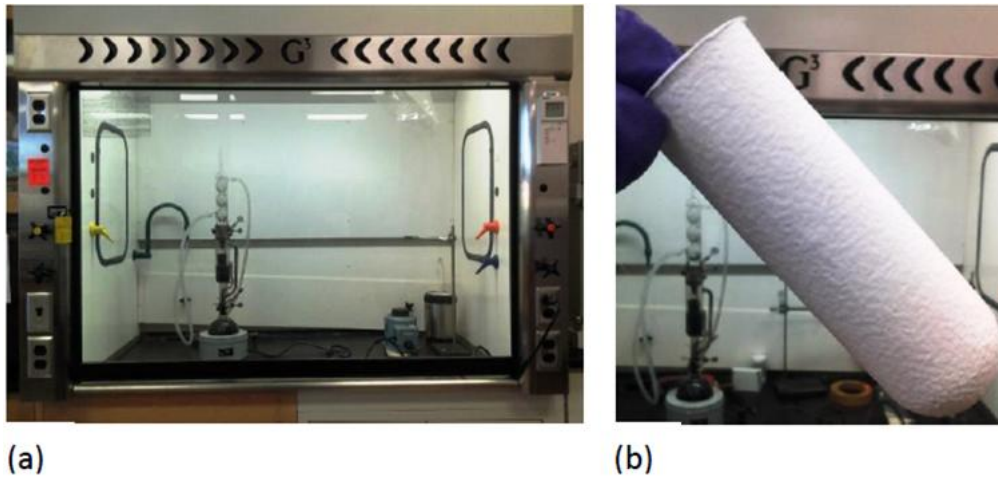


Fig 4-3 (a) Soxhlet Setup in an Experimental Fume Hood (b) 8µm Cellulose Thimble

4.2.4 Drying and Storage

After the soxhletting process, the thimble is removed from the set up and left in fume hood to dry up. Dried soot should be carefully removed from the thimble to maximize extraction and minimize waste. The dried soot is ground to fine powder using an experimental mortar and pestle. The final weight of soot is obtained using the weigh balance and recorded before storage in a glass tube properly closed in a dry environment. The soot samples are then stored for further analysis.

4.3 Elemental Composition Analysis of Used Diesel Oil

Elemental Analysis of used Diesel Oil sample shows the level of contamination from wear metals, lubricant degradation and external contaminants. Contaminations and degraded lubricant chemistries in

diesel oil under the high operating conditions of diesel engines are believed to result in formation of crystalline nano particles within soot, which are abrasive and are causes of wear in EGR Diesel Engine. Tables 4.1 below shows detail of chemical analysis for the used oil samples from which EGR soot studied was extracted.

Table 4-1 Spectrochemical Analysis of Synthetic based SAE 15-40 Used Oil Samples

SAMPLE	ENGINE AGE	ELEMENTAL COMPOSITION														
		METAL (ppm)						CONTAMINANTS (ppm)		ADDITIVES (ppm)						
		Fe	Cr	Pb	Cu	Al	Ni	K	Na	Mg	B	Ca	P	Zn	Mo	Si
		Contributions from equipment wear						From engine coolant		From detergents			From ZDDP Antiwear		Friction Modifier	Anti foam additive
AMA	127,000	35	3	0	61	25	1	44	10	1654	20	1198	1654	2417	55	13
AMB	187,000	31	3	1	58	19	1	32	11	1628	13	1595	1628	2926	57	19
AMC	248,000	49	3	0	20	17	1	24	11	1732	14	1369	1728	2914	61	8

The spectrochemical analysis measures different metals in parts per million (ppm) that represent equipment wear, lubricant additives and system contaminants. The ICP- AES (Inductively coupled plasma atomic emission spectroscopy) is necessary to observe wear metals and other contaminants in used lubricants.

4.3.1 Spectrochemical Analysis for wear metals

Abnormal wear is indicated by combination of metals and/or reaction of wear metals with degraded lubrication chemistries. There could

also be other possible secondary sources. The interpretation of sources of elements in the stochiochemical analysis of the used engine oil lubricant sample is shown in Tables 4 - 2 to 4 – 4.on pages 110 - 101.below.

Table 4-2 Spectrochemical Analysis of Wear Metals

ELEMENT	SOURCE
Iron (Fe)	Major component Material in Equipment manufacturing, housing/ blocks, bushing, bearing, shafts, valves, Rings, Rusts, etc
Chromium (Cr)	Cylinder Liners and Guides, Bushings, Bearing, Shafts, Valves, Rods, Rings, Hydraulic Cylinders
Lead (Pb)	Bearing/ Bushings, Thrust Plates, Washers
Copper (Cu)	Bearings/Bushings, Thrust Plates, Washers, Oil cooler, Pumps, Disc/ Disc Lining
Tin (Sn)	Bearings/Bushings, Pumps, Motors, Compressor, Piston, Piston skirt overlay
Aluminum (Al)	Piston, Bearings/Bushings, Thrust washers, Rings, Housing/blocks, Oil cooler, Cylinders and Cylinders Guides, Engine aftercooler
Nickel (Ni)	Gears, shafts, Rings, Valve Trains, Bearings/Bushings, Pumps

Table 4-3 Spectroscopic Analysis of Lubricant Additives

ELEMENT	SOURCES
Boron (B)	Extreme pressure additive, Detergency
Calcium (Ca)	Detergency, Alkalinity Reserve (Contributes to base number)
Molybdenum (Mo)	Extreme Pressure Additive, Lubricity Additive
Phosphorus (P)	Antiwear when present with Zinc, Extreme Pressure Additive, Friction modifier
Zinc (Zn)	Antiwear when present with Phosphorus, Antioxidant, Anticorrosive
Silicon (Si)	Anti-foam Additive

Table 4-4 Spectroscopic Analysis of External Contaminants

ELEMENT	SOURCE
Potassium (K)	Engine coolant, aftercooler brazing flux
Sodium (Na)	Engine coolant
Aluminum (Al)	Aftercooler brazing flux, Dirt if in combination with Silicon

The various elements which make up the chemistry of the used oil samples are from oil composition and possible reaction products formed under engine operating conditions. Some of the reaction products form third body nano- sized particles which are incorporated and become part of the turbostratic structure of soot. These nano- sized particles in the form of crystalline or amorphous can be source of abrasion and causes of wear in EGR engines. From the stochiochemical analysis, contributions from

equipment wear, engine oil additives and contaminants are seen in the oil. Reaction of the breakdown of additive chemistry of the oil with equipment wear product and contaminants are believed as possible result of the nano- sized crystalline and amorphous phases.

Stoichiometric result show the presence of high amount of Zinc and Phosphorus from ZDDP antiwear additive, high amount of Magnesium and Calcium from detergent, and high level of Iron from equipment wear. Possible reaction of these chemistries to form second phase crystalline and amorphous nano-sized abrasive particles which influence nature of soot formed in EGR engines were further studied using the Raman, HR-TEM, XRD and XANES studies. This will validate suggestions about formation of abrasive nano crystalline particles in EGR soot.

4.4 Raman Studies of EGR Soot Samples

Raman spectroscopy has been used to investigate short-range highly disordered graphitic structures. Studies have shown that different soot types can be distinguished based on the degree of graphitization. The integrated intensity ratio of D and G (D/G) peaks is inversely proportional to microcrystalline planer size L_a that corresponds to the in-plane dimension of the single microcrystalline domain in graphite [70-72]. Information is obtained from analyzing spectral features such as intensity, peak position, line shape and bandwidth between 800 and 2000 cm^{-1} .

4.4.1 *Experimental Procedure for Raman Studies*

The equipment used for the Raman Test was the Thermo scientific DXR spectrometer which employs a diode pumped solid-state type laser as a source of illumination. The collection system is configured to use backscattered configuration. Soot samples were analyzed by visualizing using a 10x microscope objective lens. A solid-state laser of 532 nm frequency and maximum power output of 10 mW was used. A low laser power was used to avoid excessive heating of soot sample; a laser power of 1 mW was used in analyzing the Raman Spectra. Laser spot diameter was 2 μm with 25 μm slit size for the fully focused laser beam. Spectral resolution was 5 cm^{-1} at 532 nm with wavelength range from 800 cm^{-1} to 2000 cm^{-1} .

Soot thickness of about 1 mm thick was densely pressed on a glass slide to create a macroscopically smooth surface of sample as they were analyzed. The glass slide is held by a sample holder and positioned under the microscope to focus white light. On getting a focus of sample, the white beam is replaced with laser beam which acquire the Raman spectra of sample. Curve fitting for the determination of spectral parameters was performed using the OriginLab software. Curve fit was plotted from combination of various line shapes. Best fit of the curve was accomplished

without fixing or limiting the range of any spectral parameters during iteration.

4.4.2 Raman Spectra Analysis by Curve Fitting

Studies have shown that different types of soot can be distinguished according to their degree of graphitization [73]. In this study, the Lorentzian line shape was evaluated for the analysis and determination of spectral parameters by curve fitting. Raman spectra of carbonaceous materials exhibit a broad band at approximately 1500 cm^{-1} which is associated with amorphous sp^2 bonded carbon. It is noted that sp^3 bonded carbon have vibrational frequency below 1500 cm^{-1} and this observation suggests a higher probability of sp^2 bonded amorphous carbons. The best fit for the samples was achieved combination of line shape for G, D_1 and D_3 peaks. The Lorentz line shape can be used for all four G, D_1 , D_3 and D_4 peaks or the Lorentzian line shape for G, D_1 , and D_4 peak and Gaussian line shape for D_3 peak. The Lorentzian line shape was used to fit all four peaks at approximately 1595, 1350, 1520, and 1200 cm^{-1} in this study in agreement with studies by Sadezky et al [73].

Studies from previous work showed that the intensity maximum at approximately 1590 cm^{-1} (known as G band) is analogous to ideal graphitic vibration mode. Increased degree of disorder in the graphite structure gives rise to the peak maxima at about 1350 cm^{-1} which

corresponds to disordered graphite, this peak maximum is known as D_1 peak (Defect bands). Strong signal intensity designated as $D_3(A)$ can also be noticed at about 1500 cm^{-1} which originates from the amorphous carbon fraction of soot (organic molecules, fragments or functional groups) and/ or amorphous sp^2 bonded forms of carbon. A fourth peak D_4 in the fitting took into account disordered graphitic lattice due to polyenes and/or ionic impurities.

4.4.3 Raman Spectra Analysis of Soot Samples

Further analysis of the spectra was obtained by analyzing full width half maximum (FWHM) of the peaks, peak intensity, peak position and curve fitted data to calculate the ratio of D/G peak intensity. Deconvoluted Raman peaks Carbon black and the three soot samples is shown in Fig 4.4 on page 116 below. The ratio of I_D/I_G is related to the structural defects in the basal plane of individual graphene layers. With a high amorphous content of soot, the D_3 band broadens and differences in intensities may become significant [74]. D_1 implies disordered graphitic lattice and is indicative of polycrystalline materials consisting of large number of small poly-oriented graphite-like structures. A high D_1 value will imply high intensity of disordered graphitic structures, which is caused by contributions from other crystalline phases. These other crystalline phases

are believed to come from small poly-oriented structures likely formed from thermo oxidative reaction of degraded lubricants chemistries.

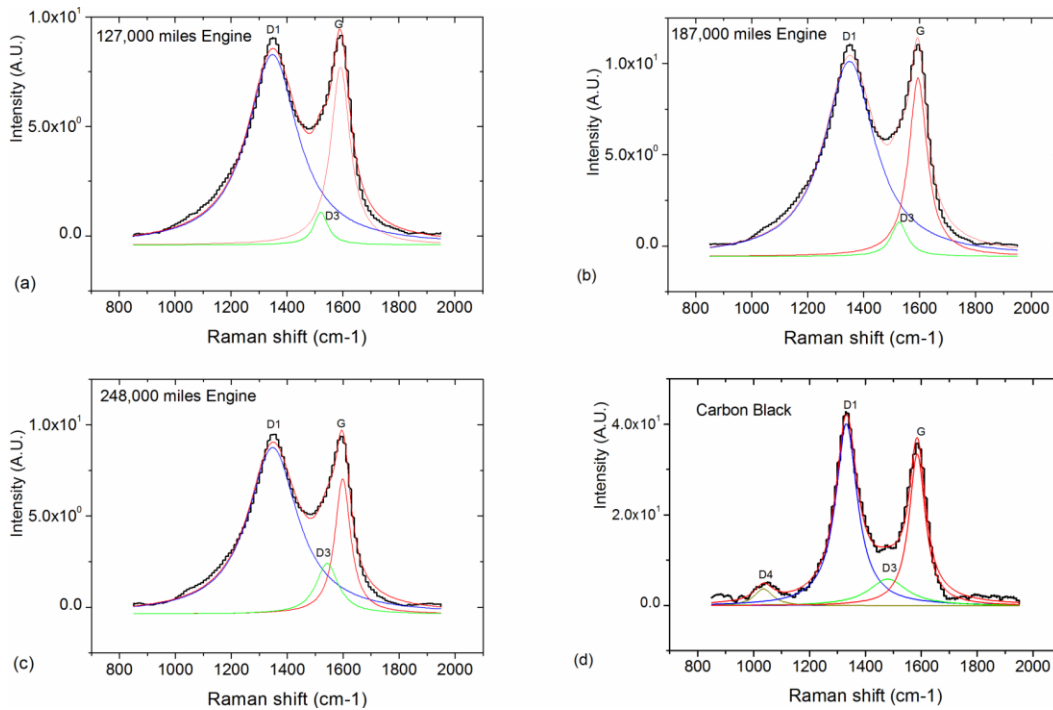


Fig 4-4 Deconvoluted Raman Spectra fitted with Lorentzian fit for G, D₁, D₃ and D₄ peaks for samples (a) AM A (b) AM B (c) AM C and (d) Carbon black

Table 4-5 Deconvoluted Raman Peak Data for Carbon Black, Samples

AM A, AM B and AM C

SAMPLE	PEAK	PEAK POSITION	INTENSITY	D ₁ /G	D ₃ /G	D ₄ /G	(D ₁ + D ₃ + D ₄) / G
AM A (127,000 miles Engine)	G	1591.11	1005.03	-	-	-	2.73
	D1	1348.29	2611.63	2.59	-	-	
	D3	1520.99	139.57	-	0.139	-	
	D4	-	-	-	-	-	
AM B (187,000 miles Engine)	G	1594.37	1145.09	-	-	-	2.98
	D1	1349.43	3221.14	2.81	-	-	
	D3	1527.38	199.14	-	0.174	-	
	D4	-	-	-	-	-	
AM C (248,000 miles Engine)	G	1598.05	751.74	-	-	-	4.14
	D1	1347.98	2712.85	3.61	-	-	
	D3	1542.61	396.87	-	0.528	-	
	D4	-	-	-	-	-	
Carbon black	G	1585.16	67.35	-	-	-	5.16
	D1	1332.19	93.96	1.40	-	-	
	D3	1480.20	182.69	-	2.71	-	
	D4	1035.90	70.24	-	-	1.04	

G = Ideal Graphitic Lattice

D1 = Disordered graphitic lattice (graphene layer edges)

D3 (A) = Amorphous carbon

D4 (I) = Disordered graphitic lattice, polyenes, ionic impurities

4.4.4 Discussion of Raman Spectra of EGR Soot

Degree of graphitization of EGR soot formed will generally decrease from loss of efficiency in combustion process in diesel engines as engine age increases. The G peak gives the intensity of the ideal graphitic lattice, with D_1 representing disordered graphitic lattice. An increase in the intensity ratio of D_1 to G (D_1/G) meaning more level of disorder as compared to ordered graphitic lattice is a means of classifying degree of graphitization in diesel soot. This is a basis used to compare level of graphitization for the three soot samples from different engine ages. The ratio of I_D/I_G is related to the structural defects in the basal plane of individual graphene layers.

The three EGR soot samples are compared with Mogul L type Carbon Black which is known to have very low degree of graphitization from its more amorphous base. From Fig 4.4 and Table 4.5 on pages 116 and 117 respectively, it is seen for samples AM A, AM B and AM C that intensity ratio D_1/G for the soot samples increased as the age of source engine increased. Quantity of soot generated in older engines is also seen to increase from increased intensity of both G and D_1 , and overall increase in $(D_1 + D_2 + D_3)/G$ ratio.

Lattice disorder of soot particles will enhance interaction of other particles with disordered graphene edges. The graphene layer edges encourage reaction and formation of other crystalline phases. Studies in

functionalizing of graphene have shown that functionalized edges of the graphene layer reacts more easily with other phases resulting in larger D_1/G ratios [75]. The graphene edges serves as preferential location for absorption of reactive decomposition species. It is seen in this study that soot samples generated in older engines has higher D_1/G which suggests that older engines will produce soot which have larger proportion of their of their graphene layer edges more easily able to react with other crystalline phases, which will result in a higher level of crystal disorder. More specific complimentary tests to validate tests were carried out using the XRD and HR-TEM.

4.5 X- Ray Diffraction studies of Diesel Soot

4.5.1 *Experimental Procedure*

The X- Ray diffraction spectra were collected using a Bruker AXS D8 High Resolution X-ray Diffractometer at the Center for Characterization of Materials and Biology (CCMB) at the University of Texas- Arlington using a $CuK\alpha$ ($\lambda = 1.54059 \text{ \AA}$) radiation. Samples were prepared by pressing soot into a Lucite holder. The Lucite holder was fixed in an orientation that ensured that the three pins of the sample holder in D8 held firmly. A Scintag counter detector was used to collect scattered x-ray from the sample. The 2θ angle ranged from 10° to 60° with step size of 0.02° and an acquisition of 1s for every step.

4.5.2 XRD Analysis of Soot Samples

XRD spectra for the soot samples AM A, AM C and AM C as seen in Fig 4.5 on page 121 below was analyzed to identify possible nano crystalline phases in the individual soot samples. Spectra peaks for the samples were matched with peaks of crystalline compounds in the Jade5 database on the Bruker ASX D8 XRD machine using metallic element composition of Ca, Zn, Fe and non - metallic composition H, C, O, S, P. The search match procedure was performed using elements of known chemical composition of lubricant chemistry and equipment wear.

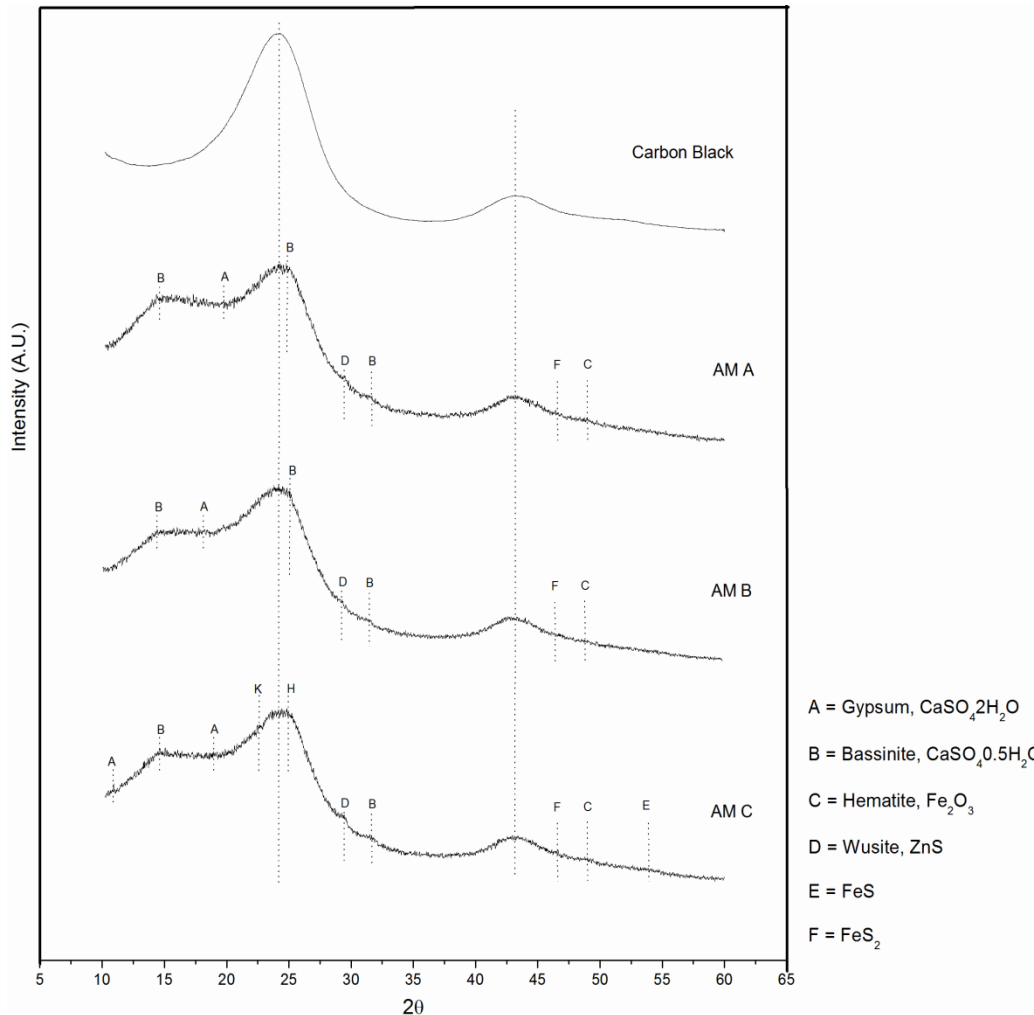


Fig 4-5 Fig 4.5 XRD spectra of Carbon black, soot samples AM A, AM B, and AM C

The three soot samples exhibited two broad peaks are at approximately 24.5° (002) and 43.5° (101) which are from the graphitic nature as matched with graphite 2H peak in the Jade5 database. There are common crystalline peaks at 14.66°, 25.49, 29.69 and 31.50 which matched with Bassinite (CaSO₄·0.5H₂O) and Gypsum (CaSO₄·2H₂O) in all

three samples. Few Hematite peaks are also noticed in various degrees of intensities, but generally low in for all three samples. Similar peaks for all three sample show higher intensity in sample from the older engines establishing the presence of nano crystal they depict. The peculiar peaks observed in individual samples gave their individual characteristics, and are as analyzed in Table 4 - 6 to 4 - 8 in pages 122 – 124 below.

Table 4-6 Analysis of nano crystalline peaks of soot sample AM A

Sample		Suspected Compounds	Crystalline Peak	Crystalline compounds	(h k l)
AM A	A	Gypsum (PDF #33-031)	20.5	CaSO ₄ .2H ₂ O (20.69)	(0 2 1)
	B	Bassinite (PDF #41-0224)	14.8	CaSO ₄ .0.5H ₂ O(14.66)	(2 0 0)
			25.1	CaSO ₄ .0.5H ₂ O(25.67)	(0 2 0)
			31.8	CaSO ₄ .0.5H ₂ O(31.90)	(2 0 4)
	C	Hematite (PDF #33-0664)	48.8	Fe ₂ O ₃ (49.48)	(0 2 4)
	D	Wurtzite, 2H (PDF #65-0309)	28.7	ZnS (28.6)	(1 1 1)
F	Iron Sulfide (PDF #65-1211)	46.8	FeS ₂ (47.43)	(0-2 2)	

Table 4-7 Analysis of Nano crystalline peaks of Soot Sample AM B

Sample		Suspected Compounds	Crystalline Peak	Crystalline compounds	(h k l)
AM B	A	Gypsum (PDF #33-031)	20.5	CaSO ₄ .2H ₂ O (20.69)	(0 2 1)
			B	Bassinite (PDF #41-0224)	14.8
	25.1	CaSO ₄ .0.5H ₂ O(25.67)			(0 2 0)
	31.8	CaSO ₄ .0.5H ₂ O(31.90)			(2 0 4)
	C	Hematite (PDF #33-0664)	35.4	Fe ₂ O ₃ (35.61)	(1 1 0)
			48.8	Fe ₂ O ₃ (49.48)	(0 2 4)
	D	Wurtzite, 2H (PDF #65-0309)	28.7	ZnS (28.6)	(1 1 1)
	F	Iron Sulfide (PDF #65-1211)	46.8	FeS ₂ (47.43)	(0-2 2)

Table 4-8 Analysis of nano crystalline peaks of soot sample AM C

Sample		Suspected Compounds	Crystalline Peak	Crystalline compounds	(h k l)
AM C	A	Gypsum (PDF #33-031)	11.5	CaSO ₄ .2H ₂ O (11.59)	(0 2 0)
			29.0	CaSO ₄ .2H ₂ O (29.11)	(4 0 0)
	B	Bassinite (PDF #41-0224)	14.8	CaSO ₄ .0.5H ₂ O(14.66)	(2 0 0)
			25.1	CaSO ₄ .0.5H ₂ O(25.67)	(0 2 0)
			31.8	CaSO ₄ .0.5H ₂ O(31.90)	(2 0 4)
	C	Hematite (PDF #33-0664)	35.4	Fe ₂ O ₃ (35.61)	(1 1 0)
			48.8	Fe ₂ O ₃ (49.48)	(0 2 4)

Table 4-9 continued

Sample		Suspected Compounds	Crystalline Peak	Crystalline compounds	(h k l)
AM C	D	Wurtzite, 2H (PDF #65-0309)	28.7	ZnS (28.6)	(1 1 1)
	E	Iron Sulfide (PDF #57-0477)	53.3	FeS (53.12)	(3 0 0)
	F	Iron Sulfide (PDF #65-1211)	46.8	FeS ₂ (47.43)	(0-2 2)

The three soot samples are dominated by Common Bassinite ($\text{CaSO}_4 \cdot 0.5\text{H}_2\text{O}$) and Gypsum ($\text{CaSO}_4 \cdot 2\text{H}_2\text{O}$) peaks, and weak Hematite (Fe_2O_3) peaks. Few other individual peaks are observed as analyzed in result above.

4.5.3 Discussion of XRD Spectra of EGR Soot Samples

Not much of other crystalline or amorphous phases are noticed in soot samples from Synthetic based oil at 50,000 mile of oil change. Peaks of Bassinite ($\text{CaSO}_4 \cdot 0.5\text{H}_2\text{O}$) and Gypsum ($\text{CaSO}_4 \cdot 2\text{H}_2\text{O}$), and minor Hematite (Fe_2O_3) peaks are observed. The samples also show sulfides and sulfates peak which has increased peak intensity and increased number of peaks with samples from increased engine. The few Sulfate and Sulfide peaks are weak and may not be strong enough to effect

abrasion in the characteristics of EGR generated in 50,000 miles of oil change.

Except for weak Hematite peaks observed, there were no strong enough oxide peaks noticed in the three sample, this can be due to the oxidation stability of the synthetic base stock used as chemistry of the oil which stayed high for more than 50,000 mile in which the samples were generated and minimized formation of oxides.

From this analysis, it is seen that lubricant chemistry in synthetic base stock may not easily be degradable by soot generated irrespective of engine age for 50,000 miles of oil use. The synthetic base stock lubricant chemistry can be said to withstand degradation ability of soot and subsequent formation of abrasive crystalline particles that are causes of wear in diesel engines. Bassinite observed in the sample is not abrasive and will not be contributor to wear, but rather improve lubrication. Hematite (Fe_2O_3) is a general constituent of EGR soot and noticed in all three samples, but with very weak peaks in new sample which may result in negligible wear.

4.6 HR-TEM Studies of EGR Soot Samples

HRTEM was used to determine possible nano-sized crystalline particles studying structure, morphology and composition of soot formed from reaction of decomposed lubricant chemistry and wear metals.

Selected Area Diffraction (SAD) was used to probe structural information. Energy Dispersive X-ray Spectrometer (EDS) coupled to the HR-TEM was used to acquire compositional information of nano crystalline particles embedded within the amorphous structure of the soot. Bright field image of the soot samples clearly shows turbostratic structure in the range of 5-35 nm in diameter.

4.6.1 Experimental Procedure for HR-TEM Soot Studies

The HR-TEM Studies of the soot samples were conducted using a Hitachi H - 9500 microscope with an accelerating voltage of 300 kV and lattice resolution of 0.18 nm. High resolution lattice image of the nanoparticle crystals from reaction of degraded lubricant chemistries with wear particles were acquired and measured. Energy Dispersive Spectra (EDS) and Selected Area Diffraction (SAED) were also obtained for various crystalline regions in the different soot samples. These were used to determine the chemical make-up of the nano-particles for each crystalline region.

4.6.2 HR-TEM Analysis of Soot Samples

Lattice fringe images, EDS spectra and SAED of the crystalline domains were taken from turbostratic region of soot. The crystalline domain was packed into hexagonal closed packed structure similar to graphite in a turbostratic fashion and an interpretation of the lattice fringes

and EDS chemical make-up gave an idea of nano-crystalline particles embedded within the individual soot samples.

4.6.2.1 Lattice Fringe Image Analysis

The lattice fringes observed within the turbostratic layers of soot samples were analyzed by manual measurement of the lattice fringe using the image J software and comparing with similar d-spacing of possible compounds from EDS result. Image of lattice fringes and EDS results for the three samples are seen in Fig 4 – 9, 4 – 10 and 4 - 11 on pages 128, 130 and 132 respectively.

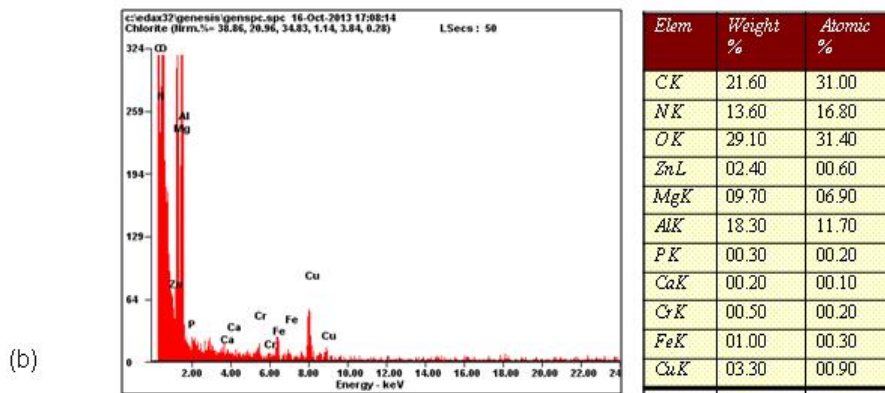
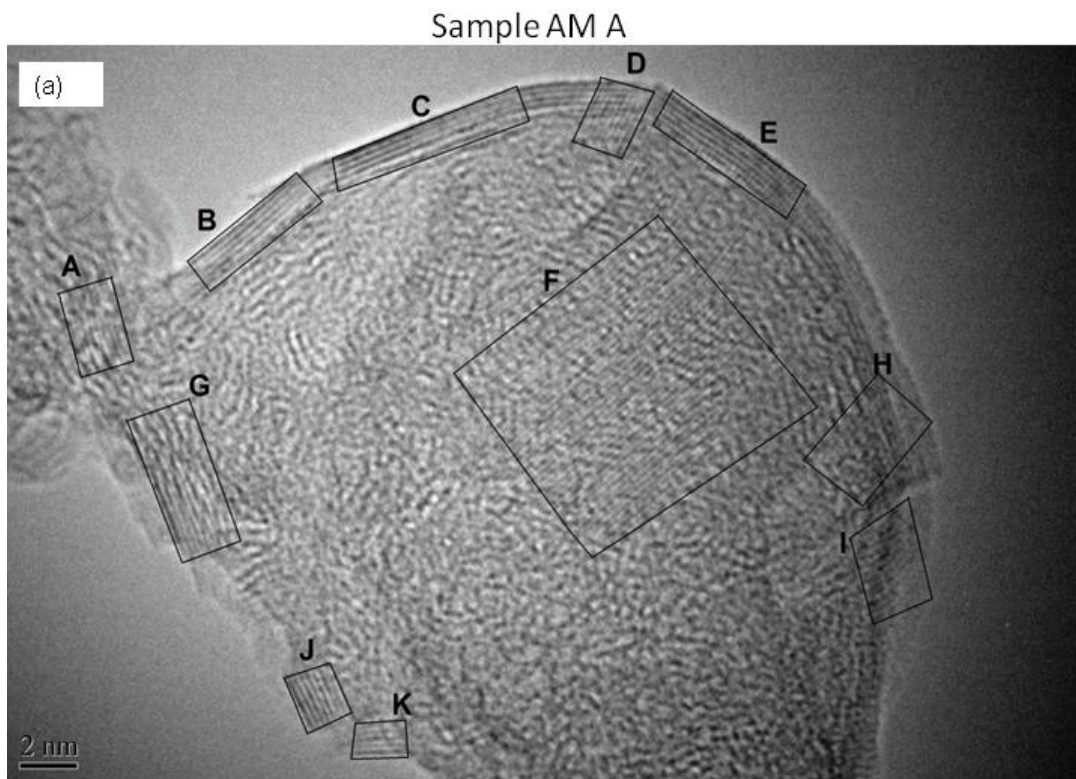


Fig 4-6 Turbostratic region of Soot Sample AM A showing (a) Crystal Fringe Lattice Image (b) EDS Spectra

Table 4-10 HR-TEM Analysis of Lattice Fringes for possible Nano Crystalline Particles in Sample AM A

Crystal Lattice Fringe	Suspected Compound	d-spacing (Å ^o)		Nano Crystalline particle
		Standard Value	Measured Value	
A	Calcium Pyrophosphate	2.30	2.32	Ca ₂ P ₂ O ₇
C	Zinc Oxide	2.45	2.46	ZnO ₂
K		2.10	2.11	ZnO
F		2.10	2.10	ZnO
B	Wustite	2.19/ 2.22	2.20	Graphite/FeO
D		2.19/ 2.22	2.21	Graphite/FeO
E		2.19/ 2.22	2.26	Graphite/FeO
G		2.19/ 2.22	2.20	Graphite/FeO
J		2.19/ 2.22	2.23	Graphite/FeO
H	Hematite	2.62	2.63	Fe ₂ O ₃
I		2.70	2.77	Fe ₂ O ₃

The lattice fringe image was matched using chemistries showed from EDS imaging, matching with Ca, Mg, Fe, Zn, P, and O in the Jade5 database. The crystal fringe matched with Calcium Pyrophosphate (Ca₂P₂O₇), Hematite (Fe₂O₃), Wustite (FeO) and Zinc Oxide (ZnO₂).

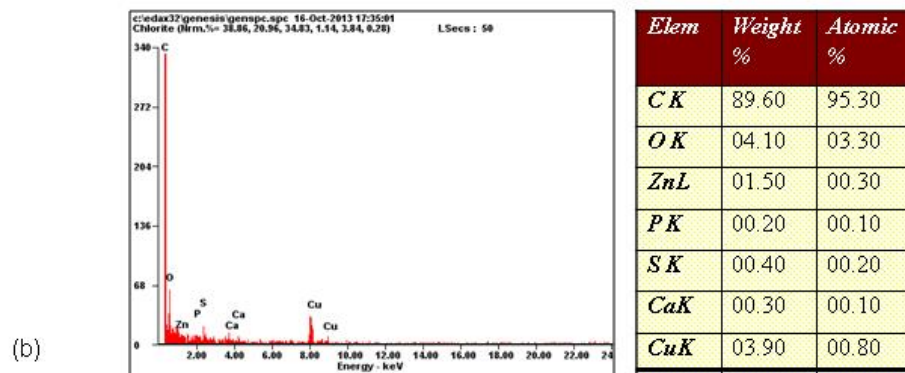
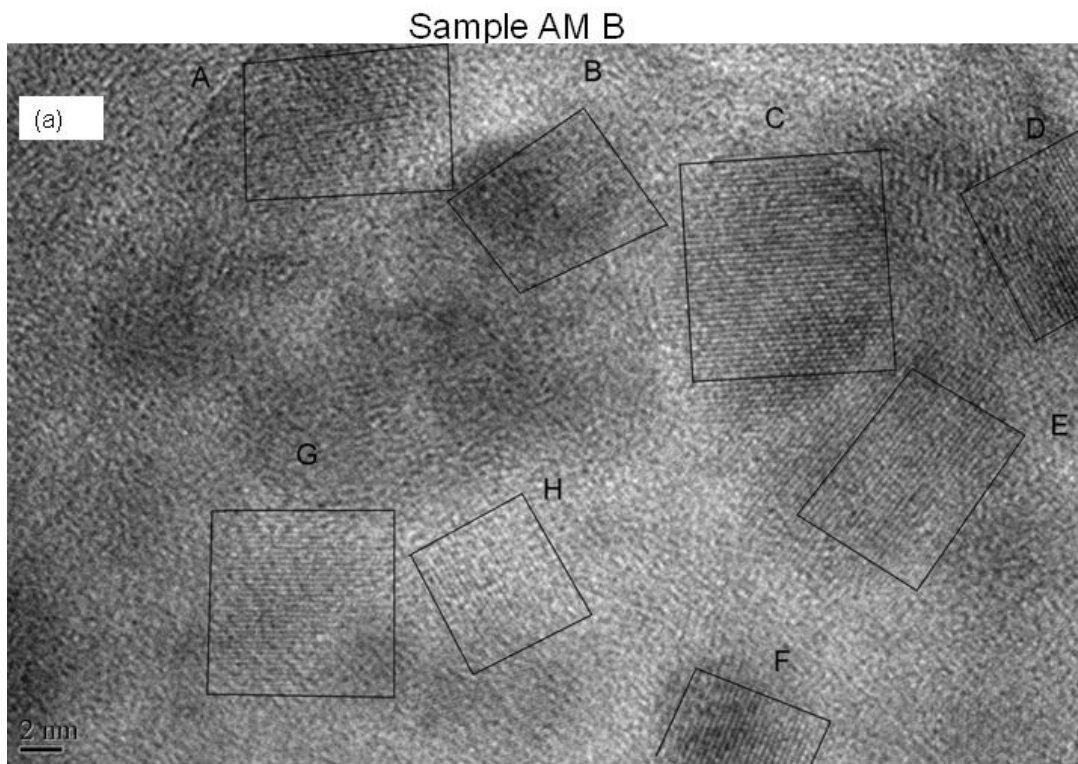


Fig 4-7 Turbostratic region of Soot Sample AM B showing (a) Crystal Fringe Lattice Image (b) EDS Spectra

Table 4-11 HR-TEM Analysis of Lattice fringes image for possible nano crystalline particles in sample AM B

Crystal Lattice Fringe	Suggested particles	Inter-planer crystal spacing d (Å)		Nano crystalline particle
		Standard Value	Measured Value	
Region A				
A	Zinc Oxide	2.43	2.43	ZnO ₂
B	Wurtzite 2H	1.91	1.87	ZnS
C		2.93	2.86	ZnS
E		2.93	2.89	ZnS
F		2.93	2.91	ZnS
H		2.93	2.88	ZnS
D	Wustite	2.59	2.59	FeO
G	Hematite	2.52	2.50	Fe ₂ O ₃

Crystal fringe image and EDS for sample AM B in the turbostratic region of soot sample show few nano crystalline phases within the turbostratic Soot. Zn, P, S, O, Mg, and Fe are recorded in the EDS which are from contamination in diesel oil. Matching of the lattice fringes from manual measurement with lattice fringes in Jade5 database software showed possible presence of Wurtzite 2H (ZnS), Zinc Oxide (ZnO₂), Hematite (Fe₂O₃) and Wustite (FeO).

Sample AM C

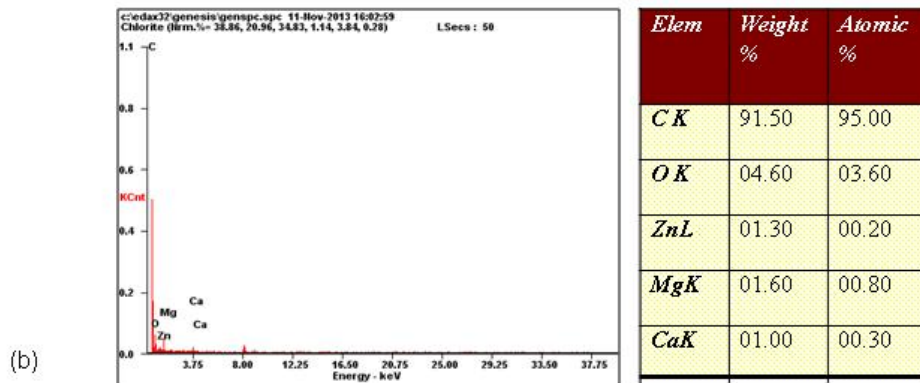
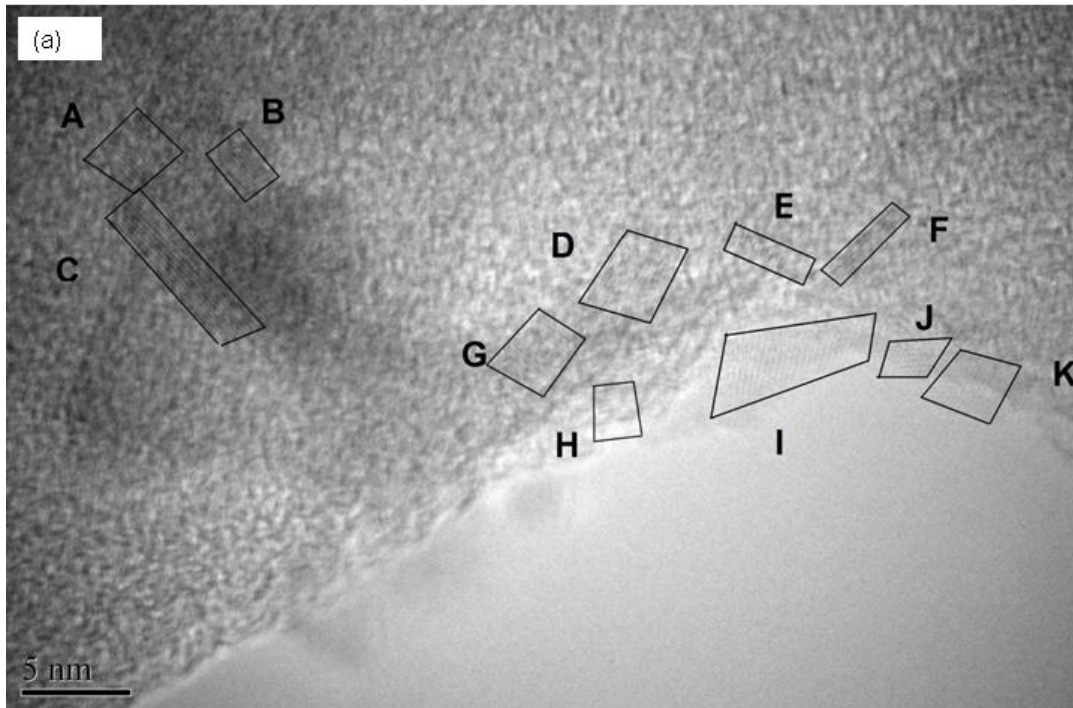


Fig 4-8 Turbostratic region of Soot Sample AM C showing (a) Crystal Fringe Lattice Image (b) EDS Spectra

Table 4-12 HR-TEM Analysis of Lattice Fringes for Possible Nano crystalline particles

Crystal Lattice Fringe	Suggested Particle	d-spacing (Å ^o)		Crystalline Particle
		Standard Value	Measured Value	
B	Calcium Oxide	1.88	1.80	CaO
J		3.00	3.04	CaO
C	Graphite/ Zinc Oxide	2.19/ 2.14	2.16	C/ ZnO
K		2.19/ 2.14	2.16	C/ ZnO
D	Graphite	2.19	2.25	C
F		2.19	2.22	C
A	-	-	2.27	-
E	-	-	2.31	-
G	-	-	2.76	-
H	-	-	2.32	-
I	-	-	3.30	-

Soot sample from oldest engine AM C of 248,000 miles did not give much result. Matching of EDS result and lattice fringes in turbostratic region of soot sample was only able to identify Zinc Oxide and Calcium Oxide. Result from EDS was able to reflect on faint values of Magnesium, Zinc Oxygen and Calcium. There is the possibility of other crystal particles

embedded in the soot but not reflected by EDS, those cannot however be matched.

4.6.2.1 SAED Analysis of Soot Samples

SAED analyses are used for structural characterization of sample. Interpretation and Analysis for the samples AM A, AM B and AM C are compared in Fig 4.9 below and Table 4.12 on page 135.

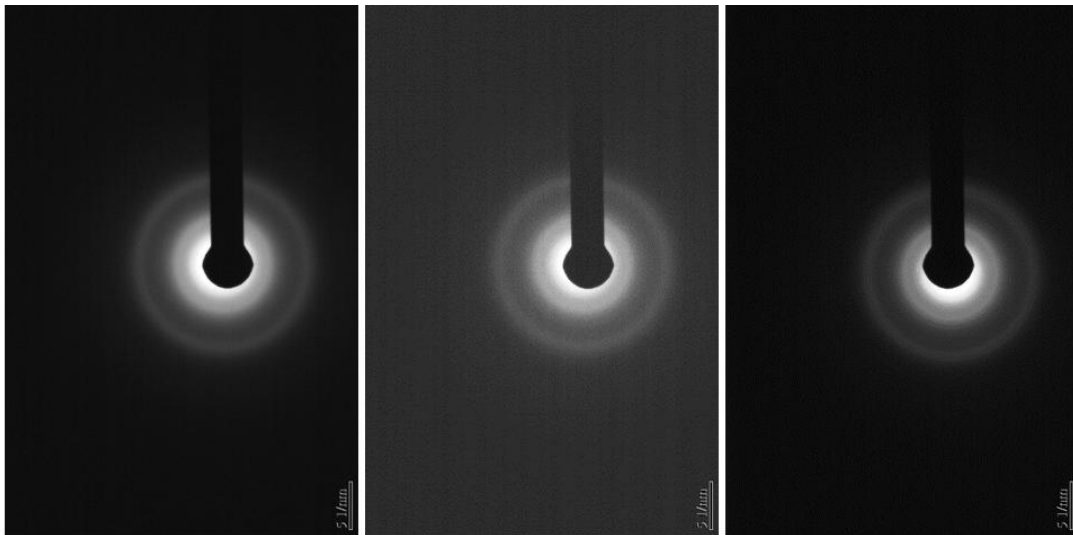


Fig 4-9 SAED Lattice Image of Soot Samples (a) AM A (b) AM B and (C)
AM C

Reciprocal lattice of other crystalline phases is not revealed in the SAED result of soot samples. This is an indication of low formation of other crystal particle phases in synthetic based diesel oil with recirculation from EGR system. EGR soot generated from EGR recirculation in

dominated by graphitic phases and only graphitic rings are observed in the SAED image.

Table 4-13 d- spacing Measurement of Electron Diffraction Patterns for Samples AM A, AM B and AM C

Sample	1 st ring d-spacing (R ₁)	2 nd ring d-spacing (R ₂)	3 rd ring d-spacing (R ₃)	R ₂ /R ₃	R ₁ /R ₃
SP A	0.317 (002)	0.199 (10)	0.112 (11)	1.77	2.83
SP B	0.322 (002)	0.198 (10)	0.114 (11)	1.74	2.82
SP C	0.332 (002)	0.208 (10)	0.120 (11)	1.73	2.77

The SAED diffraction patterns majorly has the intense rings arising from (200) basal planes, (10) prismatic plane and (11) from the pyramidal planes. The diffraction patterns primarily arise from the crystalline portion of the turbostratic structure. The d- spacing that give rise to the rings are calculated from the electron patterns representing the graphitic phase. Other crystal patterns for other crystalline phases in the samples are not revealed, but lattice fringe images showed evidence of their presence.

4.6.3 Discussion of HR-TEM Analysis of EGR Soot Samples

Analysis of EGR soot from synthetic based chemistry did not reveal much of other crystalline particles within soot. EDS result show little quantities of chemistries with majority of Carbon indicating low presence of third body crystalline and amorphous formations with soot.

PAO which is the building block of synthetic based diesel oil in which the EGR soot are produced generally have great oxidative stability, extremely high viscosity index, and pure petrochemical feedstocks; which will prevent thermo-oxidative reaction which are precursor to formation of other abrasive and amorphous phases that can be founded within EGR soot and are causes of abrasive wear in diesel engines.

4.7 XANES Studies of EGR Soot Samples

The X-ray Absorption Near Edge Spectroscopy (XANES) is used as a non-destructive tool to characterize chemical substances at nano scale [76]. It employs high energy/ soft X-ray photon from synchrotron radiation source with high flux where photon beam of known energy is directed incident on a sample surface with sufficient energy which excites a core level electron of an atom in the sample. On excitation, a photoelectron is created which moves into unoccupied states of the atom and photon is absorbed. Holes created in either of the K or L levels from movement of photoelectron are filled up by electrons from other shells. These electron movement to fill the 'holes' generate an emission of a Fluorescent Yield (FLY) Spectra. Another approach used is to ground the sample and measure neutralization current which yields Total Electron Yield (TEY) spectra. Total Electron Yield is surface sensitive while the Fluorescent Yield spectra give information to higher depth of sample [77]. The

Absorption Edge of photon energy in samples can be used as finger-print to identify their chemical make-up.

4.7.1 Experimental Procedure for XANES Studies

The XANES experiment was carried out at the Canadian Light source, Saskatoon, Canada using the 2.9 GeV storage ring. Two beam lines were used to obtain the K and L absorption edge spectra. Phosphorus and Sulphur L Edge were obtained using the Variable Line Grating – Plane Grating Monochromator (VGM – PGM) beam line covering region of 5 – 250eV with photon resolution of 0.2eV and spot size of 500 μ m x 500 μ m. Phosphorus K Edge was recorded using the Soft X-ray Micro-characterization Beamline (SXRMB) covering region of 1700 – 10000 eV with photon resolution of 0.2eV and spot size of 300 μ m x 300 μ m. XANE spectra for the L edge were all acquired in both the Total Electron Yield (TEY) and Fluorescent Yield (FLY) modes while XANES spectra for the K edge was acquired in FLY mode. The spectra data for the soot samples were analyzed with the OriginPro software to get final XANES spectra. The absorption spectra of the various chemistries incorporated in the soot were compared with that of model compounds for the Phosphorus and Sulphur L edge, and for Phosphorus K edge.

4.7.2 XANES Analysis of Soot Samples

XANES Spectroscopy of extracted soot samples from used Diesel Oil were acquired in the Total Electron Yield (TEY) mode for chemical information of surface or near surface regions and the fluorescence Yield (FLY) mode was acquired to determine chemical property of bulk soot sample. The sampling depths for the soot sample in the TEY mode of the Phosphorus and Sulfur L Edge are at about 5 nm at the L- Edge and about 50 nm at the K- Edge. Sampling depth for the FLY mode was taken at about 50 nm at the L Edge and about 400 nm at the K Edge [78].

4.7.2.1 Phosphorus L Edge XANES Spectral Analysis

The FLY spectra and the TEY spectra of nano particles created with soot are compared with model compounds of FePO_4 , $\text{Zn}_3(\text{PO}_4)_2$, $\text{Ca}_2\text{P}_2\text{O}_7$, $\text{Ca}_3(\text{PO}_4)_2$ as shown in Fig 4.10 on page 139 below. Iron phosphates have a slightly higher energy states than zinc phosphates. FePO_4 is at 139 eV and $\text{Zn}_3(\text{PO}_4)_2$ is at 138.7 eV).

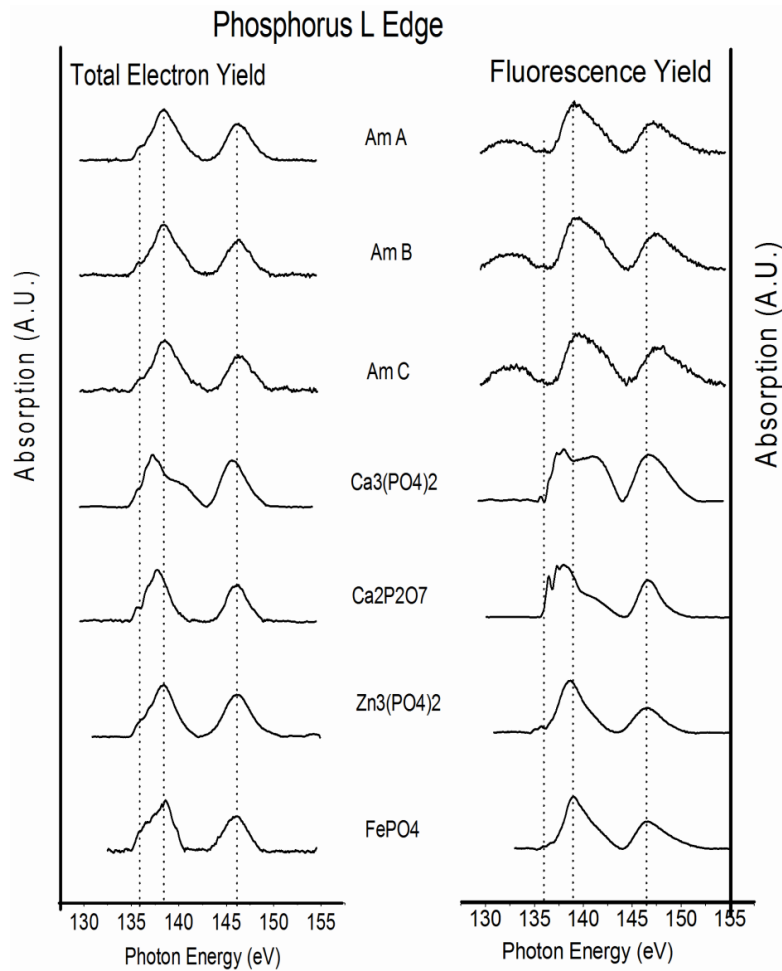


Fig 4-10 Normalized TEY and FLY Phosphorus L Edge spectra of soot samples AM A, AM B, AM C and model compounds

Spectra of soot sample AM A, AM B and AM C are similar, and they closely matched with Zinc Phosphate and Iron Phosphate. The spectra of the samples look more similar to Zinc Phosphate, but the presence of Iron Phosphate can also not be ruled out. There is a huge possibility of the

presence of both Calcium Phosphate and Iron phosphate nano particles in the samples.

4.7.2.1 Sulphur L Edge XANES Spectra Analysis

Sulfur L edge provides local coordination of sulfur near the surface of the tribofilm [79,80]. The Sulfur L Edge Spectra taken in the TEY and FLY modes is shown in Fig 4.11 on page 141 below. Spectra of soot samples are compared with model compounds of sulfates and sulfides to determine possible presence of any similar compound. All sulfates and sulfides have unique features which distinguish them except FeSO_4 and $\text{Fe}_2(\text{SO}_4)_3$. Iron sulfide (FeS) and Iron sulfate (FeSO_4 or $\text{Fe}_2(\text{SO}_4)_3$) have two main peaks, while iron sulfide has a sharp peak at lower energy that is missing in the sulfates. Zinc sulfate has three small peaks at first main peak.

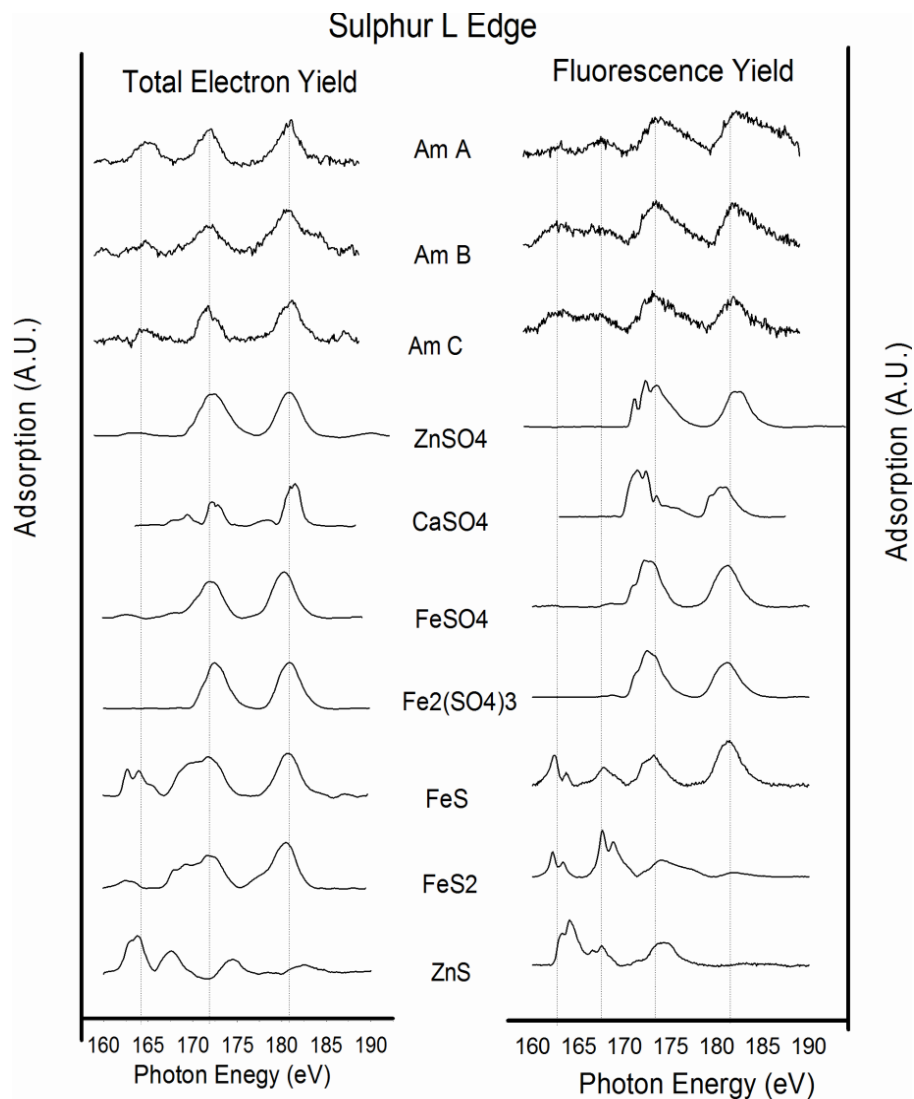


Fig 4-11 Normalized TEY and FLY Sulfur L Edge Spectra of Soot Samples
AM A, AM B, AM C and Model Compounds

The XANES spectra of the soot samples indicate the presence of sulfates and sulfides of Iron. All three soot samples are confirmed to contain Iron Sulfide with the possibility of other sulfates, which are most likely Iron Sulfate.

4.7.1.3 Phosphorus K edge XANE Spectra Analysis

Absorption peak in phosphorus K- edge spectrum arises from transition of 1s electrons to unoccupied 2p shells. Soot spectra for the three samples are compared with phosphates of zinc, calcium, and iron as shown in Fig 4.12 below.

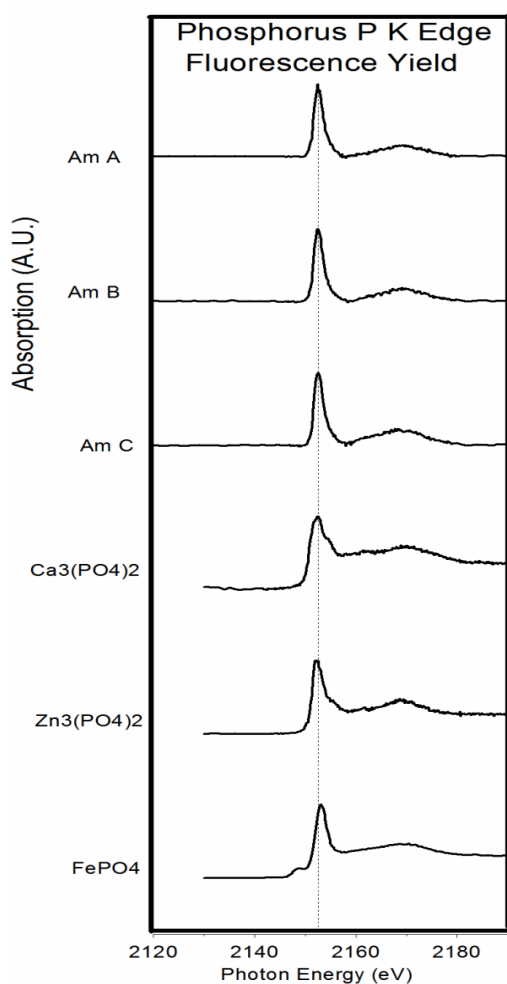


Fig 4.12 Normalized FLY Phosphorus K Edge Spectra of Soot Samples

AM A, AM B, AM C and Model Compounds

The peaks observed for the three samples AM A, AM B and Am C are similar. The P K Edge which is at a higher dept can be used to confirm result in the P L Edge where samples closely matched with Iron phosphate and Zinc phosphates. In this case of the P K Edge, the phosphate peak is also closer matched to Zinc phosphate, but the presence of Iron phosphate will not be ruled out. The absence of pre edge peak at 2148eV in the soot sample which is seen in Iron can also be used to corroborate the match.

4.7.2 Discussion of XANES Spectra

XANES Analysis result was able to show the presence of a number of crystalline particles formed with EGR Soot. The presence of Iron Sulfide, Iron Sulfate and the possibility of other sulfates is confirmed in results from the Sulphur L Edge. Results from both Phosphorus L end K Edge also confirm the presence of Iron Phosphate and a high likelihood of Zinc phosphates. These nano particles reveals by the XANES analysis are all abrasive and are believed to cause and encourage wear in Diesel engines. Their ease of formation and effect on wear will be more aggravated in older engines with less operating combustion efficiency.

Chapter 5

Conclusion

The stoichiometric chemical analysis of used Mineral and Synthetic based Diesel Oil studied showed that Synthetic base stock possesses less additive composition in its oil formulation. The synthetic base stock is more stable in its oxidative ability. In both cases of Diesel Oil, almost same types of additives were used in the formulation of oil but in much different quantities. Besides the properties of basestock used in oil formulation, quantities of lubricant additives added to oil which are degradable overtime will play a role to determine nature of other crystalline and amorphous third particle phases formed in EGR soot. From the ICP- AES (Inductively coupled plasma atomic emission spectroscopy) test of used oil, it is seen that less ZDDP antioxidant is required to reach desired properties anti-oxidation and wear protection in Synthetic Diesel Oil than required to achieve desired properties in Mineral Diesel Oil.

It is seen from the Raman studies of soot that newer engines because of their more efficient combustion system generated better graphitized soot which are less reactive and less able to degrade lubricant chemistry. Less graphitized soot generated in the older and oldest engine have more disordered graphene edges that more easily react and degrade

lubricant chemistry. The more disordered graphene edges serve as functionalized absorptive sites for third body particles formed from degradation of lubricant chemistries.

The XRD studies which studied bulk quantity of the samples revealed that soot generated in the new engine is dominated by more of calcium based nanoparticles (Bassinite, $\text{CaSO}_4 \cdot 0.5\text{H}_2\text{O}$) than any other particles Bassinite has a hardness of 2 on the mohr hardness scale and will not be a cause of wear in diesel engine. The studies showed that more nano particles are formed in EGR soot as the engine of the EGR engine increases.; it showed that older engines generated soot incorporating more of other phases with the engine of 247,000 miles showing presence of additional Wurtzite 2H (ZnS) phase, and the oldest engine of 306,000 miles generating soot with additional Calcium Pyrophosphate ($\text{Ca}_2\text{P}_2\text{O}_7$), Wurtzite, Magnetite (Fe_3O_4), Wustite (FeO), and Zinc Sulfate particles. Most of these additional phases observed in the older engines, aside Calcium pyrophosphate are abrasive and will be causes of wear in diesel engines; and they are determinant of the abrasive characteristics of EGR soot in old diesel engines.

Result from HR-TEM also showed domination of Calcium based crystalline compound with few oxides in the new engine. The Calcium based particles are from the detergency action of calcium sulfonate; and

they have low hardness of 2 on a scale of 10 which will not be threat to wear in Diesel engines. It can be concluded that lubrication is more effective in new engine and the detergents circulating in oil to reduce formation of second in both oil and soot. Diverse crystal particles are observed in both samples from older engines ranging from the three phases of Iron Oxides, multiple other oxides and sulfates. The Iron Oxides; Magnetite, Hematite and Wustite observed in samples from the older engines above 200,000 miles are abrasive with hardness comparable to 9 on a scale of 10, and will result in wear in EGR diesel engines.

XANES also corroborated the findings of XRD where abrasive sulfates, sulfide and phosphates were observed in soot samples generated across increasing diesel engine age

Chapter 6

Suggested Future Work

This work has studied and understood the characteristics of EGR soot as a function of engine age and lubricant chemistries, and it is seen that older engines will generate more of other crystalline and amorphous particles in EGR soot than in newer engines. Most of these particles are abrasive and are determinant of the abrasive nature of EGR soot. It will be suggested that tribological tests be carried out in future to test the relationship between abrasive nature of soot to wear in engines.

Asides the engine age and lubricant chemistries studied, other factors influencing formation of soot such as engine design and operating conditions can also be studied to determine nature of EGR soot formed as a result of such factors.

Appendix A
API Diesel Oil Grades [81]

DIESEL ENGINE		
Category	Status	Service
CJ-4	Current	Introduced in 2006. For high-speed, four-stroke engines designed to meet 2007 model year on-highway exhaust emission standards. CJ-4 oils are compounded for use in all applications with diesel fuels ranging in sulfur content up to 500 ppm (0.05% by weight). However, use of these oils with greater than 15 ppm (0.0015% by weight) sulfur fuel may impact exhaust after-treatment system durability and/or oil drain interval. CJ-4 oils are effective at sustaining emission control system durability where particulate filters and other advanced after-treatment systems are used. Optimum protection is provided for control of catalyst poisoning, particulate filter blocking, engine wear, piston deposits, low- and high-temperature stability, soot handling properties, oxidative thickening, foaming, and viscosity loss due to shear. API CJ-4 oils exceed the performance criteria of API CI-4 with CI-4 PLUS, CI-4, CH-4, CG-4 and CF-4 and can effectively lubricate engines calling for those API Service Categories. When using CJ-4 oil with higher than 15 ppm sulfur fuel, consult the engine manufacturer for service interval
CI-4	Current	Introduced in 2002. For high-speed, four-stroke engines designed to meet 2004 exhaust emission standards implemented in 2002. CI-4 oils are formulated to sustain engine durability where Exhaust Gas Recirculation (EGR) is used and are intended for use with diesel fuels ranging in sulfur content up to 0.5% wt. Can be used in place of CD, CE, CF-4, CG-4, and CH-4 oils. Some CI-4 oils may also qualify for the CI-4 PLUS designation
CH-4	Current	Introduced in 1998. For high-speed, four-stroke engines designed to meet 1998 exhaust emission standard. CH-4 oils are specifically compounded for use with diesel fuel ranging in sulfur content up to 0.5% wt. Can be used in place of CD, CE, CF-4, and CG-4 oils
CG-4	Obsolete	Introduced in 1995. For severe duty, high-speed, four-stroke engines using fuel with less than 0.5% weight sulfur. CG-4 oils are required for engines meeting 1994 emission standards. Can be used in place of CD, CE, and CF-4 oils
CF-4	Obsolete	Introduced in 1990. For high-speed, four-stroke, naturally aspirated and turbocharged engines. Can be used in place of CD and CE oils.
CF-2	Obsolete	Introduced in 1994. For severe duty, two-stroke-cycle engines. Can be used in place of CD-II oils.
CF	Obsolete	Introduced in 1994. For off-road, indirect-injected and other diesel engines including those using fuel with over 0.5% weight sulfur. Can be used in place of CD oils.
CE	Obsolete	Introduced in 1985. For high-speed, four-stroke, naturally aspirated and turbocharged engines. Can be used in place of CC and CD oils.
CD- II	Obsolete	Introduced in 1985. For two-stroke cycle engines.
CD	Obsolete	Introduced in 1955. For certain naturally aspirated and turbocharged engines.
CC	Obsolete	CAUTION: Not suitable for use in diesel-powered engines built after 1990.
CB	Obsolete	CAUTION: Not suitable for use in diesel-powered engines built after 1961.
CA	Obsolete	CAUTION: Not suitable for use in diesel-powered engines built after 1959.

References

- [1] C. J. Morey, J Mark. Diesel Passenger Vehicles - Can They Meet Air Quality Needs and Climate Change Goals?. 2000-01-1599 2000;01.
- [2] Yu RC, Shahed SM. Effects of Injection Timing and Exhaust Gas Recirculation on Emissions from a D.I. Diesel Engine. 811234 2000.
- [3] Yamaguchi ES, Utermann M, Roby SH, Yeh S. Soot Wear in Diesel Engines. Proceedings of the Institute of Mechanical Engineers Pt: J Automobile Eng 2006;220: 463-9.
- [4] Dennis AJ, Garner CP, Taylor DHT. The Effect of EGR on Diesel Engine Wear. SAE Technical Paper 1999: Paper Number 1999-01-0839.
- [5] Gautam M, Chitoor K, Durbha M, Summers JC. Effect of diesel soot contaminated oil on engine wear— investigation of novel oil formulations. Tribol Int 1999; 32:687-99.
- [6] Aldajah S, Ajayi OO, Fenske GR, Goldblatt IL. Effect of exhaust gas recirculation (EGR) contamination of diesel engine oil on wear. Wear 2007; 263:93-8.
- [7] Moran RC, Kazacik AP. Mineral oil composition. Socony-Vacuum Oil Company Inc 3/21/1939; 2,151,300.

[8] Green DA, Lewis R. The Effects of Soot- contaminated Engine Oil on Wear and Friction: A Review. Proceedings of the Institute of Mechanical Engineers Pt D: J Automobile Eng 2008;222: 1669-89.

[9] Singh SK, Agarwal AK, Sharma M. Experimental investigations of heavy metal addition in lubricating oil and soot deposition in an EGR operated engine. Appl Therm Eng 2006; 26:259-66.

[10] Kuo CC, Passut CA, Jao T, Csontos AA, Howe JM. Wear mechanism in Cummins M-11 high soot diesel test engines. 1998;1368: 21-32.

[11] Yamaguchi ES, Utermann M, Roby SH, Ryason SH, Yeh SW. Soot wear in diesel engines. Proc Inst Mech Eng Part J 2006; 220:463-9.

[12] Bardasz EA, Carrick VA, Ebeling VL, George HF, Graf MM, Kornbrekke RE et al. Understanding soot mediated oil thickening through designed experimentation-part 2: GM 6.5L. 1996.

[13] Bardasz EA, Carrick VA, George HF, Graf MM, Kornbrekke RE, Pocinki SB. Understanding soot mediated oil thickening through designed experimentation - Part 5: Knowledge enhancement in the GM 6.5L. 1997.

[14] Braun A, Huggins FE, Shah N, Chen Y, Wirick S, Mun SB et al. Advantages of soft X-ray absorption over TEM-EELS for solid carbon

studies- A comparative study on diesel soot with EELS and NEXAFS. Carbon 2005;43:117-24.

[15] Braun A, Shah N, Huggins FE, Kelly KE, Sarofim A, Jacobsen C et al. X-ray scattering and spectroscopy studies on diesel soot from oxygenated fuel under various engine load conditions. Carbon 2005;43:2588-99.

[16] Cuesta A, Dhamelinourt P, Laureyns J, Martinez-Alonso A, Tascon JMD. Raman microprobe studies on carbon materials. Carbon 1994;32:1523-32.

[17] Dillon RO, Woollam JA. Use of raman scattering to investigate disorder and crystallite formation in as-deposited and annealed carbon films. 1983:291-2.

[18] Antusch S, Dienwiebel M, Nold E, Albers P, Spicher U, Scherge M. On the tribochemical action of engine soot. Wear 2010;269:1-12.

[19] Rounds FG. Effect of lubricant additives on the prowear characteristics of synthetic diesel soots. Lubrication Engineering 1987; 43: 273-82.

[20] Ryason PR, Chan IY, Gilmore JT. Polishing wear by soot. 1990; 35:250.

[21] Nagai I, Endo H, Nakamura H, Yano H. Soot and valve train wear in passenger car diesel engines. 1983.

[22] Soejima M, Ejima Y, Uemori K, Kawasaki M. Studies on friction and wear characteristics of cam and follower: Influences of soot contamination in engine oil. *JSAE Rev* 2002;23:113-9.

[23] Truhan JJ, Covington CB, Wood L. The classification of lubricating oil contaminants and their effect on wear in diesel engines as measured by surface layer activation. 1995.

[24] Truhan J, Covington C. The use of direct method surface layer activated to measure wear in diesel engine. 1993.

[25] Pang KM, Ng HK, Gan S. Simulation of temporal and spatial soot evolution in an automotive diesel engine using the Moss–Brookes soot model. *Energy Conversion and Management* 2012;58:171-84.

[26] Lawrence L. Heavy- Duty Diesel Engine Oil Development and Trends. In: Lawrence L, editor. *Machinery Lubrication*; 2007.

[27] Gill SS, Tsolakis A, Dearn KD, Rodríguez-Fernández J. Combustion characteristics and emissions of Fischer–Tropsch diesel fuels in IC engines. *Progress in Energy and Combustion Science* 2011;37:503-23.

[28] Tree DR, Svensson KI. Soot processes in compression ignition engines. *Progress in Energy and Combustion Science* 2007;33:272-309.

[29] Akihama K, Takatori Y, Inagaki K, Sasasaki S. Mechanism of the Smokeless Rich Diesel Combustion by Reducing Temperature. 2001-01-0655 2001.

[30] Park SW. Optimization of combustion chamber geometry for stoichiometric diesel combustion using a micro genetic algorithm. Fuel Process Technol 2010;91:1742-52.

[31] Rakopoulos CD, Kosmadakis GM, Pariotis EG. Investigation of piston bowl geometry and speed effects in a motored HSDI diesel engine using a CFD against a quasi-dimensional model. Energy Conversion and Management 2010;51:470-84.

[32] Maiboom A, Tautzia X, Hétet J. Experimental study of various effects of exhaust gas recirculation (EGR) on combustion and emissions of an automotive direct injection diesel engine. Energy 2008;33:22-34.

[33] Kim HJ, Lee KS, Lee CS. A study on the reduction of exhaust emissions through HCCI combustion by using a narrow spray angle and advanced injection timing in a DME engine. Fuel Process Technol 2011;92:1756-63.

[34] Thurnheer T, Edenhauser D, Soltic P, Schreiber D, Kirchen P, Sankowski A. Experimental investigation on different injection strategies in a heavy-duty diesel engine: Emissions and loss analysis. Energy Conversion and Management 2011; 52:457-67.

[35] Lockwood FC, Naguib AS. The prediction of the fluctuations in the properties of free, round-jet, turbulent, diffusion flames. *Combust Flame* 1975;24:109-24.

[36] Arcy D. Proposed 'PC- 11' Diesel oil. Shell North America Technology Seminar 2012.

[37] Noria Corporation. Understanding the Differences in Base Oil Groups. *Industrial Lubricant* 2012.

[38] Hsu SM. Molecular basis of lubrication. *Tribol Int* 2004; 37:553-9.

[39] Stachowiak GW, Batchelor AW. *Engineering Tribology*. Butterworth Heinemann, 2001.

[40] Vander Wal RL, Tomasek AJ. Soot nanostructure: dependence upon synthesis conditions. *Combust Flame* 2004; 136:129-40.

[41] Zhu J, Lee KO, Yozgatligil A, Choi MY. Effects of engine operating conditions on morphology, microstructure, and fractal geometry of light-duty diesel engine particulates. *Proceedings of the Combustion Institute* 2005;30: 2781-9.

[42] Clark NN, Kern JM, Atkinson CM, Nine RD. Factors affecting heavy-duty diesel vehicle emissions. *Journal of the Air and Waste Management Association* 2002; 52:84-94.

[43] Wade RW. Light-Duty Diesel NO_x-HC-Particulate Trade-Off Studies. SAE Technical Paper 1980.

[44] Needham DM. The Low NO_x Truck Engine. SAE Technical Paper 1991.

[45] Smith O I. Fundamentals of soot formation in flames with application to diesel engine particulate emissions. Progress in Energy and Combustion Science 1981;7:275-91.

[46] Haynes BS, Wagner Gg. H. Soot formation. Progress in Energy and Combustion Science 1981;7:229-73.

[47] Glassman I. Soot formation in combustion processes. Symp Int Combust 1989;22:295-311.

[48] Zhou Z, Ahmed TU, Y. Choi M. Measurement of dimensionless soot extinction constant using a gravimetric sampling technique. Exp Therm Fluid Sci 1998;18: 27-32.

[49] Echavarria CA, Jaramillo IC, Sarofim AF, Lighty JS. Studies of soot oxidation and fragmentation in a two-stage burner under fuel-lean and fuel-rich conditions. Proceedings of the Combustion Institute 2011;33: 659-66.

[50] Bryce D, Ladommatos N, Xiao Z, Zhao H. Investigating the effect of oxygenated and aromatic compounds in fuel by comparing laser

soot measurements in laminar diffusion flames with diesel-engine emissions. *J Inst Energy* 1999;72:150-6.

[51] Mitchell JBA, Le Garrec JL, Florescu-Mitchell A, Di Stasio S. Small-angle neutron scattering study of soot particles in an ethylene-air diffusion flame. *Combust Flame* 2006;145:80-7.

[52] Peck J, Timko MT, Yu Z, Wong H, Herndon SC, Yelvington PE et al. Measurement of volatile particulate matter emissions from aircraft engines using a simulated plume aging system. 2011;2:1249-58.

[53] Sato H, Tree DR, Hodges JT, Foster DE. A study on the effect of temperature on soot formation in a jet stirred combustor. *Symp Int Combust* 1991;23:1469-75.

[54] Pinson J, Mitchell D, Santoro R, Litzinger T. Quantitative, Planar Soot Measurements in a D.I. Diesel Engine Using Laser-induced Incandescence and Light Scatterin. *SAE Technical Paper* 1993.

[55] Nakanishi K, Kadota T, Hiroyasu H. Effect of air velocity and temperature on the soot formation by combustion of a fuel droplet. *Combust Flame* 1981; 40:247-62.

[56] Nagle J, Strickland-Constable RF. Oxidation of Carbon between 1000-2000°C. *Fifth Conference on Carbon* 1962:154-64.

[57] Rounds FG. Generation of synthetic diesel engine oil soot for wear studies. *Lubrication Engineering* 1984;40: 394-401.

[58] Rounds FG. Soots from used diesel engine oils - Their effects on wear as measured in 4-ball wear tests. SAE Technical Paper 1981:Paper Number 810499.

[59] Rounds FG. Carbon: Cause of diesel engine wear? SAE Technical Paper 1977:Paper Number 770829.

[60] Berbezier I, Martin JM, Kapsa P. The role of carbon in lubricated mild wear. Tribol Int 1986;19:115-22.

[61] Kim B. Tribological Performance of Ashless Antiwear Additives Under Extreme Pressure Conditions. 2009.

[62] Castilloa C, Spikes HA. The behavior of diluted sooted oils in lubricated contacts. Tribology Letters May, 2004;16:317.

[63] Needelman WM, Madhavan PV. Review of Lubricant contamination and Diesel Engine Wear. SAE Technical Paper 1988.

[64] Cadman W, Johnson JH. Study of the effect of exhaust gas recirculation on engine wear in a heavy duty diesel engine using analytical ferrography. 1986:SAE, Warrendae, PA, USA.

[65] Corso S, Adamo R. The Effect of Diesel Soot on Reactivity of Oil Additives and Valve Train Materials. SAE Technical Paper 1984.

[66] Corso S, Adamo R. Incipient Scuffing Detection by Ferrography in a Diesel Valve Train System. SAE Technical Paper 1985.

[67] Akiyama K, Masunaga K, Kado K, Yoshioka T. Cylinder Wear Mechanism in an EGR-Equipped Diesel Engine and Wear Protection by the Engine Oil. SAE Technical Paper 1987.

[68] Gautam, M., Durbha, M., Chitoor K, Jaraiedi Mea. Contributions of Soot Contaminated Oils to Wear. SAE Technical Paper 1998.

[69] ASTM International. ASTM E2412- 10 Standard Practice for Condition Monitoring of Used Lubricant by Trend Analysis Using Fourier Transform Infra red Spectroscopy. ASTM International 2010;E2412.

[70] Jawhari T, Roid A, Casado J. Raman spectroscopic characterization of some commercially available carbon black materials. Carbon 1995;33:1561-5.

[71] Nikiel L, Jagodzinski PW. Raman spectroscopic characterization of graphites: A re-evaluation of spectra/ structure correlation. Carbon 1993;31:1313-7.

[72] Tuinstra F, Koenig J L. Raman Spectrum of Graphite. J Chem Phys 1970;53:1126-30.

[73] Sadezky A, Muckenhuber H, Grothe H, Niessner R, Poschl U. Raman microspectroscopy of soot and related carbonaceous materials: Spectral analysis and structural information. Carbon 2005;43:1731-42.

[74] Ferrari AC. A model to interpret the Raman spectra of disordered, amorphous and nanostructured carbons. 2001; 675: W11.5.1, W11.5.12.

[75] Sharma R, Baik JH, Perera CJ, Strano MS. Anomalous Large Reactivity of Single Graphene Layers and Edges toward Electron Transfer Chemistries. Nano Letters 2010;10:398-405.

[76] Kasrai M, Lennard WN, Brunner RW, Bancroft GM, Bardwell JA, Tan KH. Sampling depth of total electron and fluorescence measurements in Si L- and K-edge absorption spectroscopy. Appl Surf Sci 1996; 99:303-12.

[77] Ankudinov AL, Rehr JJ, Low JJ, Bare SR. Theoretical interpretation of XAFS and XANES in Pt clusters. 2002; 18:3-7.

[78] www.wisconsin-med.edu, The Synchrotron Radiation Center (SRC).

[79] Nicholls MA, Norton PR, Bancroft GM, Do BH. Nanometer scale chemomechanical characterization of Antiwear Films. Tribol Lett 2004; 17:205-16.

[80] Bukanin VN, Kasrai M, Kuzmina GN, Bancroft GM, Parenago OP. Influence of temperature and ZDDP concentration on tribochemistry of surface-capped molybdenum sulfide nanoparticles studied by XANES spectroscopy. Tribol Lett 2007;26:33-43.

[81] Kiely G. Environmental Engineering , McGraw Hill International Editions, Chemical and Petroleum Engineering series. UK 123, 1998, McGraw - Hill International Edition, UK

Biographical Information

Olusanmi Adeniran was born and raised in South West, Nigeria. He has his bachelor's degree in Metallurgical and Materials Engineering at the Obafemi Awolowo University, Ile-Ife, Nigeria where he worked with Dr. Oluleke Oluwole on the developing Nickel Coated manganese steel for Oil and gas applications. After graduation, he had a one year National Service to the Government of Nigeria from 2008 – 2009, a time at which he also served as a Relationship Officer with Oceanic Bank Plc, Lagos, Nigeria. He worked as a Piping Engineer with ASB Valiant Limited which is the sole representative of Turbomach Gas Turbines in Nigeria, and resigned from the job in 2011 to pursue graduate degree in Materials Engineering at the University of Texas at Arlington.

He has a student cooperative work training at LuK USA LLC-Schaeffler Group from January – August 2013, and he was offered a full time position as a Development Engineer from January 2014 upon his graduation. Olusanmi is a certified Project Management Professional (PMP), Society of Tribologist and Lubrication (STLE) volunteer and is active in many other professional bodies. Olusanmi is interested in Tribology and Corrosion research and plans on pursuing a PhD degree in the future.